Planktonic foraminiferal response to the Last Glacial Termination and their application to Holocene biostratigraphy in the western Mediterranean Sea

By

Teresa Carmel Broggy

A thesis submitted for the degree of

DOCTOR OF PHILOSOPHY

Supervisor: Dr. Angela Hayes

Submitted 13 Sept 2011

Department of Geography
Mary Immaculate College
(Coláiste Mhuire Gan Smál)
University of Limerick

ABSTRACT

Planktonic foraminiferal response to the Last Glacial Termination and their application to Holocene biostratigraphy in the western Mediterranean Sea

By Teresa Broggy

This research presents the planktonic foraminiferal assemblage variation of four western Mediterranean Sea cores since the Last Glacial Termination.

The Holocene epoch represents the current interglacial since the Last Glacial Termination ~11,600 cal years ago. Extensive palaeoenvironmental research has verified the ability of planktonic foraminiferal abundances to record climatic and environmental variations. This research utilises planktonic foraminiferal abundance and morphological asymmetry to establish new biostratigraphic applications and to reconstruct Holocene palaeoenvironmental conditions. The chronology of this research is validated by ^{14}C-AMS dating.

The potential of utilising variations in the coiling direction of *Globorotalia truncatulinoides* as a biostratigraphic tool was first noted in the early 1950s. This research has provided a detailed investigation into the Holocene coiling variation of *G. truncatulinoides*. Four cores identify a synchronous mid Holocene coiling variation event indicating a change in dominance from the sinistral to the dextral coiling variant. This coiling event was identified ~5.0 cal kyr BP in the initial sampling of the total population of *G. truncatulinoides* and at the later time of ~ 4.4 cal kyr BP in the faunal abundance record. The synchronous coiling events in all four cores indicate the significance of *G. truncatulinoides* as a biostratigraphic tool in the western Mediterranean Sea and suggest its possible biostratigraphic significance for other geographical locations. Sea Surface Temperatures (SSTs) were reconstructed for each core via faunal assemblage variations using Artificial Neural Network (ANN) software. Our findings suggest that SSTs was not a controlling factor on coiling direction, but rather ecological conditions relating to water column stability. This finding allows for a palaeoenvironmental reconstruction of the water column as indicated by the abundance and coiling variation of *G. truncatulinoides*. Three phases of abundance identified the ecological response of the species to environmental changes since the last glacial termination, recording the change from a weakly stratified, stratified and unstratified water column between ~11.2-8.6, ~8.6-5.1 and ~5.1 cal kyr BP-present respectively.

Faunal abundance records established the identification of 3 ecozones (EZ) for the previously undefined areas of the Gulf of Lion and the Balearic Basin (EZ1:11.2-8.6 cal kyr BP, EZ2:8.6-5.1 cal kyr BP and EZ1:5.1 cal kyr BP-present). This new proposed ecozonation provides a means of rapid chronological constraint within a local sub-basin scale.

Core M40/4 82-2 SL provided the means to present a high (1-2 cm) resolution palaeoenvironmental reconstruction for the hydrologically significant Gulf of Lion region. SST reconstructions identified three phases of climatic variability and four significant cooling events that can be recognised in both North Atlantic and/or Mediterranean Sea proxies at ~ 7.2, 5.2, 2.4 and 1.2 cal kyr BP. These findings indicate the ability of the Gulf

of Lion to record global climatic variations and its potential as a palaeoenvironmental research location.

Declaration

I, Teresa Broggy declare that this thesis is my own work and has never been previously submitted by me or any other individual for the purpose of obtaining a qualification.

Signed:

Teresa Broggy

Date:

_____

Acknowledgements

Firstly I would like to thank my supervisor Dr. Angela Hayes who opened my eyes to a world beneath the sea floor, and offered me the opportunity to study the mysteries of the Mediterranean Sea. I couldn't have done it without you! Thank you for all your advice, support and guidance they will always be appreciated. Finally I would like to thank you for your friendship, and for being the world's best supervisor!

I would like to thank *all* of my family especially my sisters, your love and support has kept me grounded with never a dull moment. I would especially like to thank my twin Joanne and my best friend, who is always there for me, never faltering and full of good advice. I would like to thank my parents Noel and Bridget Broggy for their love and for always encouraging me to succeed and finally for teaching me there really is no place like home.

I would like to thank my fiancé Padraic, for your support, love and laughter during all the years. Thank you for all the good times and all the good music and the wonderful future we will have together.

I would like to thank Mary Immaculate College and all the wonderful people and friends I have met there. I would like to thank the Geography Department, Prof Des McCafferty, Prof. Mick Healy, Dr Catherine Dalton, Dr Helene Bradley, Dr Brendan O Keefe and Anne Kane and the postgraduate community, especially Darren Barry with the final preparations! Sean Halligan, Philip Cremin, Shane O Sullivan, Philipo Cassina, Karen Sparber, Treasa Sheehan, thanks for all the chats, advice and your valued friendship.

Finally I would like to express my sincere gratitude and thanks to Prof. Michal Kucera and Dr Pauhla McGrane, thanks for making the Viva and submission a great experience, it was a pleasure to work with you both.

Dedicated to my Godchild Bridget (Broggy) Moloney

With Love x x x

List of Figures

List of Tables

Table of Contents

Chapter 1: Introduction

1.1. Introduction

The Holocene, the most recent epoch of geological time, represents the current interglacial period from ~11,600 years ago, up to and including the present day (O'Brien et al., 1995; Davis et al., 2003). The climatic signals of the Holocene may have appeared relatively stable compared to glacial periods however, further investigation provides evidence to the contrary (Alley at al., 1997; Barber et al., 1999; Bond et al., 1997, 2001; Mayewski et al., 2004; Alley and Ágústsdóttir., 2005; Rohling and Pälike, 2005; Fleitmann et al., 2008). The change from glacial to interglacial climates is transitional as is illustrated by the last glacial termination, where early to mid Holocene marine sediments records post glacial adjustments such as sea level rise. Post glacial sea level rise has significant hydrological and ecological responses, altering water column structure and circulation patterns and, as such, faunal responses to post glacial sea level rise have been quite dramatic. Providing a temporal progression for these Holocene climatic responses is facilitated by radiocarbon dating and as the timeframe encompassing the Holocene falls well within the time limits of radiocarbon dating, the timing and frequency of faunal changes are quite accurate.

1.2. Area of Study: The Mediterranean Sea

The Mediterranean Sea is almost completely landlocked, bounded by Europe to the north, Africa to the south and Asia to the East. The Mediterranean Sea is further divided into the main western and eastern basins via the Strait of Sicily, with each basin comprising several smaller sub-basins *(figure 1.1)*. As a semi enclosed sea, connected to the open North Atlantic Ocean via the relatively narrow Straits of Gibraltar *(figure 1.1)*, the Mediterranean Sea has the ability to record and amplify climatic events and as such, proves a valuable area of study for Holocene climatic variations (Cacho et al., 2001). Climate sensitive organisms such as planktonic foraminifera record Holocene climatic changes and provide the proxy information that allow for its reconstruction (Fischer and Wefer, 1999; Armstrong and Brasier, 2005; Kucera, 2007). The effects of climatic variations are observed in changes of atmospheric trends and patterns, land/sea ice ratios and ocean circulation, all of which directly affect the hydrographical features of the Mediterranean Sea and subsequent ecosystems it supports.

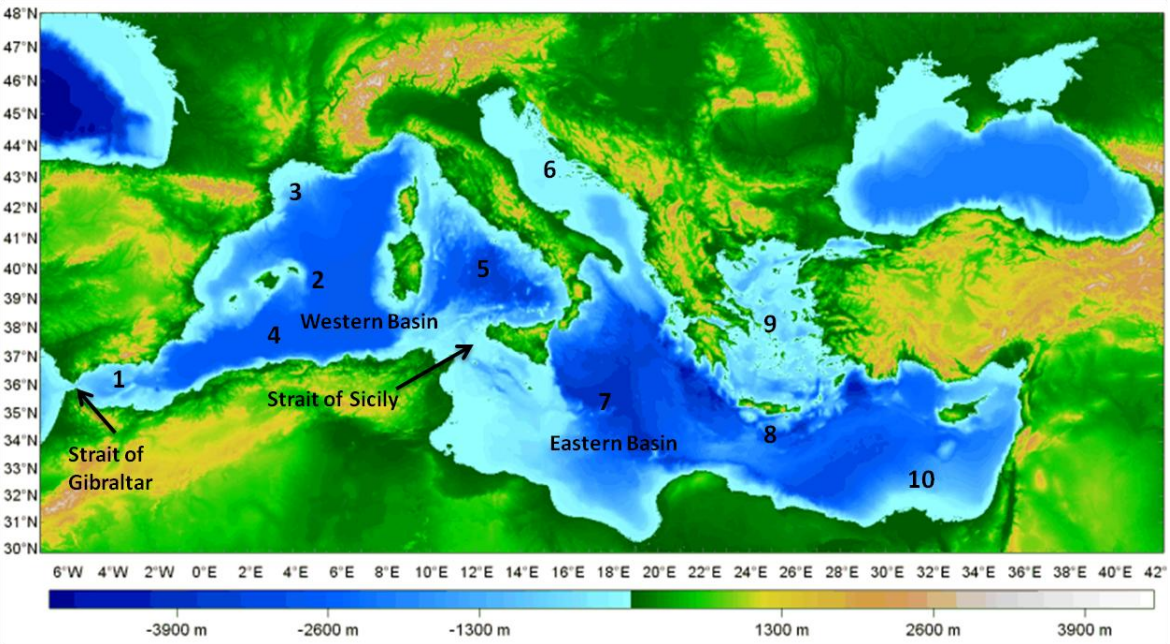

Figure 1.1. Map representing the main basins, sub basins and straits of the Mediterranean Sea 1=Alboran Sea, 2=Balearic Basin, 3=Gulf of Lion, 4=Algerian Sea, 5=Tyrrhenian Sea, 6=Adraitic Sea, 7=Ionian Sea, 8=Cretan Sea, 9=Aegean Sea, 10=Levantine Basin (Modified from CIBRA).

Modern day conditions establish the Mediterranean Sea as a concentrated basin (Reddy, 2001), where excess evaporation over precipitation produces relatively high salinities that increase in an easterly direction. Atmospheric patterns including local winds initiate further evaporation, such as the winter mistral winds that are channelled orographically into the Gulf of Lion region (*figure 1.1*) (Robinson et al., 1999). The modern day salinity and temperature profiles of the Mediterranean Sea determine water stability, this is particularly evident for the western basin where local temperature, salinity and density patterns facilitate the formation of deep water and subsequent deep vertical mixing in the Gulf of Lion region. The stability of the water column controls the vertical distribution of key elements such as nutrients and the resulting abundance and vertical movement of organisms including planktonic foraminifera. Using the principles of uniformitarianism, the present day distribution of planktonic foraminifera is applied to this study to reconstruct palaeoclimatic trends.

1.3. Planktonic Foraminifera

The distribution of planktonic foraminifera is governed by environmental parameters providing palaeoceanographic studies with a significant array of proxy data such as primary production, salinity and temperature (Fischer, and Wefer, 1999). Such proxies include

fossilised planktonic foraminiferal assemblages whereby sea surface temperatures (SSTs) are reconstructed via their species abundances and/or isotopic compositions. The applicability of planktonic foraminifera as a palaeoenvironmental tool was first noted by Murray (1897) who observed an association between their distribution and global belts of SST. Downcore analysis revealed the abundance variation of planktonic foraminifera reflected alterations between glacial and interglacial periods (Schott, 1935). This led the way for further palaeoclimatological reconstructions, of which the largest project being the reconstruction of temperatures during the last glacial maximum (LGM) (CLIMAP), 1976) which laid the foundations for the most recent Multiproxy Approach for the Reconstruction of the Glacial Ocean Surface (MARGO) project. In addition to palaeoenvironmental reconstruction, planktonic foraminifera provide valuable biostratigraphic tools in aiding temporal correlation between events and/or climatic zones. Planktonic foraminiferal biostratigraphy can be utilised via faunal assemblage zonation and/or morphological variation, such as the variation between the sinistrally (left) and dextrally (right) coiling planktonic foraminiferal species *Globorotalia truncatulinoides*

1.4 Purpose and Aims of this Research

This research identified a gap in the literature pertaining to biostratigraphy and palaeoclimatic studies in the western Mediterranean Sea and set about to address this issue.

A primary component of this research is to address the issue of coiling variation in the planktonic foraminiferal species *G. truncatulinoides*. Previous biostratigraphic studies based on the coiling variation of this species have only included the North Atlantic (Erricson, 1951) and the eastern Mediterranean Sea (Herman, 1972), this research aims to add to the existing literature by providing the first high resolution Holocene coiling variation data of *G. truncatulinoides* in the western Mediterranean Sea and determine if a coiling pattern exists, thereby providing a local scale biostratigraphic marker. As we know the modern day ecology of the sinistral and dextral variants of *G. truncatulinoides* downcore analysis would also provide a useful palaeoenvironmental indicator, while previous research have indicated the potential of SST on the coiling variation, this research would now provide the means to test that hypothesis.

The second focus of this research will utilise variations in planktonic foraminiferal assemblages to provide the first Holocene ecozonation for the Gulf of Lion and the Balearic Basin (*figure 1.1*), as previous research on ecozonation in the western Mediterranean is

spatially confined to the Alboran and Tyrrhenian Seas. This research will provide a Holocene stratigraphic framework based on faunal assemblage variations which will thereby facilitate further researchers in the areas defined to identify initial significant Holocene boundaries based on faunal variations alone.

In addition a palaeoclimatic study was undertaken across the western Mediterranean basin utilising SST reconstructions with particular emphasis on the Gulf of Lion region. The Gulf of Lion region represents the present day site of Western Mediterranean Deep Water (WMDW) formation and is subject to the effects of local winds intensified by the regional orography. Despite its particularly sensitive location for hydrological and atmospherical changes there have been limited palaeoenvironmental studies in this area (Melki et al., 2009). This study will present a high resolution faunal and SST reconstruction of the Gulf of Lion during the Holocene thereby highlighting Holocene climatic variations. These findings will provide a valuable addition to the limited palaeoclimatic research in this area.

In order to fulfil the research objectives four western Mediterranean Sea cores were utilised and the following **aims** were set out:

1. To assess the potential of coiling variation in *G. truncatulinoides* as a biostratigraphic marker in the western Mediterranean Sea during the Holocene and to examine the relationship of coiling variation with environmental parameters such as sea surface temperatures (SSTs).
2. To establish a new ecozonation from the last deglacation to the Holocene for the Gulf of Lion and Balearic Basin based on planktonic foraminiferal variations.
3. To provide a palaeoenvironmental reconstruction of the climatically sensitive Gulf of Lion employing the use of artificial neural networks (ANNs).

In order to appreciate the significance of our findings an understanding of the previous literature in the areas concerned is necessary. The following literature review will be presented in three chapters, the first will present an introduction to the present day climatology and oceanography of the Mediterranean, the second will address the proxy in question, planktonic foraminifera and outline its modern day abundance and distribution in the Mediterranean Sea. The third and final literature review chapter will address the

climatological variations associated with the time-frame of this research (The Holocene). These introductory chapters will then be followed by a material and methods and the chronological framework of the thesis. Finally the results will be presented in three distinct chapters corresponding with the three aims as outlined above.

Chapter 2: Mediterranean Sea Present Day Climatology and Physical Oceanography

2.1 The Mediterranean Climate

Based on the Köppen-Geiger climate classification system, figure 2.1 illustrates the climatic zones of the Mediterranean Sea (Peel et al., 2007). Each climatic zone is identified by an initial letter, and subsequent letters correspond to various climatic features within each zone *(Table 2.1)*. As is evident from figure 2.1 the Mediterranean Sea is situated in a transitional region between a more temperate European zone (Cs) north of the western Mediterranean basin, a cold European zone north of the eastern Mediterranean basin (Ds) and an arid North African zone directly to the south (Bs). Its transitional location reflects the fact that the Mediterranean Sea is affected by the various atmospheric forces that influence the climatic zones to its north and south. In the Northern Hemisphere descending air, associated with the mid latitude and Hadley cells, create a belt of high pressure known as the Subtropical High (*figure 2.2*). The resultant diverging winds travel poleward (westerlies) and towards the equator (Trade winds) *(figure 2.2)*. Consequently, central and northern Europe is influenced by the continuous year round flow of the westerlies which greatly influence winter precipitation (*figure* 2.2) (Boucher, 1975; Luterbacher and Xoplaki, 2003; Lionello et al., 2006). The typical warm and dry summer that characterise the Mediterranean climate is attributed to a strong high pressure extending from the Azores subtropical high (Xoplaki et al., 2003).

The topography surrounding the Mediterranean Sea also has a significant influence on the regions climate (Lionello et al., 2006). In particular, the Alps and the Pyrenees mountain ranges orographically channel local winds towards the Mediterranean Sea, ultimately influencing the hydrographic circulation *(figure 2.3)*. The principal influencing winds of the Mediterranean region are the Mistral, Westerly, Levante, Bora, Bora/Etesian and Sirocco *(figure 2.3)*. The Bora and Bora/Etesian flow into the Adriatic and Aegean Seas respectively, as cold northerly winds while the Sirocco winds are warm/hot southeast winds originating from the Sahara desert, Libya and Egypt. More significant to this research however, are the prevailing winds affecting the western Mediterranean Sea, the Mistral, Westerly and Levante as they are directly associated with the hydrographic and climatic features of the basin (Alpert et al., 2006: Rohling et al., 2009).

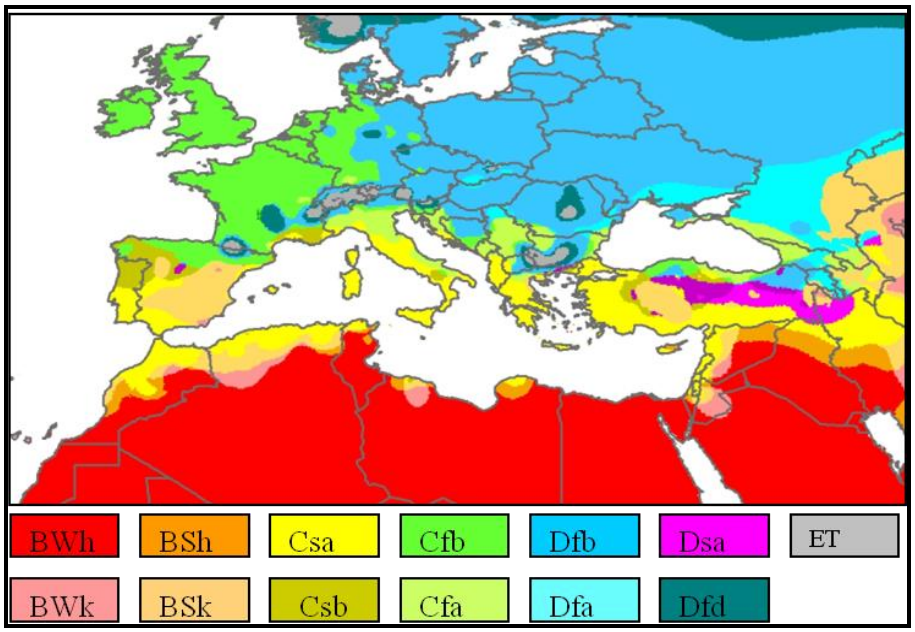

Figure 2.1. Climatic zonation of the Mediterranean region based on the Köppen-Geiger climate classification. Each zone is represented by a different colour shade (see legend) which subsequently identifies with a sequence of letters representing various precipitation and temperature characteristics. See Table 2.1 for an explanation of each letter used in the classification sequence (from Peel et al., 2007).

1st letter	Zone	2nd Letter: Precipitation	3rd Letter: Temperature
A	Tropical	**f** : rainforest **m**: monsoon **w**: savannah	
B	Arid	**W**: desert **S**: steppe	**h**: hot **k**: cold
C	Temperate	**s**: dry summer **w**: dry winter **f**: without dry season	**a**: hot summer **b**: warm summer **c**: cold summer
D	Cold	**s**: dry summer **w**: dry winter **f**: without dry season	**a**: hot summer **b**: warm summer **c**: cold summer **d**: very cold winter
E	Polar	**T**: tundra **F**: frost	

Table 2.1. Köppen's classification index, using a sequence of letters to denote the precipitation and temperature characteristics that govern each climatic zone. Each letter is representative of a particular climatic feature (see figure 2.1 for the location of each climatic zone) (from Peel et al., 2007).

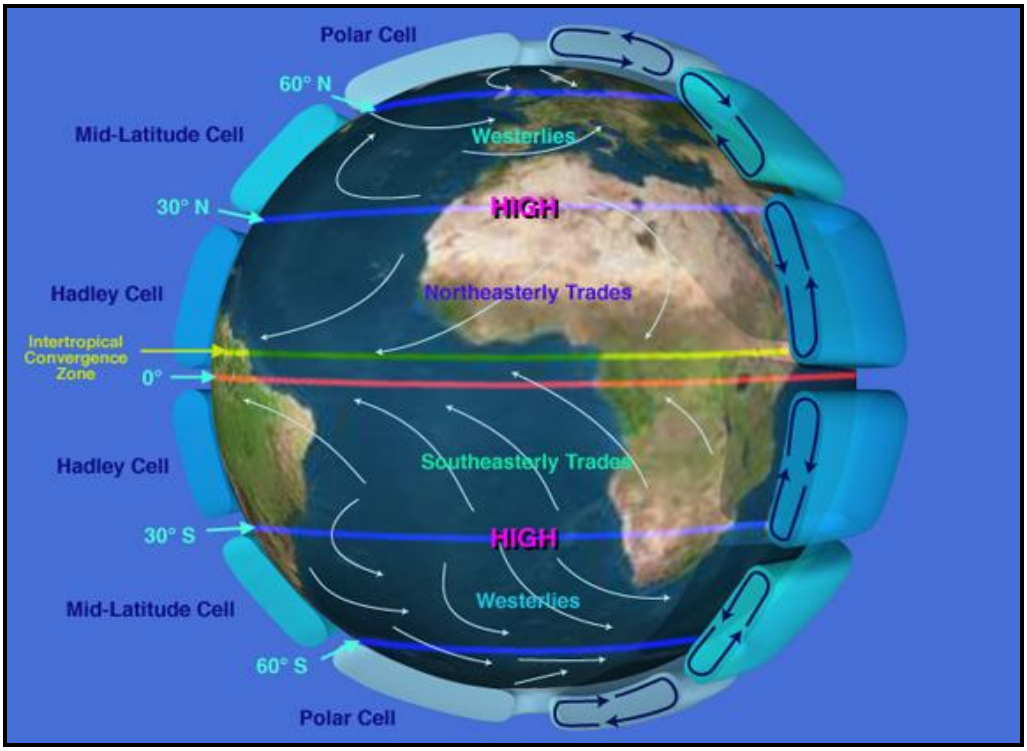

Figure 2.2. Schematic representation of global atmospheric circulation. The westerlies are the most significant prevailing winds influencing the Mediterranean Sea, particularly in the western basin (from NASA, 2009).

2.2.1 Local Prevailing Winds

Mistral winds are cold, northerly katabatic winds that travel into the Gulf of Lion from the south coast of France. Channelled between the Massif Central, the Alps and Pyrenees mountain ranges they are often associated with depressions or cyclonic events (Campins et al., 2006). Mistrals are at their strongest during the winter and spring months and in some cases, their affects can be seen to extend as far as the eastern basin (*figure* 2.4). High evaporation rates, due to the cold dry winds contribute to the formation of western Mediterranean Deep Water (WMDW) in the Gulf of Lion (Rohling et al., 2009). Westerly winds are channelled through the Spanish Sierra Nevada mountain range and the Strait of Gibraltar from the Atlantic Ocean (*figure* 2.3). They occur all year round, however during winter, cyclones that develop in the North Atlantic Ocean are steered towards the western Mediterranean Sea by the prevailing westerly winds inducing precipitation (Alpert et al., 2006). In contrast, Levante are warm, moisture rich easterly winds blowing from Corsica into the Alboran Sea and through the Strait of Gibraltar (*figure* 2.3). High levels of

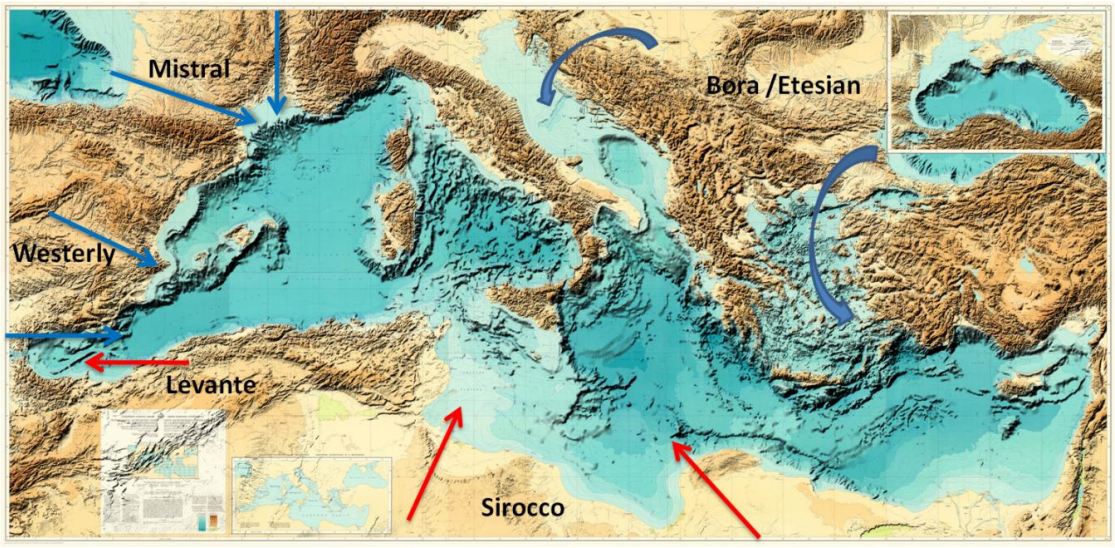

Figure 2.3. Map illustrating the direction and location of the prevailing winds across the Mediterranean region. Cold winds include the Westerly, Mistral, Bora and the Bora/Etesian indicated by the blue arrows while the warm winds (red arrows) include the Levante and Sirocco. Brown and cream shaded areas represent elevated topography. Modified from NOAA international bathymetric chart of the Mediterranean.

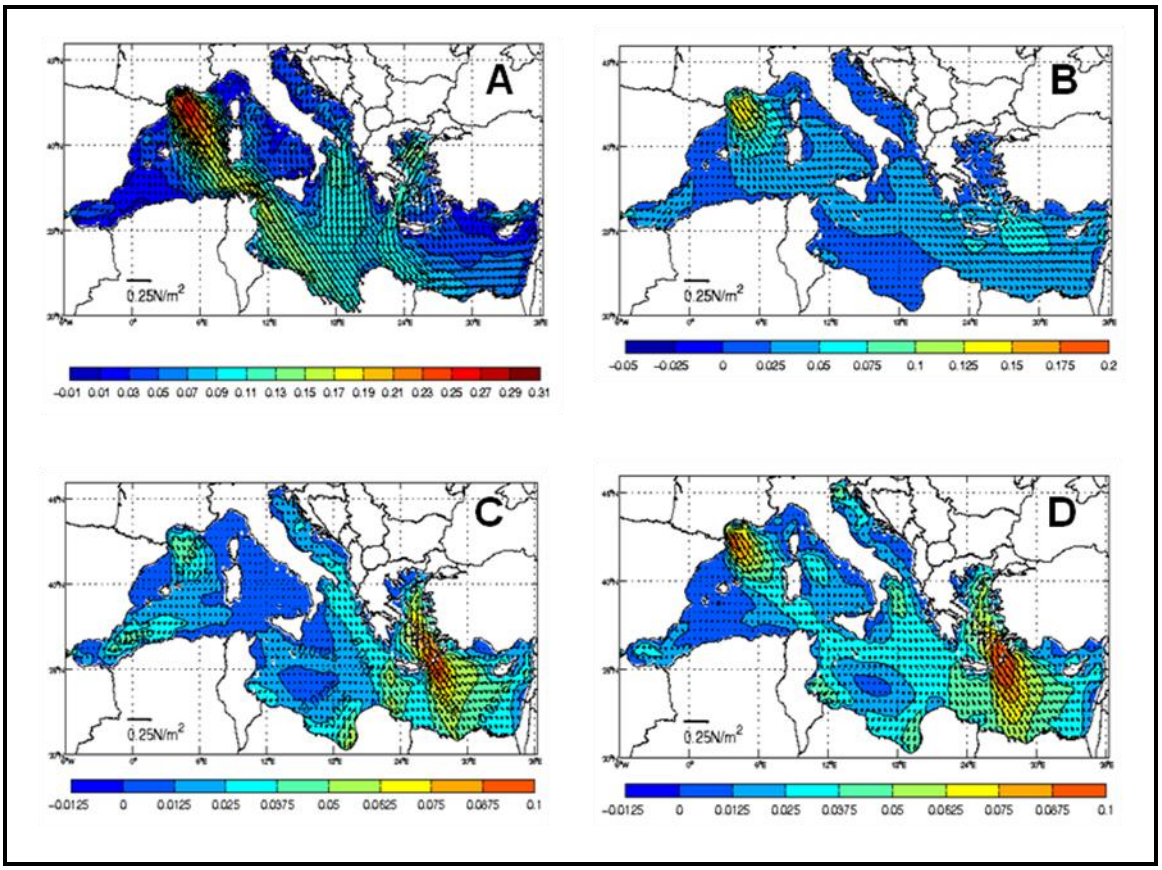

Figure 2.4. Seasonal wind stress patterns across the Mediterranean Sea during A) Winter, B) Spring, C) Summer and D) Autumn. The data refers to measurements obtained in 2005 (from MFSTEP, 2009).

moisture associated with the Levante can lead to the formation of fog (Naval Research Laboratory, 2010).

2.1.2 Cyclogenesis

The transitional location of the Mediterranean Sea affects the intensity and variability of cyclonic systems. The arid subtropical African deserts and the high precipitation levels in northern regions (the Dinaric Alps in the eastern basin have the greatest annual precipitation totals in Europe) provide the heat and moisture required for cyclogenesis (Lionello et al., 2006). The most intense area of cyclonic activity in the Mediterranean Sea is in the western basin, particularly the Gulf of Genoa and to a lesser extent the Algerian Sea, the Catalan-Balearic basin and the Gulf of Lion (Lionello et al., 2006). Data gathered from June 1995 to May 2003 highlights the variety in size and intensity of Mediterranean cyclones with season and geographical region (Campins et al., 2006) *(Table 2.2, figure 2.5)*. Often categorised according to their depth, cyclones can be shallow (weak) or deep (strong). In the Mediterranean Sea, summer marks the highest intensity of shallow cyclones whereas winter, influenced by the Mistral, has the highest percentage of deep cyclones. The overall percentage of cyclones in the western Mediterranean is higher in the summer, however those that occur during winter are associated with more severe weather conditions *(Table 2.2)* (Campins et al., 2006).

Cyclone type:	Summer	Autumn	Winter	Spring
Shallow	46	18	11	25
Middle depth	30	23	19	29
Deep	18	25	28	30
Total Western Mediterranean	33	21.	18	27

Table 2.2. Frequency (%) of seasonal shallow, middle and deep cyclone events, and the overall frequency, in the western Mediterranean basin (from Campins et al., 2006).

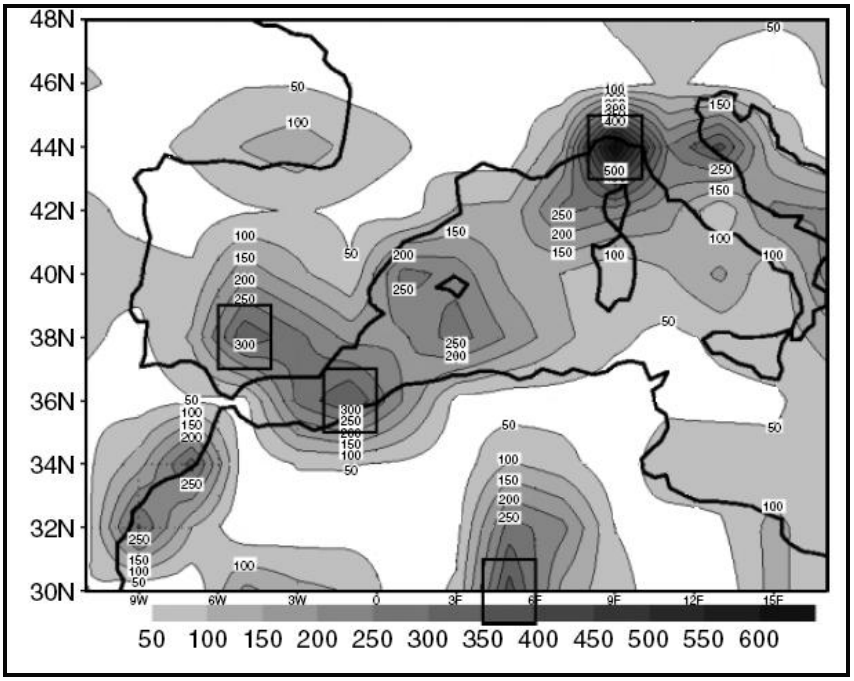

Figure 2.5. Map illustrating the total number of cyclone centres (darkest shaded areas represent highest number of cyclone centres) in the Mediterranean Sea, (from Campins et al., 2006).

2.1.3 North Atlantic Oscillation (NAO)

The climate of the Mediterranean Sea is influenced by a phenomenon known as the North Atlantic Oscillation (NAO). Associated with the Icelandic Low polar cyclone and the Azores High subtropical anticyclone, differences in atmospheric pressure result in a large scale circulation pattern which defines the NAO (Hurrell, 1995). Large variations in atmospheric pressure are represented as a positive or high NAO index while reduced pressure differences are represented as a negative or low NAO index *(figure 2.6)*.

The variability of the NAO has direct implications on North Atlantic weather systems, such as the westerly winds, which influence the weather systems in the western Mediterranean Sea (Hurrell, 1995). A positive NAO index (large pressure gradient) increases the strength of the westerlies resulting in cool, dry summers and mild wet winters in central Europe and the Mediterranean Sea (*figure 2.6*). In contrast, a negative NAO index causes a weakening of the westerlies allowing Atlantic Ocean storm tracks to flow in a more southerly direction towards the Mediterranean Sea resulting in increased storm activity and rainfall over southern Europe and North Africa (*figure 2.6*).

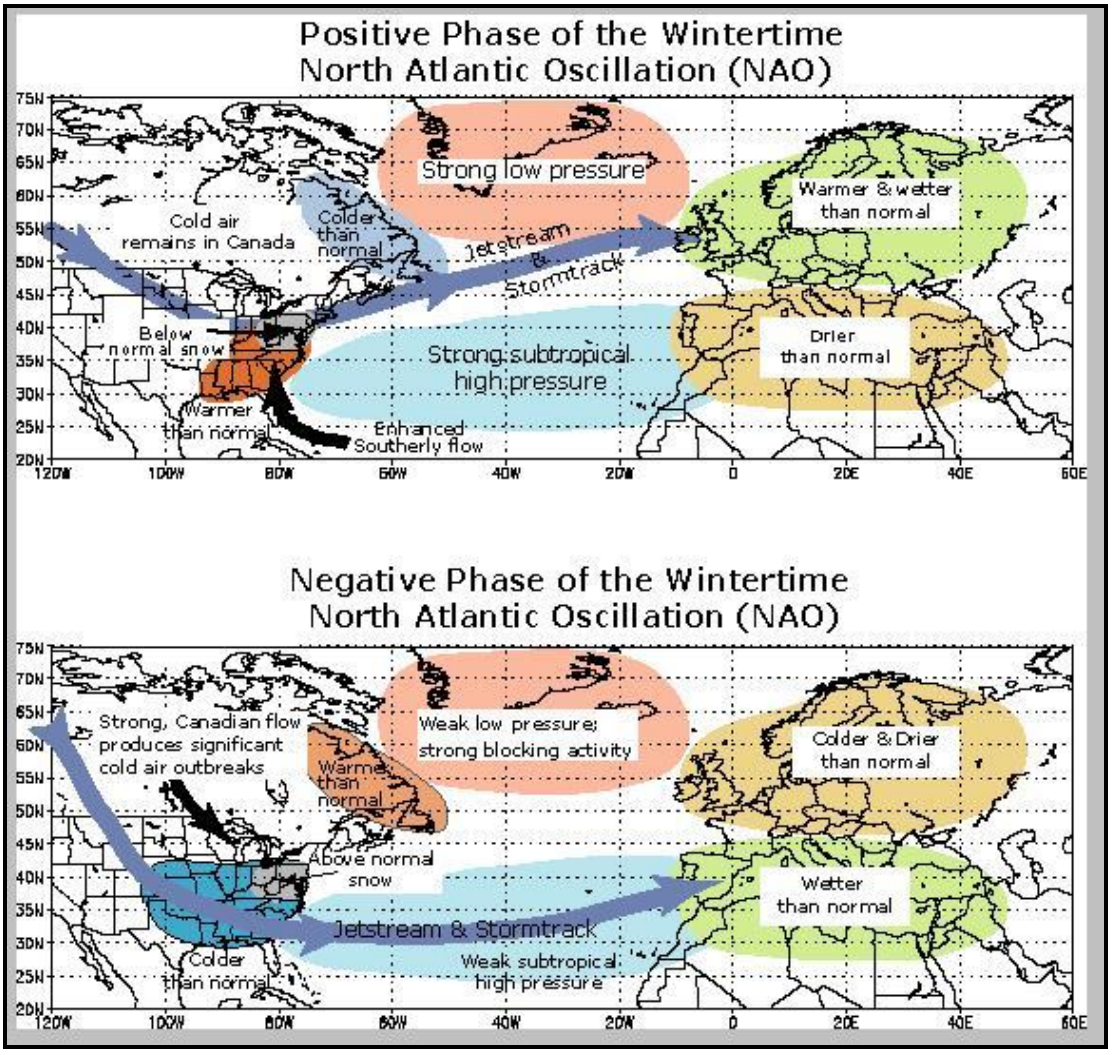

Figure 2.6. Map illustrating atmospheric pressure systems and associated circulation patterns for both the positive and negative phases of the North Atlantic Oscillation (from National climatic data centre, 2009).

2.1.4 The El Niño Southern Oscillation (ENSO)

While it is quite clear that the Mediterranean climate is influenced by the NAO, evidence suggests that a correlation also exists with the El Niño Southern Oscillation (ENSO), albeit to a lesser extent (Rodó et al., 1997). Occurring approximately every 3-7 years ENSO is a natural event related to the warming of the eastern Pacific Ocean for a period of 6-12 months (Allan, 2000). Under normal conditions, due to the strength of the trade winds, the western Pacific Ocean experiences warm SSTs and subsequent abundant rainfall. In contrast, upwelling occurs in the eastern Pacific producing lower SSTs (*figure 2.7A*). However, during El Niño years, the trade winds weaken allowing warm SSTs and a low

pressure system to migrate to the eastern Pacific Ocean (*figure 2.7B*). These abnormally warm waters stimulate cloudiness and increased precipitation for the region, while countries such as Australia experience a reduction in rainfall (Washington, 2005).

Observed precipitation levels across Europe and the Mediterranean Sea correlate with ENSO events, where the western Mediterranean region records an approximate 10% increase in seasonal rainfall during El Niño, and a subsequent decrease in precipitation following El Niño events (Rodó et al., 1997). The importance of ENSO for the Mediterranean climate may be significant, however, it is difficult to isolate the effects in the North Atlantic/European Sector from the dominating mid-latitude dynamics (Rodó, 2001; Alpert et al., 2006).

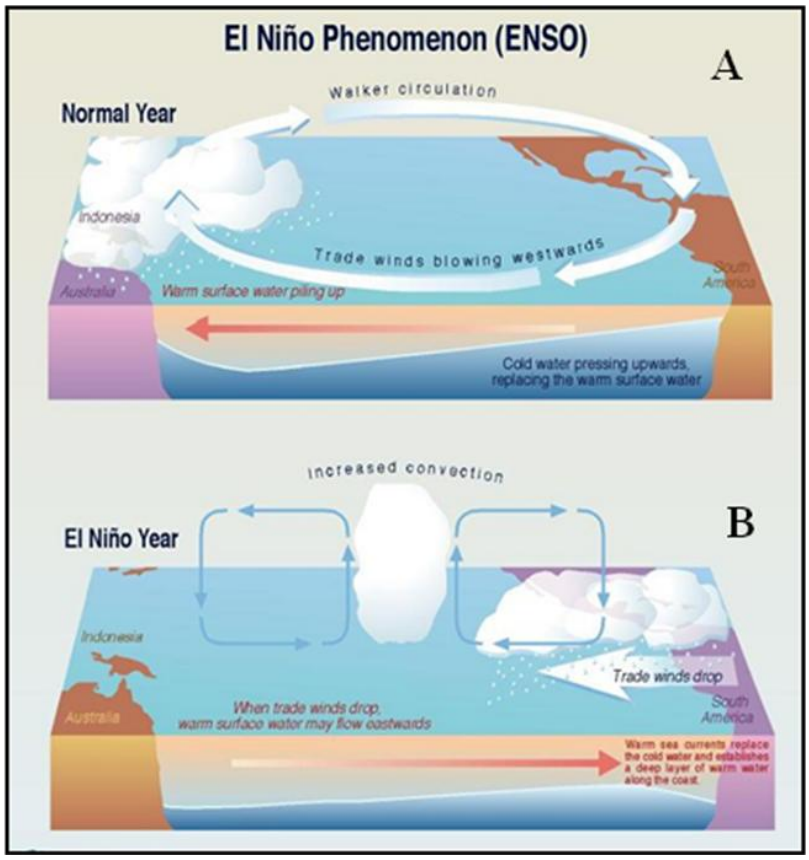

Figure 2.7. Schematic representation of the atmospheric and hydrological processes in the western and eastern Pacific Ocean during a normal (non El Niño year) and those that occur during an El Niño year (Climate Prediction Centre, 2009).

2.2 Mediterranean Sea Physical Oceanography

Connected to the North Atlantic Ocean via the Strait of Gibraltar, the Mediterranean Sea is considered a concentrated basin (Reddy, 2001). An excess of evaporation over precipitation results in high salinity levels that increase in an easterly direction. These high salinities and subsequent buoyancy loss encourage a two level exchange of water through the Strait of Gibraltar, consisting of a saline subsurface outflow and a comparatively fresh surface inflow of Atlantic water (AW). The high level of evaporation however, creates an imbalance in the amount of water exchange through the strait of Gibraltar, where a relatively small excess of inflow occurs over the outflow (La Violette, 1994; Reddy, 2001). A complex sill structure at the Strait of Sicily further divides the Mediterranean Sea into the western and eastern basins.

The maximum depth of the western basin is ~3400m, with the major deep basins being the Balearic, the Algero-Provençal and the Tyrrhenian Sea. The eastern basin is slightly deeper reaching ~4200m at its maximum depth and comprises the Adriatic, Aegean, Ionian and Levantine basins (*figure* 1.1) (Reddy, 2001). The oceanic circulation in the Mediterranean Sea is controlled by the complex relationship between temperature, salinity, density, wind stress, surface buoyancy flux and the exchange of water through the various straits (Robinson et al., 2001; Macdonald et al., 2004).

2.2.1. Temperature and Salinity

Figures 2.8 and *2.9* illustrate the mean monthly temperature and salinity gradients recorded in winter (January), spring (March) summer (June) and late summer/autumn (September) during 2005. Basinwide trends are apparent, highlighting an increase in both temperature and salinity in an easterly direction. Correlating with the influx of relatively fresh Atlantic Water (AW), the lowest salinities are recorded in the Alboran Sea and can be traced along the Algerian coastline (*figure 2.8).*

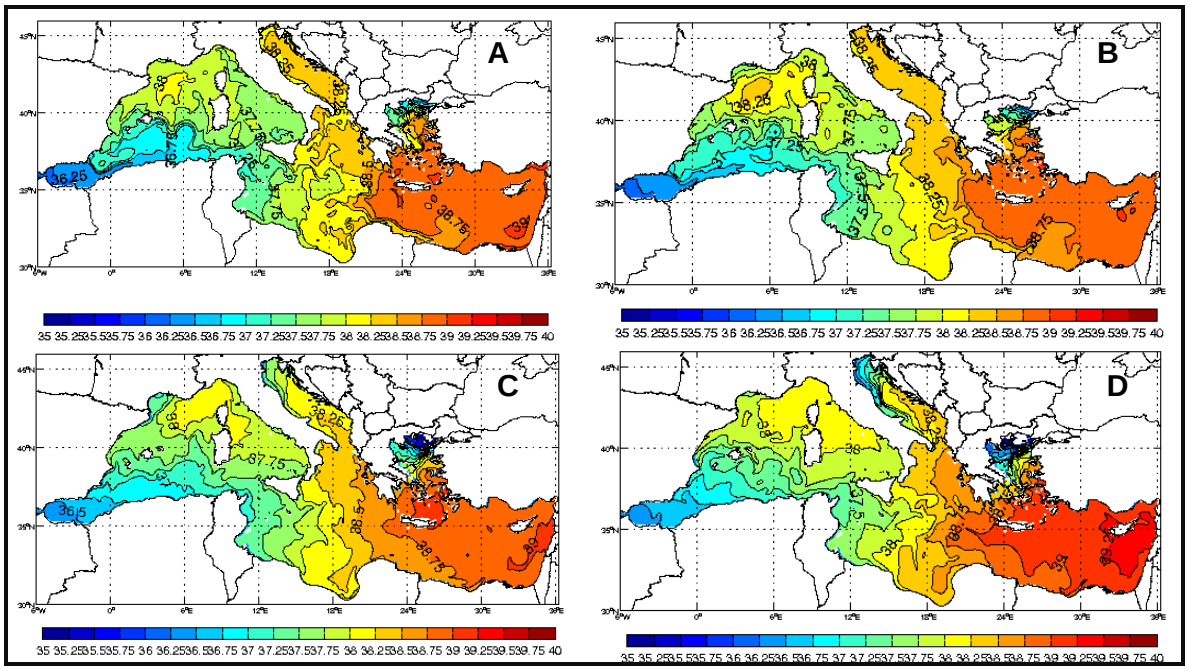

Figure 2.8. Seasonal mean surface salinity ‰ during 2005 for A) Winter B) Spring C) Summer and D) Autumn (data from MFSTEP Mediterranean Forecasting System, 2009).

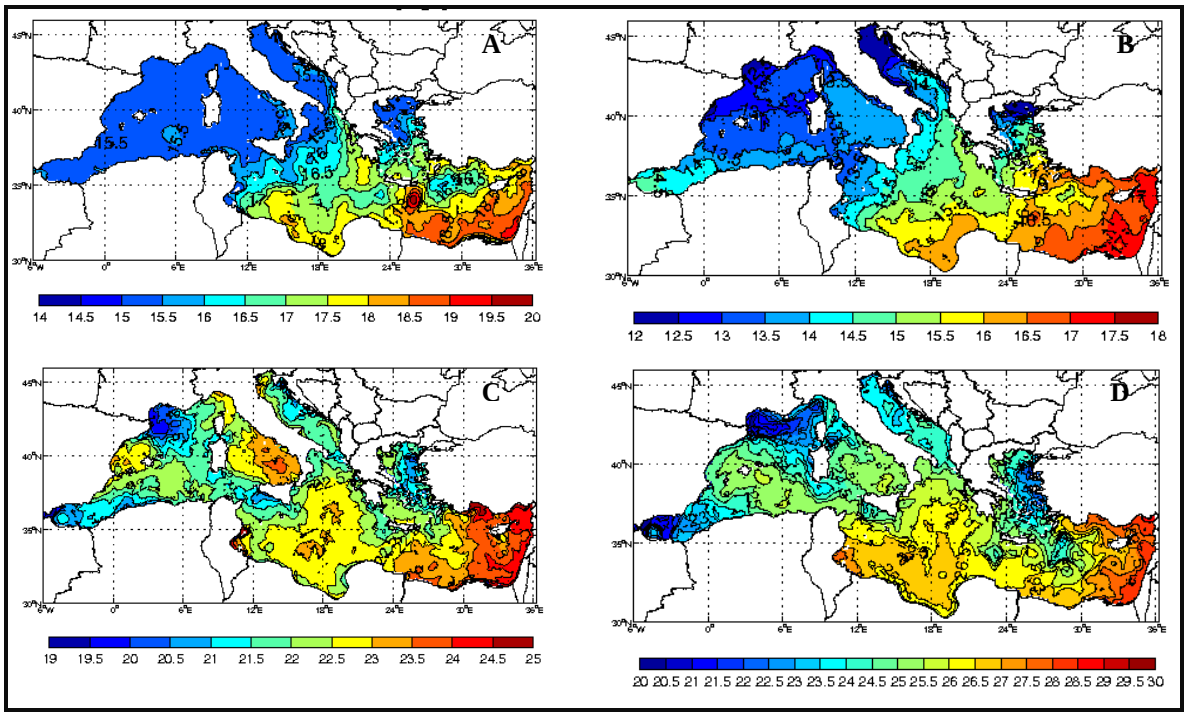

Figure 2.9. Seasonal Mean SST (°C) during 2005 for A) Winter, B) Spring, C) Sumer and D) Autumn (data from MFSTEP Mediterranean Forcasting System, 2009).

In contrast, the highest salinities are recorded in the most easterly parts of the Mediterranean Sea, reaching values of 39.2‰ (parts per mille) during September (*figure 2.8D)*. The Gulf of Lion recorded the lowest temperatures (12.5°C during March), correlating with the cooling effect of the mistrals and the site of deep water formation, in contrast to the highest recorded temperatures in the eastern basin at 28.5°C during September (*figure 2.9D)*.

2.2.2 Western Mediterranean Water Masses

Characterised by a thermohaline circulation system, *figure 2.10* illustrates the different water masses throughout the Mediterranean Sea. The dominant water masses within the western basin consist of an eastward surface layer of Modified Atlantic Water (MAW), a westward subsurface layer of Levantine intermediate water (LIW) and the western Mediterranean deep water (WMDW) mass. La Violette (2004) observed a further water mass beneath the WMDW displaying different temperature and salinity properties. Referred to as bottom water (BW), this water mass occurs at depths greater than 3000m.

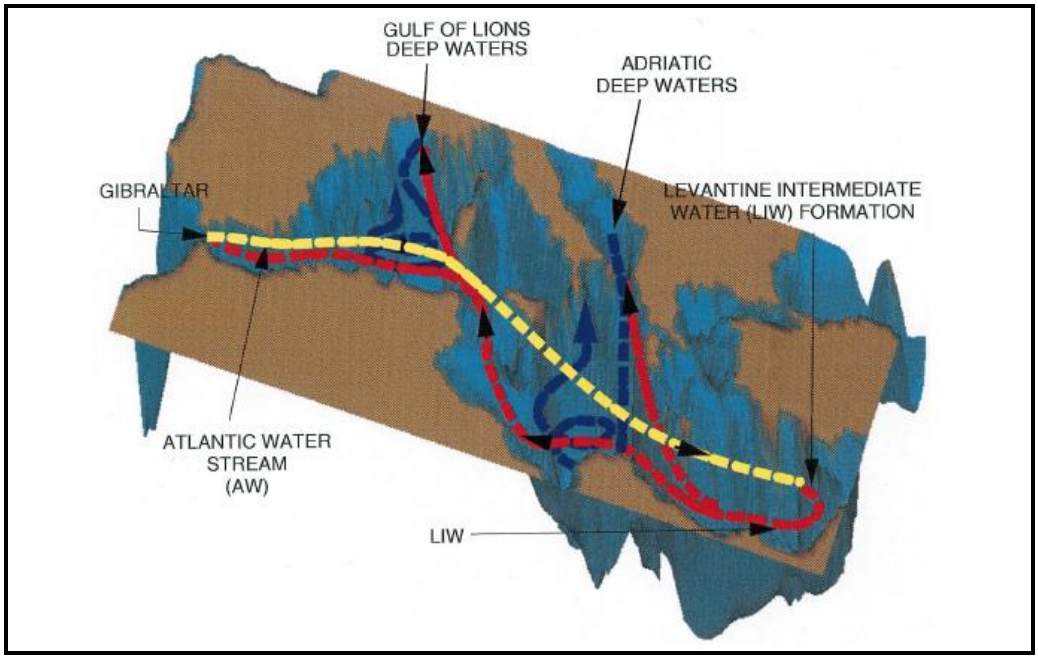

Figure 2.10. Schematic illustration of the thermohaline circulation in the Mediterranean Sea. The major circulation systems are indicated by different coloured lines. The red line represents the LIW, the blue represents the deep water masses from both the eastern and western basins and the yellow line represents the surface MAW (from Pinardi and Masetti, 2000).

2.2.2.1 Modified Atlantic Water (MAW)

Inflowing Atlantic water (AW) has a salinity range of 36.5-37.5‰ with a temperature of approximately 16°C (Robinson et al., 1999; Smith et al., 2008). MAW, as indicated by its name, is Atlantic water that has been modified in the western Mediterranean Sea due to evaporation and mixing with LIW (Robinson et al., 1999). The newly formed MAW exists as a relatively low density water mass in the upper 200m of the water column and can be traced throughout the Mediterranean Sea due to its low salinity (La Violette, 2004). In the Alboran Sea, AW is directed north-eastwards through the Strait of Gibraltar where immediate mixing occurs. The resultant MAW forms two anticyclonic gyres, induced by a strong jet with speeds up to several kilometres an hour, before migrating eastward along the Spanish coast as part of the Algerian Current (Pinardi et al., 2004). Along the Algerian coast, MAW forms cyclonic coastal eddies and anticyclones (*figure 2.11).* The coastal eddies are relatively short lived, while the anticyclones can last for weeks or months (Robinson et al., 1999). At the Strait of Sicily, the Algerian Current bifurcates with part of the current continuing eastward into the Ionian and Levantine basins identified in the upper 150-200m of the water column by its low salinity (<37.5‰) (Pinardi et al., 2004). The remainder of the Algerian Current travels into the Tyrrhenian Sea where the southern and northern Tyrrhenian gyres are formed (*figure 2.11).*

2.2.2.2 Levantine Intermediate Water (LIW)

Formed by enhanced winter cooling in the Levantine basin, LIW is characterised by peak salinities (up to 38.7‰) in the Mediterranean Sea and is identified by this salinity maximum in water column vertical profiles (La Violette, 2004; Smith et al., 2008). From its source, LIW migrates westward through the Strait of Sicily in a generally cyclonic fashion beneath the MAW layer between a depth of 200 and 800m (La Violette, 2004). LIW comprises much of the subsurface outflow from the Mediterranean Sea through the Strait of Gibraltar, however, with westward migration temperature and salinity changes occur due to mixing. During the winter in the Gulf of Lion, MAW and LIW combine to create the largest water mass by volume in the western Mediterranean, WMDW (La Violette, 1994).

1a Liguro-Provencal-Catalan current (LPC)
1b Gulf of Lyon Gyre
1c Western Corsica Current
2 Northward Tyrrhenian current and gyres:
2a Northward current and Southern Tyrrhenian Gyre
2b Northern Tyrrhenian Gyre
2c Eastern Corsica Current
3 Gibraltar-Atlantic current system
3a Alboran basin Gyres and meanders
3b Algerian current gyres, eddies and meanders
3c Tyrrhenian bifurcation/current
3d Atlantic-Ionian Stream
3e African MAW (Modified Atlantic Water) Current
3f Mid-Mediterranean Jet
3g Southern Levantine current
4 Rhodes Gyre
5 Western Cretan cyclone
6 Western Ionian cyclonic Gyre
7 Syrte Gyre
8 Anticyclonic system of the South-eastern Levantine basin
8a Mersa-Matruh Gyre system
8b Shikmona Gyre system
9 Asia Minor current
10 Iera-Petra Gyre
11 Pelops Gyre
12 Southern Adriatic cyclonic Gyre
13 Western Adriatic Coastal Current
14 Western Ionian anticyclonic Gyre

Figure 2.11. Schematic representation of surface water circulation in the Mediterranean Sea. The red line prefixed with the number 3 highlights the main flow of MAW as described in text. Other mesoscale circulation patterns are denoted by numbers referenced in the key (from Pinardi et al., 2004).

2.2.2.3 Western Mediterranean Deep Water (WMDW)

Formed in the Gulf of Lion, the site of WMDW is characterised by the 'Lion cyclonic gyre' (*figure 2.11)*. According to Theocharis and Lascaratos (2006), the mechanism responsible for the formation of WMDW is open-ocean convection in the Gulf of Lion. The increased intensity of the cold, dry mistral winds during the winter (January/February) *(figure 2.4)* enhances evaporation increasing the density of the surface water, leading to instability within the water column. The resultant mixing and convection causes surface waters to sink combining with LIW, to form WMDW (MEDOC group, 1970; Rohling et al., 2009). Three phases have been identified during the process of WMDW formation: the preconditioning phase, the violent mixing phase and the sinking and spreading phase (*figures 2.12 and 2.13)* (MEDOC group, 1970, Rohling et al., 2009).

2.2.2.3.1 The Preconditioning Phase

The onset of winter cooling from the local mistral winds reduces surface water temperatures (10-12°C) while increasing the water density by 29.1 gm^{-3} and salinity to 38.4‰ creating an instability within the water column (MEDOC group, 1970). The resultant intensification of the cyclonic circulation causes a shallowing of the pycnocline from a typical depth of 200-250m, to less than 100m (Rohling et al, 2009). This induces mixing within the surface waters. At this point stratification of the water column remains intact, with a relatively cold, fresh surface water layer, an intermediate layer of higher temperatures and salinities and a cold saline deep layer (*figure 2.12*) (Leaman, 1994, Rohling et al., 2009).

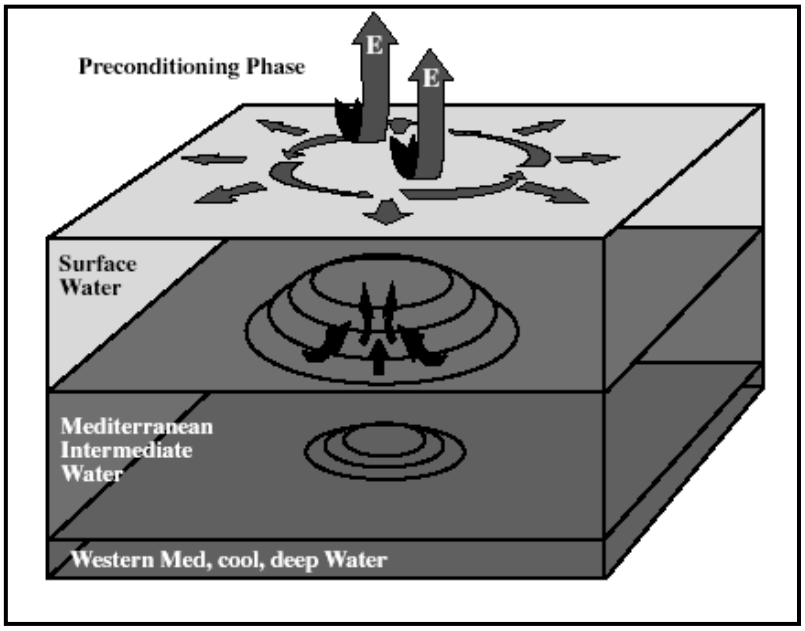

Figure 2.12. Schematic representation of the preconditioning phase of WMDW. Enhanced evaporation (E), increased salinities and reduced sea surface temperatures induces the shoaling of the pycnocline. It should be noted that during this stage the water column stratification remains intact (see text) (from Rohling et al., 2009).

2.2.2.3.2 The Violent Mixing Phase

The onset of violent mixing phase is characterised by a large surface buoyancy loss resulting from continued cooling and evaporation. The subsequent decrease in density results in the breakdown of stratification between the surface and intermediate waters. This

instability within the water column results in a deep (> 2000m) "chimney" (width 30-40km) of convective mixing that develops within the centre of the gyre (*figure 2.13*) (Leaman, 1994; Theocharis and Lascaratos, 2006, Rohling et al., 2009). Deep vertical mixing allows for the exchange of properties such as heat, salt, oxygen and nutrients between the euphotic zone and the abyssal depths (Theocharis and Lascaratos, 2006).

2.3.3.3.3 The Sinking and Spreading Phase

After the violent mixing phase the water sinks rapidly to form WMDW. From its location in the Gulf of Lion WMDW spreads east and southwards towards the Balearic basin, the Tyrrhenian Sea and the Alboran Sea. The resultant water mass (WMDW) lies between 800 and 3000m and is characterised by low temperatures (~13°C) and high salinities (~38.4‰) (La Violette, 1994) *(Table 2.3)*. The WMDW migrates throughout the western Mediterranean, where it eventually flows westward to remix in the Alboran Sea with the upper waters and exit the Mediterranean via the Strait of Gibraltar. The WMDW contributes to approximately 25% of the Mediterranean outflow through the Strait of Gibraltar (Rohling et al, 2009). Table 2.3 provides an overview of the characteristic main water masses affecting the western basin.

Depth (M)	Water Mass
Surface **200-400-**	**Modified Atlantic Water (MAW)** **Source:** Strait of Gibraltar **Temperature:** 15-16°C at Gibraltar up to 20-28°C **Salinity:** 36.5-37.5‰
200-400 **700/800**	**Levantine Intermediate Water (LIW)** **Source:** winter formation in Levantine Basin (eastern Mediterranean basin) **Temperature:** 15.5°C **Salinity:** 38.45-38.7‰
<800 **3000**	**Western Mediterranean Deep Water (WMDW)** **Source:** Winter formation in the Gulf of Lion (western Mediterranean basin) **Temperature:** 12.6-12.90°C **Salinity:** 38.40 – 38.6‰

Table 2.3. The water masses in the western Mediterranean and their associated characteristics (Reddy, 2001; La Violette, 2004; Millot and Taupier Letage, 2005).

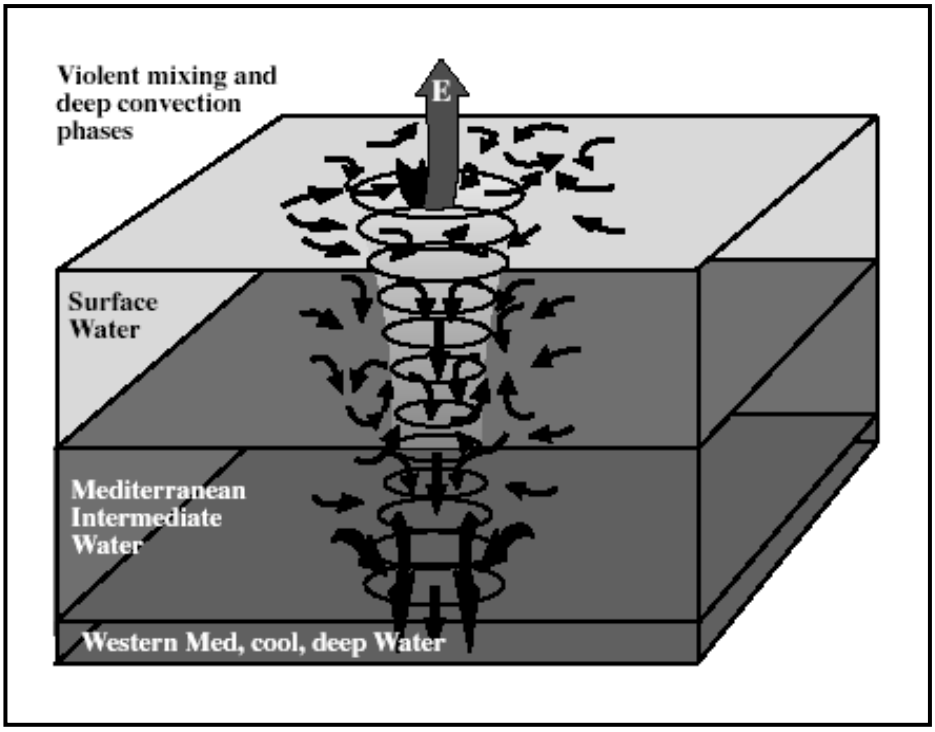

Figure 2.13. Schematic representation of the violent mixing and deep convection phases in the western Mediterranean Sea, where E= evaporation (from Rohling et al., 2009).

Chapter 3: Holocene Climatic Variability in the Western Mediterranean Sea

3.1 Introduction

The aim of this chapter is to highlight the main climatic events and trends that have affected the western Mediterranean region during the Holocene epoch. Northern Hemisphere Holocene climatic variations, in particular those that occurred in the North Atlantic Ocean, will be addressed highlighting the impact of North Atlantic teleconnections on the western Mediterranean Sea.

The Holocene, the most recent epoch of geological time, represents the current interglacial period from ~11,600 years ago, up to and including the present day (O'Brien et al., 1995; Davis et al., 2003). Despite its relatively stable climate, the Holocene epoch exhibits numerous short term climatic variations, the forcing mechanisms of which can include latitudinal position, local atmospheric changes, glacial variations and tectonic activity (Bond et al., 1997; Davis et al., 2003; Mayewski et al., 2004: Rasmussen et al., 2007; Fleitmann et al., 2008). Oscillations in the production rates of the North Atlantic Deep Water (NADW) and poleward heat transport could also have triggered or amplified these rapid climatic events (Bond et al., 1997; Cacho et al., 1999). However, changes in insolation as a result of orbital and solar variations is considered the primary forcing mechanism during the early Holocene (Mayewski et al., 2004; Frigola et al., 2007), while internal oceanic forcing is considered to play a more dominant role during the mid to late Holocene (Debret et al., 2007, 2009).

3.2 Holocene SST Trends

Global Holocene insolation changes reflect changes in SST and as insolation varies spatially this can result in opposing SST trends. Lorenz (2006) suggested that opposing Mid-Late Holocene trends of cooling in the extratropics and warming in the tropics was the result of changes in the seasonal insolation cycle as a result of orbital forcing. A multi proxy approach utilising alkenone and foraminiferal Mg/Ca derived SSTs identified a general Holocene warming trend in the western Mediterranean Sea (Leduc et al., 2010). SST variations between the two methodologies were attributed to a strong contrast in the ecological response of coccolithophors and planktonic foraminifera to winter and summer oceanographic conditions, indicating the significant seasonal impact on palaeotemperature reconstructions *(figure 3.1).*

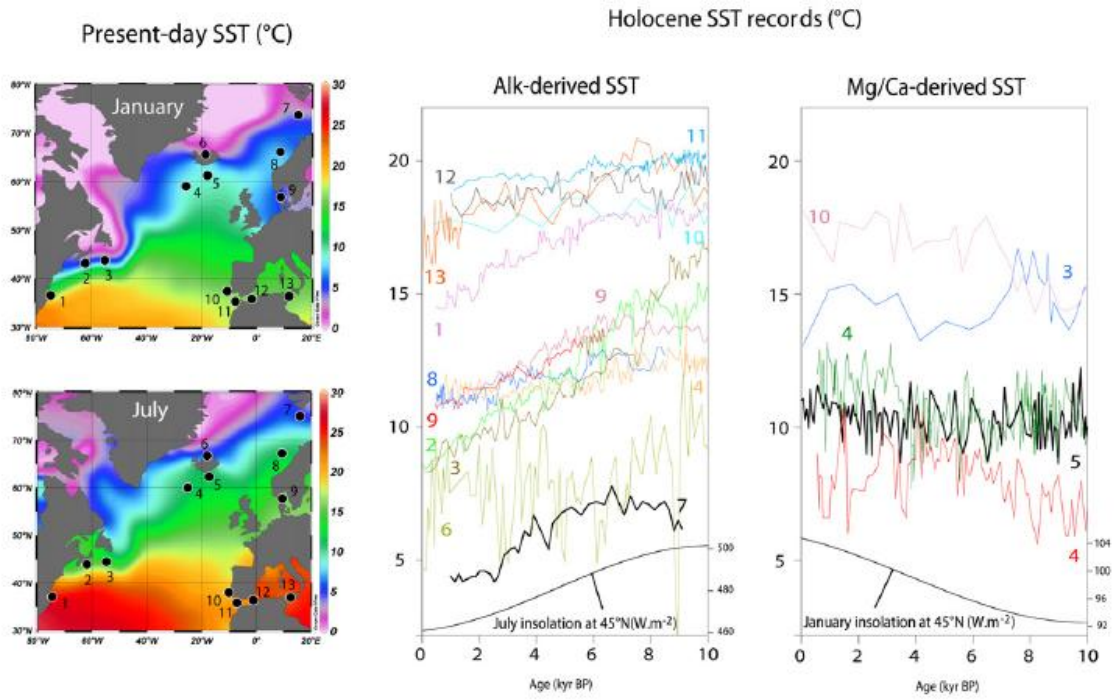

Figure 3.1. Holocene SST evolutions in the North Atlantic as determined from alkenone and MG/Ca derived SSTs. Present day SST are presented for winter and summer seasons with insolation changes indicated for 45°N. (References for SST records are listed in Table 2 Leduc et al., 2010) (from Leduc et al., 2010).

3.2.1 Holocene Thermal Optimum

The Holocene thermal optimum (HTO) signified a warm period in the early to mid Holocene occurring between ~9.0–6.0 ka in the Northern Hemisphere (Kerwin et al., 1999; Kaufman et al., 2004). Temperature increases between 1.67±0.8°C up to 4°C have been recorded during this HTO, however, these temperature increases refer primarily to summer temperatures with winter recording temperatures cooler than the present day (Kerwin et al., 1999; Kaufman et al., 2004) (*figure. 3.2*). In addition the HTO temperatures were not uniform, with maximum warming varying with latitude. Alaska and northwest Canada record a HTO between ~ 11 and 9 ka, a difference of ~4 kyr for the same event in the northeast of Canada thereby highlighting the lack of synchronicity of this event on a geographical scale (Kaufman et al., 2004) *(figure 3.2)*..

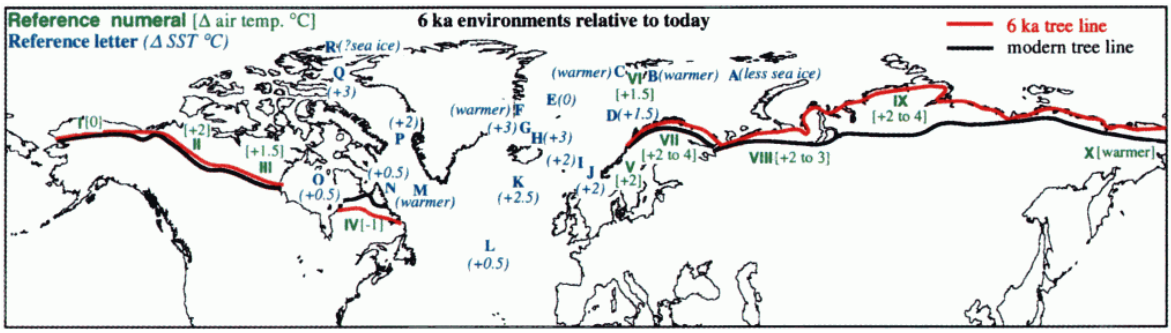

Figure 3.2. Mid Holocene Northern Hemisphere temperature changes relative to the present day. SST changes are represented in blue, and air temperatures represented in green (from Kerwin et al., 1999).

European proxies indicate that the traditional HTO was observed over northern Europe and principally during the summer. This was then balanced by a mid-Holocene cooling over southern Europe (Davis et al., 2003). Central Europe experienced a HTO at ~6.0 cal kyr BP, however it was more defined in the west than the east with southern climate patterns varying considerably from the north (Davis et al., 2003).

The HTO in the western Mediterranean Sea has been correlated with the North Atlantic Ocean (Sbaffi et al., 2001; Cacho et al., 2001; Jimenez-Espejo et al., 2007). However, the response of these climatic changes is not always synchronous within the western basin. For example, the SST maximum that defines the HTO occurs between 11.5–10.2 kyr BP in the Gulf of Cadiz. In the Alboran Sea the same event is recorded between 10–9.0 kyr, whereas in the Tyrrhenian Sea the event is recorded between 8.9-8.4 kyr BP. Buccheri (2002) identified a longer lasting warming phase in the Tyrrhenian Sea corresponding to the HTO between 9.5-6 cal kyr BP. Cacho et al. (2001, 2002) observed a general cooling trend once the HTO was reached.

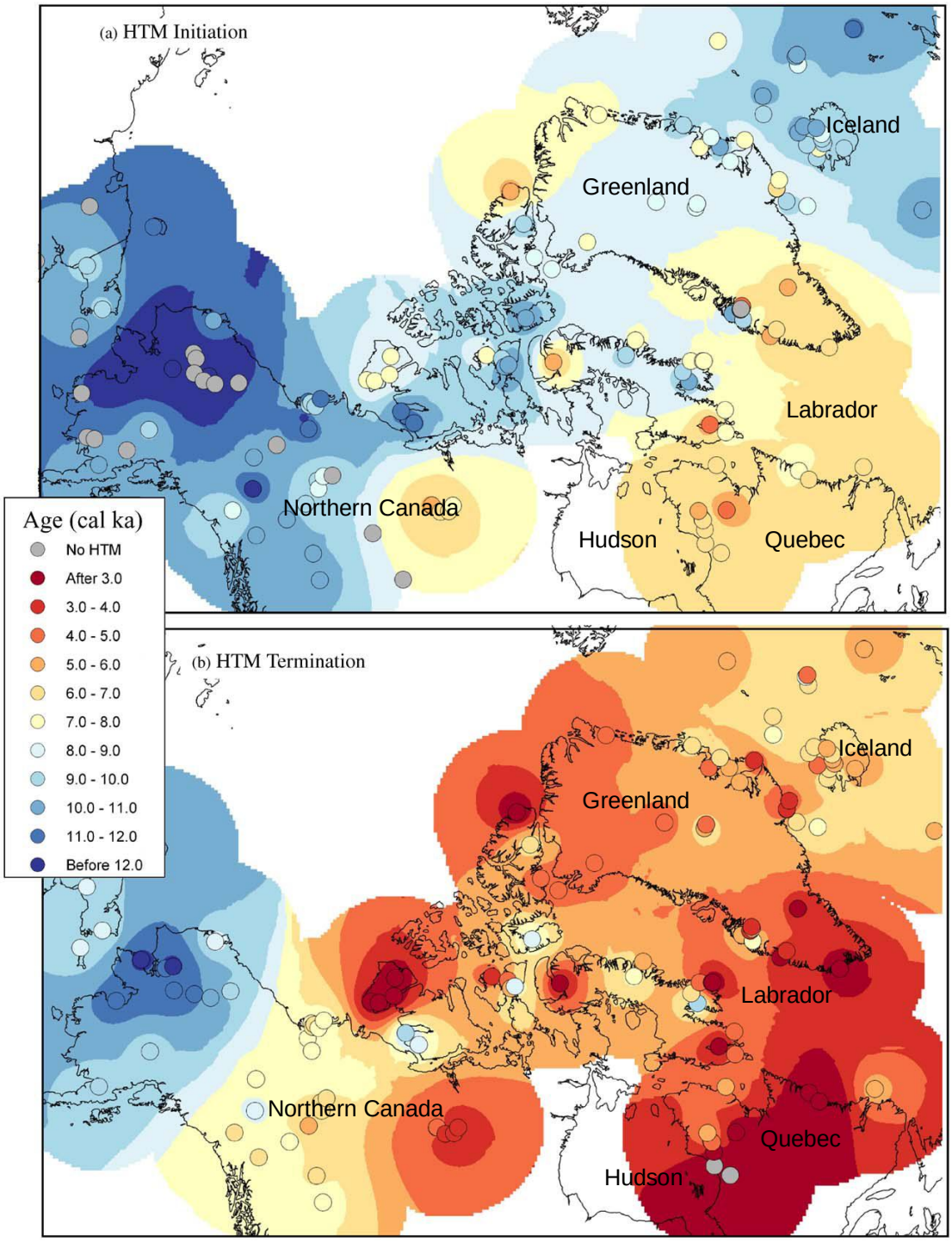

Figure 3.3. Pattern of (a) initiation and (b) termination of the Holocene thermal optimum in the western Arctic (from Kaufman et al., 2004).

3.3 The Mediterranean Sea and North Atlantic Ocean Teleconnections

The Mediterranean Sea has acted as a concentration basin for the North Atlantic Ocean during the last 20 kyr where climatic events are amplified by the confined nature of the sea (Rohling and De Rijk, 1999; Cacho et al., 2001). The connection between both regions can

be directly related to the entrance of cold North Atlantic surface waters into the western Mediterranean Sea through the Strait of Gibraltar (Cacho et al., 2001; 2002) (see chapter 2 section 2.1). Indeed, the presence of Dansgaard-Oeschger cycles and Heinrich events, in sediment cores from the western Mediterranean Sea, highlights the sensitivity of the region to short-term climatic variability in the North Atlantic Ocean (Cacho et al., 1999, 2001; Llave et al., 2006). In addition, climatic cooling in the North Atlantic can directly impact atmospheric forcing in the Mediterranean region intensifying the westerly winds (Mayewski et al., 2004). This atmospheric teleconnection was the main control over the western Mediterranean thermohaline circulation during the Holocene (Frigola et al., 2007).

During the Holocene the western Mediterranean Sea records declining SSTs whereas the eastern Mediterranean Sea and the Red Sea show an increase (Duplessy et al., 2005). This SST pattern has been interpreted as a continuous weakening of the NOA from the early to late Holocene (Duplessy et al., 2005). Increased solar radiation in response to the Earth's precessional cycle could be sufficient to weaken the NAO, thereby attributing to low latitude tropical warming during the winter. This illustrates the significant role of insolation forcing on the Northern Hemisphere and consequently the climatic variability in the Mediterranean Sea (Duplessy et al., 2005).

3.3.1 The 9.2 and 8.2 Cooling Events

Early Holocene Northern Hemisphere climatic events were influenced by the presence of large Northern Hemisphere ice sheets (Mayewski et al., 2004). The subsequent melting of these ice sheets associated with early Holocene warming interrupted the ocean circulation pattern which had direct consequences on the North Atlantic Ocean and Mediterranean Sea Research in the Northern Hemisphere (Greenland, Alaskan Subartic, Central Europe, Germany and China) identified a short term (200-150 years) cold and wet climatic anomaly at ~ 9.2 kyr BP, it has been suggested that this "9.2 cooling Event" (~1.6 ºC) was the result of a melt water pulse (MWP) through the Gulf of Laurence into the North Atlantic Ocean, within close proximity to the site of NADW formation (Fleitmann et al., 2008). It is inferred that the MWP weakened the thermohaline circulation inducing atmospheric cooling and subsequent formation of sea ice. The rapid duration of the 9.2 Event makes it difficult to be recognised in sedimentary sequences (Fleitmann et al., 2008) however, it is possible that this event correlates to the 9.4 cooling event identified in the Tyrrhenian Sea

(Cacho et al., 2001) as part of the Bond Cycles (Bond et al., 1997). A later cooling event known as the 8.2 Event is more widely recognised with European and North American proxies (Barber et al., 1999; Baldini et al., 2002; Veski et al., 2004; Fleitmann et al., 2008 among others). Cooling events at ~ 8.2 cal kyr BP have been recorded in the Alboran (Frigola et al., 2007) and Tyrrhenian Seas (Sbaffi et al., 2001) in addition the 8.2 Event also correlates with the interruption of S1 deposition in the eastern Mediterranean Sea (Casford et al., 2001: Jimenez-Espejo et al., 2007). The correlation of these events with those in the Mediterranean Sea highlights the teleconnection with the North Atlantic Ocean. Similar to the 9.2 Event, the 8.2 Event is associated with a MWP (Alley et al., 1997) thought to be the final MWP in a series of at least 14 similar events recorded during the early Holocene (Rohling and Pälike, 2005). The discharge of a MWP into the North Atlantic Ocean weakened the thermohaline circulation causing sudden and widespread cooling in the region (Alley at al., 1997; Barber et al., 1999; Mayewski et al., 2004; Alley and Ágústsdóttir., 2005; Rohling and Pälike, 2005; Fleitmann et al., 2008). The 8.2 Event was the largest of 3 cooling events occurring at 8.5, 8.2 and 8.06 cal kyr BP (Lal et al., 2007). The 8.2 Event correlates with a reduction of European and North American temperatures by 4-8 ˚C in central Greenland and by 1.5-3˚C at marine and terrestrial sites around the north eastern North Atlantic Ocean indicative of reduced heat transfer from the ocean to the atmosphere in the North Atlantic Ocean.

3.3.2 Dansgaard-Oeschger Cycles and Bond Events

Important evidence emerging from ice core records suggests that climate change within the Quaternary Period were often very rapid with significant warm interstadial and cool stadial episodes occurring just a few centuries apart. These records quite clearly illustrate that glacial periods were punctuated by several short warming episodes. First identified in the Greenland ice core record, Dansgaard et al (1993) identified 24 cycles of abrupt warming (interstadials) followed by a gradual cooling between 80 and 20 kyr BP *(figure 3.4)*. These interstadials, termed Dansgaard-Oeschger (D-O) cycles have a frequency of ~ 1479±532 years and appear to continue into the Holocene (Bond et al., 2001). Bond (1997) observed similar abrupt climatic shifts during the Holocene with similar periodicities to the D-O events (1470 ±500 yrs).

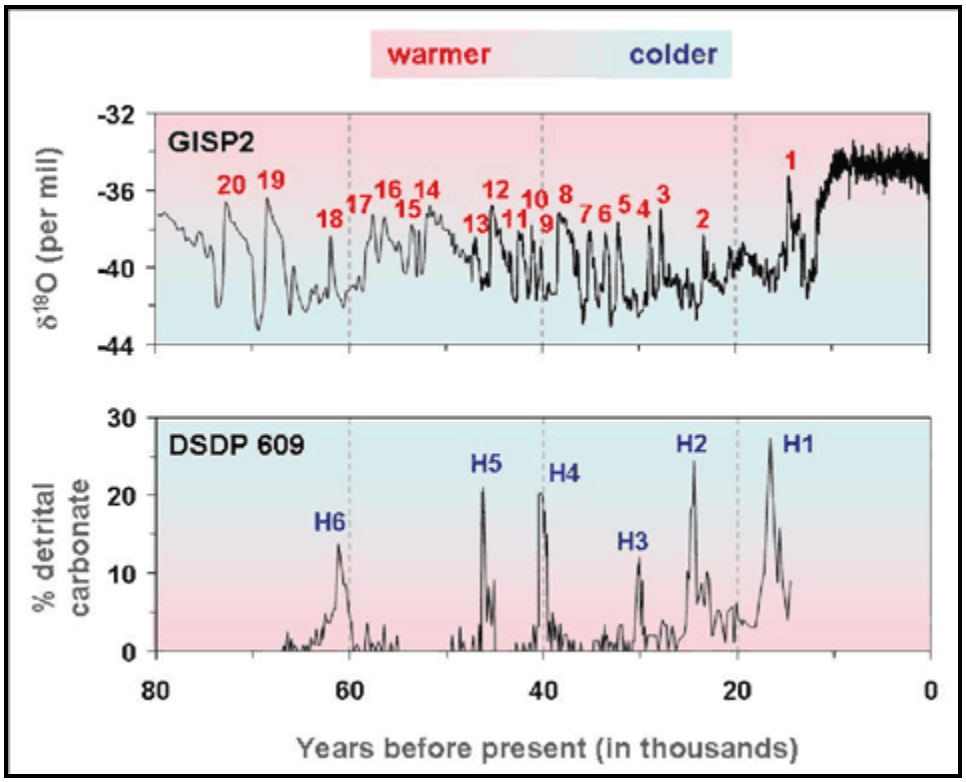

Figure 3.4. The top graph depicts the Dansgaard-Oeschger events as identified in the $\delta^{18}O$ record during the last glacial period from the Greenland ice core (GISP2) (Grootes et al., 1993). The lower graph depicts Heinrich events (HE) 1-6 as indicated by peaks in IRD from a core in the North Atlantic Ocean (Bond and Lotti, 1995) (from National climatic data centre, 2010).

These climatic shifts indicate that the climate events occurring during the Holocene are part of a continuous climatic cycle that operates independently of the glacial-interglacial climatic state. The D-O cycles combined with the cooling that follows are referred to as Bond Cycles. The culmination of this cooling is often associated with a Heinrich event (HE), intense short term cold periods characterised by the deposition of ice rafted debris (IRD) (Bond et al., 1997, 2001) *(figure 3.4)*. Based on planktonic foraminiferal, lithic and petrologic proxies Bond et al., (1997) recorded several cooling (Bond) events in the North Atlantic Ocean and Nordic sea during the Holocene *(figure 3.5)*. Associated with increased concentrations of lithic grains and an increase in the relative abundance of *N. pachyderma* (sinistral), these events occur at ~ 1400, 2800, 4200, 5900, 8100, 9400, 10,300 and 11,100 yrs *(figure 3.5)*.

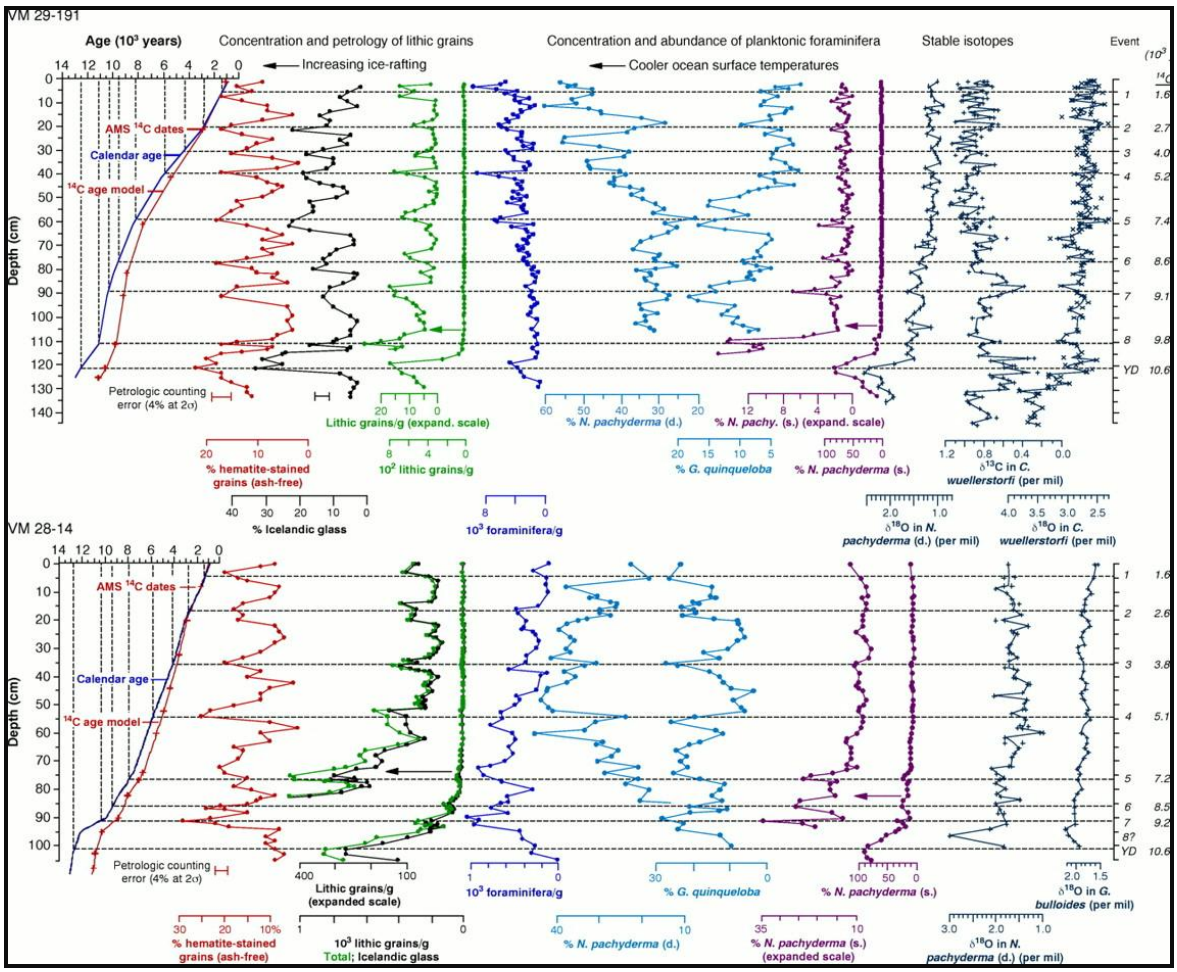

Figure 3.5. Graphs illustrating the range of evidence used to identify a series of abrupt cooling events (Bond Events) in the North Atlantic Ocean. Data is obtained from cores VW 29-191 (North Atlantic) and VW 28-14 (Nordic seas) (from Bond et al., 1997).

Research in the western Mediterranean Sea has identified cold events that show direct correlation with many of the Bond events in the North Atlantic Ocean *(figure 3.6)* (*Table 3.1*) (Bond et al., 1997; Jalut et al., 2000; Cacho et al., 2001; Sbaffi et al., 2001; Frigola at al., 2007). Frigola et al., (2007) identified 8 cooling events in the northwestern Mediterranean Sea which they associated with an intensification of the north westerly winds. Of these 8 events, 5 show almost direct comparison with those of the North Atlantic Ocean Bond events (*Table 3.1*). Similarly using pollen records Jalut et al. (2000) identified 6 major changes in vegetation cover which they attributed to phases of aridification. These phases occurred between 10.9-9.7, 8.4-7.6, 5.3-4, 4.3-3, 2.85-1.73 and 1.3-0.75 cal kyr B P and also correspond to most of the North Atlantic Ocean Bond events (Jalut et al., 2000) *(Table 3.1)*.

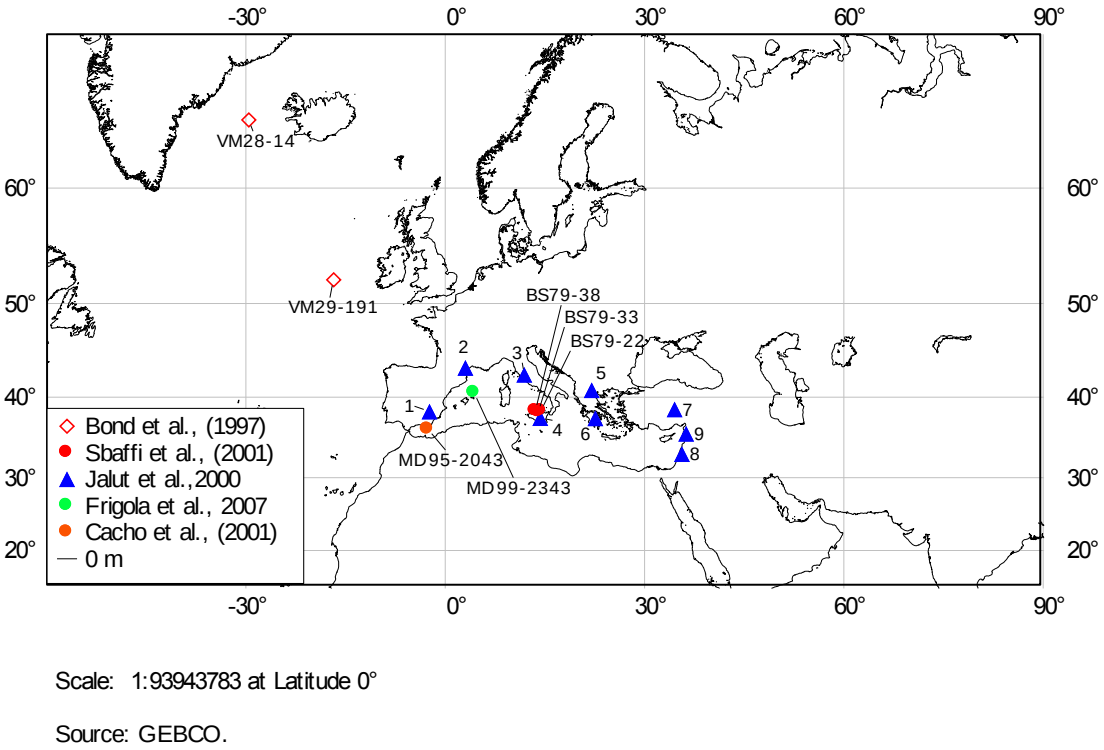

Figure 3.6. Map depicting core and site location where short term cooling events have been identified with similar periodicities to the Bond Events identified in the North Atlantic (see Table 3.1 for timing of these events). Jalut et al., (2000) locations are: 1=Villaverde, 2=Capestang, 3= Lagaccione 4=Lago di Pergusa, 5=Lake Leena, 6=Lake Edessa, 7=Eski Acigöl, 8=Lake Hula, 9=Valley of the Ghab.

North Atlantic Bond events cal kyr BP Bond et al., 1997	Aridification phases centred at cal kyr BP Jalut et al., 2000	Cooling phases centred at cal kyr BP Frigola at al., 2007	Cooling phases centred at cal kyr BP Cacho et al., 2001	Cooling phases centred at cal kyr BP Sbaffi et al., 2001
		0.5		
1.4	1.025	1.6	1.39	1.4
2.8	2.29	2.5	2.95	2.7
		3.2		
4.3	3.65	4.1		
		5		
5.9		6.2	5.93	5.4
		7.2		
8.2	8	8.2		8.2
9.5			9.45	
10.3	10.3		9.87	10.1
11.1			11.58	
12.5			12.51	

Table 3.1. North Atlantic Bond Events and western Mediterranean Sea climatic events associated with aridification and cooling.

The HTO was reached between 8.9 – 8.4 kyr BP in the Tyrrhenian Sea followed by a general cooling trend interrupted by rapid periods of cooling (Cacho et al., 2001; 2002, Sbaffi et al., 2001). The coldest of these cooling events (SST decrease of -4°C) occurred at

~5.4 cal kyr BP in comparison to the more widely recognised 8.2 cold event that recorded a temperature decrease of 1.5°C. These cooling events are likely associated with similar cooling events in the North Atlantic (Bond et al., 1997).

The Mediterranean Sea has recorded the climatic response since the last glacial termination; the early to mid Holocene was a significant time for climatic variations in the Western Mediterranean Sea. Post glacial post glacial sea level rise until ~5.0-6.0 kyr cal BP (Goy et al., 2003; Zazo et al., 2008; Lesine at al., 2009; Sabatier at al., 2010) attributed to the influx of meltwater into the Mediterranean from the North Atlantic Ocean, (Rohling et al., 1995; Perez Folgado et al., 2003; Jimenez Espejo et al., 2006) which had direct consequences on salinity and subsequent hydrological conditions. This early to mid Holocene time frame is coeval with the African Humid period associated with warmer temperatures and enhanced precipitation and river runoff (de Menocal et al., 2000; Lezine et al., 2009). Evidence of reduced sea surface salinities (SSSs) in the western basin, coeval with S1 deposition, is present in proxies from the Tyrrhenian Sea (Kallel et al., 1997, 2004; Bernasconi and Pika-Biolzi, 2000; Di Donato et al., 2008) and the Gulf of Lion (Melki et al., 2009). A speleothem record from Poleva Cave in the south west of Romania provides a high resolution climatic reconstruction for the area utilising 115 isotopic measurements between 11.5-2.0 cal kyr BP (Constantin et al., 2007). The isotopic signal indicated a gradual post glacial warming between 11.5-5.2 cal kyr BP associated with the African Humid period , that was interrupted by cooling events at ~8, 7.2 and 4.2 cal kyr BP. These cooling events may coincide with similar cooling events identified by Frigola et al., (2007) at 8.2, 7.2 and 4.1 cal kyr BP and also the 8.2 and 4.3 Bond events (Bond et al., 1997). The end of the early-mid to mid Holocene phase is associated with numerous changes across the Mediterranean region, coinciding with the end of the humid period (between 5.5 and 6.0 kyr cal BP) (De Menocal et al., 2000; Lezine et al., 2009) while proxies in the Tyrrhenian Sea indicate a re-establishment of winter mixing (Di Donato et al., 2008). Two warming events were observed in South west Romania based on increased $\delta^{18}O$ values the first at ~5.2 and the second a warm and wet phase at 3.3 cal kyr BP that corresponds to the beginning of the Bronze age (Constantin et al., 2007). An increasing salinity trend is evident in the Gulf of Lion after 5.0 kyr cal BP (37.5‰) until ~1.0 kyr cal BP this increase in surface salinities as a result of reduced precipitation, would reduce stratification allowing

convective overturning and facilitating the formation of WMDW and the initiation of modern day conditions in the Western Mediterranean Sea (Melki et al., 2009).

Chapter 4: Present Day Distribution of Planktonic Foraminifera in the Mediterranean Sea

4.1 Introduction

Belonging to the Phylum Protozoa, foraminifera are microscopic single celled animals first classified in 1826 by Alcide d'Orbigny. The method of classification was based on the composition and structure of the test (shell) of which three types were recorded: organic, agglutinated and secreted calcium carbonate. The lower taxonomic groups such as super-families and genera are further classified according to morphological variations within the test, such as chamber number, shape and arrangement, and aperture structure (Armstrong and Brasier, 2005). This research uses the classification system of Hemleben et al., (1989). Based on their mode of living foraminifera can be benthic (bottom dwelling) or planktonic (free floating within the water column) and occupy a diverse range of marine environments (Williams et al., 1998). Possessing a calcareous test, planktonic foraminifera are divided into three super-families based on the test structure: Non-spinose (Globorotaliidae), Spinose (Globigerinidae) and Microperforate (*figures 4.1a and b*)

Modern day foraminiferal species analysis indicates that planktonic foraminifera live within specific ecological environments primarily governed by temperature, salinity and productivity, where maximum relative abundance of species correlates with their ecological optima (Bé, 1959, 1960; Kustanowich, 1963; Jones, 1967; Schmuker et al., 2002). Based primarily on temperature, recent planktonic foraminiferal distribution has been classified into the following biogeographic regions: tropical, subtropical, temperate, Arctic, subpolar and polar (Bé and Tolderlund, 1971; Kucera, 2007) (*figure 4.2*). While planktonic foraminiferal species can exist within a broad range of temperatures, an optimum range is associated with maximum absolute and relative abundances (Kucera, 2007). The distribution of species has been identified as bipolar, in that species existing in northern waters also exist symmetrically in southern regions (Armstrong and Brasier, 2005).

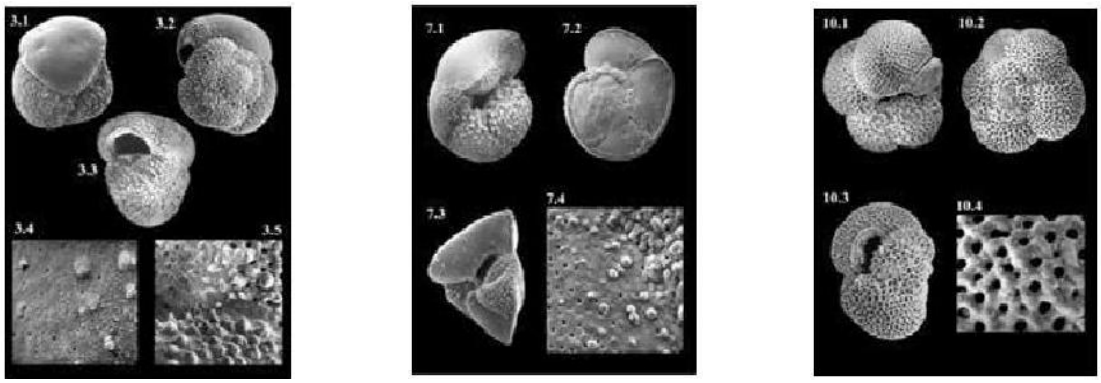

Figure 4.1a. Non spinose species of the Super-Family **Globorotaliidae**: *G. inflata, G. truncatulinoides* and *N. pachyderma* respectively (from Coloma et al., 2005).

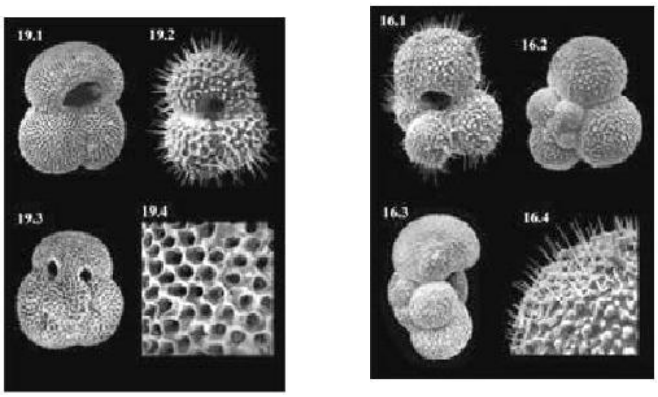

Figure 4.1b. Spinose species of the Super-Family **Globigerinidae**: *G. bulloides,* and *G. ruber* respectively (from Coloma et al., 2005).

This chapter provides an overview of the present day distribution of planktonic foraminifera within the Mediterranean Sea using data extracted from surface sediments (Thunell, 1978) and live plankton tows (Pujol and Vergnaud-Grazzini, 1995). Both research processed their samples utilising a >150µm sieve, as did our research, this allowed for the direct comparison of faunal distribution patterns Understanding the ecological preferences and resultant distribution of various planktonic foraminiferal species is recognised as a modern analog which can be subsequently used in palaeoenvironmental reconstructions.

4.2. Surface Sediment Cores

Figures 4.3-4.11 illustrate the distribution of the relative frequency of 9 primary species of planktonic foraminifera in the Mediterranean Sea as observed by Thunell (1978). The results are based on 66 surface (0-2cm) sediment samples, 26 of which are located in the western Mediterranean Sea. Cluster, factor and species diversity analysis were applied to

the faunal assemblages indicating temperature and salinity as primary controlling factors related to faunal distribution (Thunell, 1978).

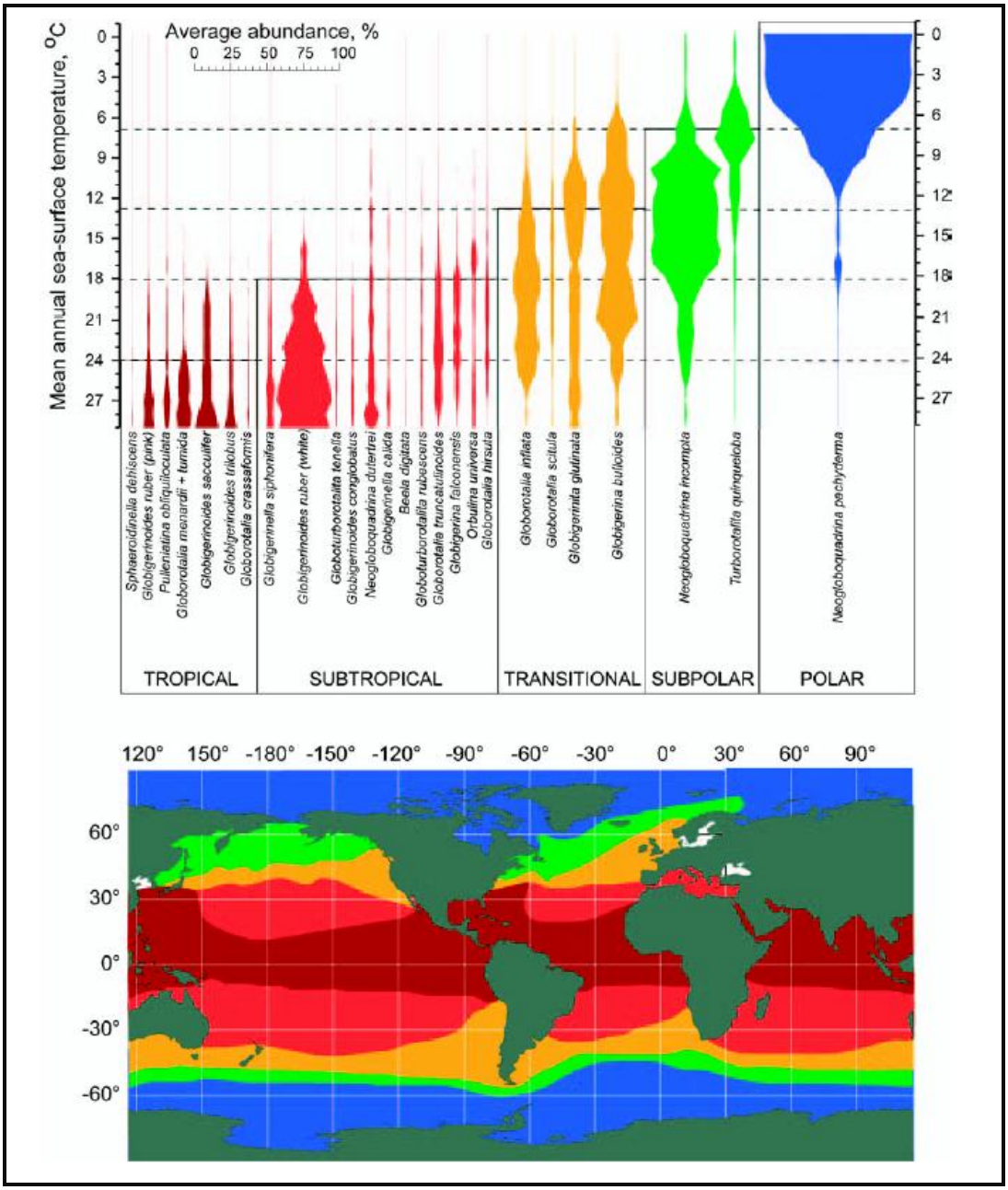

Figure 4.2. Modern planktonic foraminiferal biogeographic regions associated with SST distribution. Each region is associated with a colour as indicated in the species abundance plots. The abundance plots are based on surface sediment data from the Atlantic Ocean (Kucera et al., 2005).

Reaching values greater than 60% in the far eastern Mediterranean basin, *G. ruber* is the most dominant species in the surface sediments (*figure 4.3*). Its temperature

dependence is clearly evident along a west-east gradient, with minimal abundances coinciding with the lower temperatures occurring in the Gulf of Lion region.

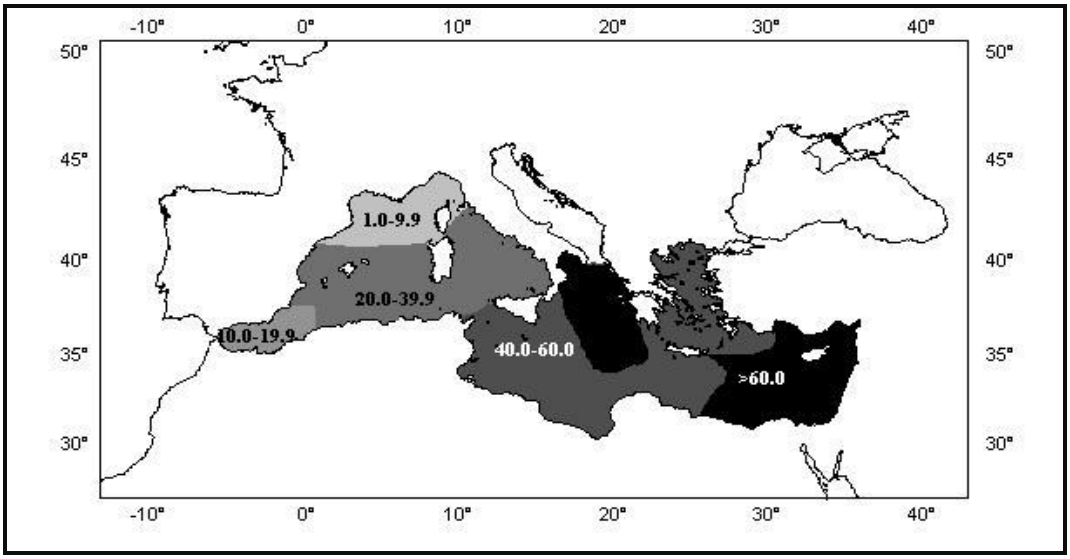

Figure 4.3. Relative abundance (%) of *G. ruber* in the surface sediments of the Mediterranean Sea (modified from Thunell, 1978).

In contrast to *G. ruber*, *G. bulloides* records its highest frequencies (20-40 %) in the western basin. Lowest values (1.0-9.9 %) occur in the eastern basin, with the exception of the Aegean Sea (*figure 4.4*). Cluster analysis identified *G. bulloides* as a cool-subtropical species (Thunell, 1978), correlating with Bé (1960) who recorded an increase in *G. bulloides* where temperatures ranged between 18-23°C.

N. pachyderma is classified as a polar non spinose species (*figure 4.2*). Thunell (1978) grouped both the left and right coiling variants into one entity as the left coiling variety had minimal abundances with the highest values reaching only 1% of the faunal assemblage. The left coiling variant dominates faunal assemblages in cooler high latitudes while the right coiling variant tends to be associated with more temperate climates (Darling et al., 2006). The highest frequencies (>20%) of *N. pachyderma* occur in the cooler Gulf of Lion (*figure 4.5*). In contrast the abundance of *N. pachyderma* significantly decreases (<1.0%) in the central and eastern Mediterranean basins. However, since the distribution of *N. pachyderma* is also associated with the depth of the pycnocline (Kuroyanagi et al., 2004), it is not surprising to find high abundances associated with the site of WMDW formation (see chapter 2 section 2.2.2.1).

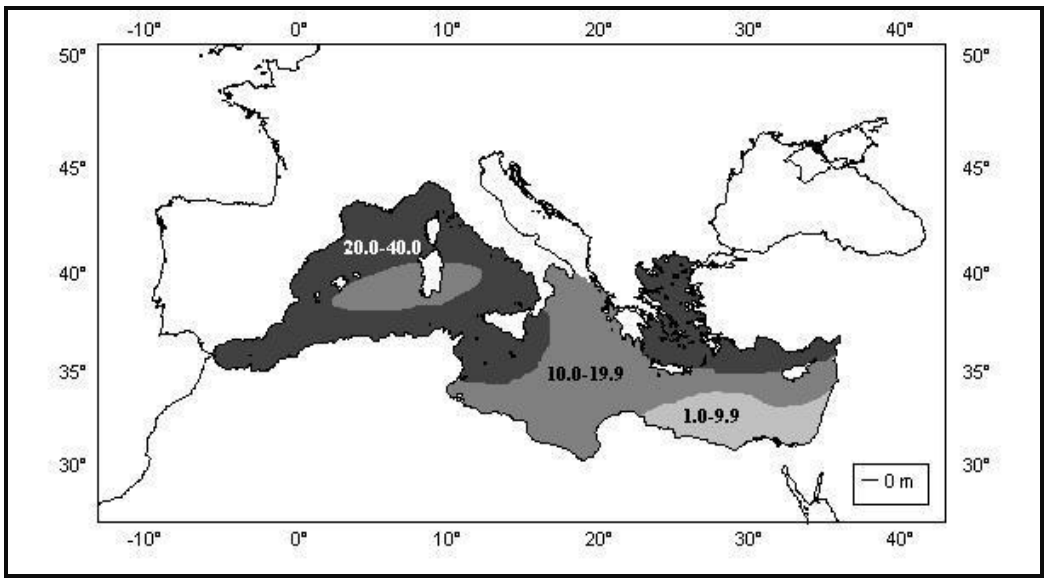

Figure 4.4. Relative abundance (%) of *G. bulloides* in the surface sediments of the Mediterranean Sea (modified from Thunell, 1978).

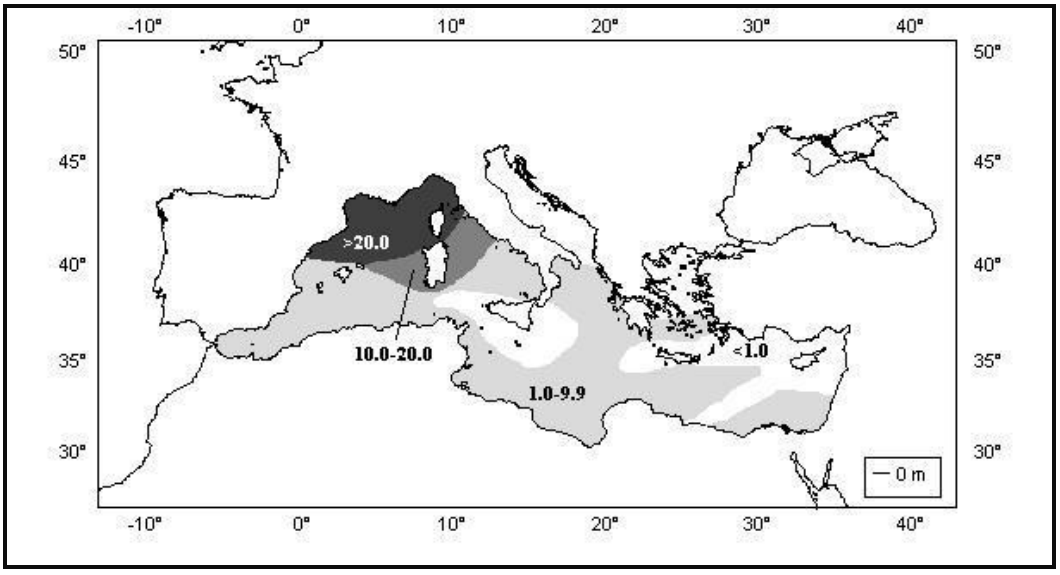

Figure 4.5. Relative abundance (%) of *N. pachyderma* in the surface sediments of the Mediterranean Sea (modified from Thunell, 1978).

Figure 4.6 highlights the uneven distribution of *G. inflata* in the Mediterranean Sea. Identified as a transitional species, *G. inflata* has an optimum temperature range of ~18°C (*figure 4.2*), this would explain its virtual absence in the eastern basin and greater abundances (>20%) in the western basin.

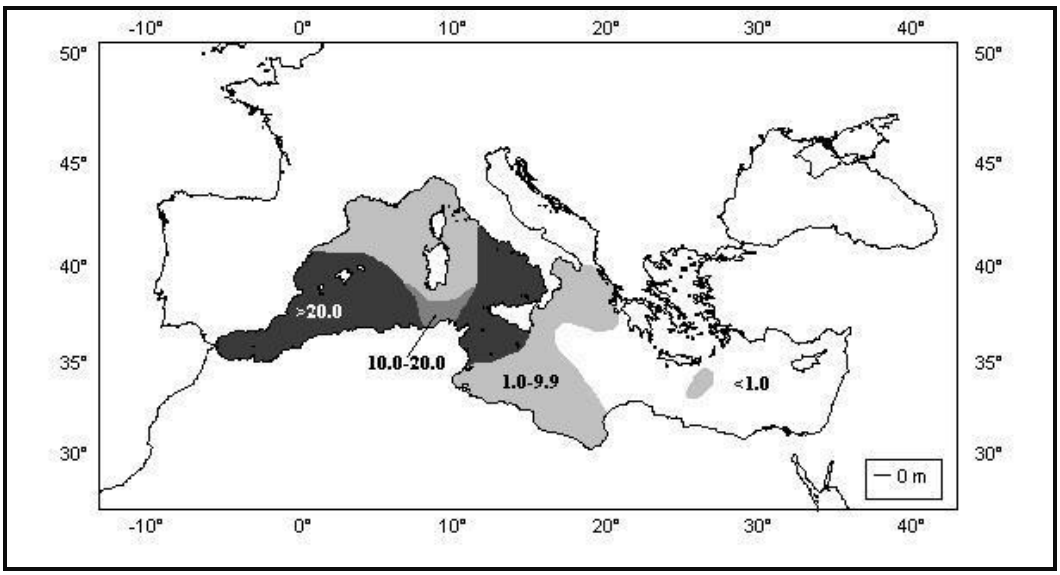

Figure 4.6. Relative abundance (%) of *G. inflata* in the surface sediments of the Mediterranean Sea (modified from Thunell, 1978).

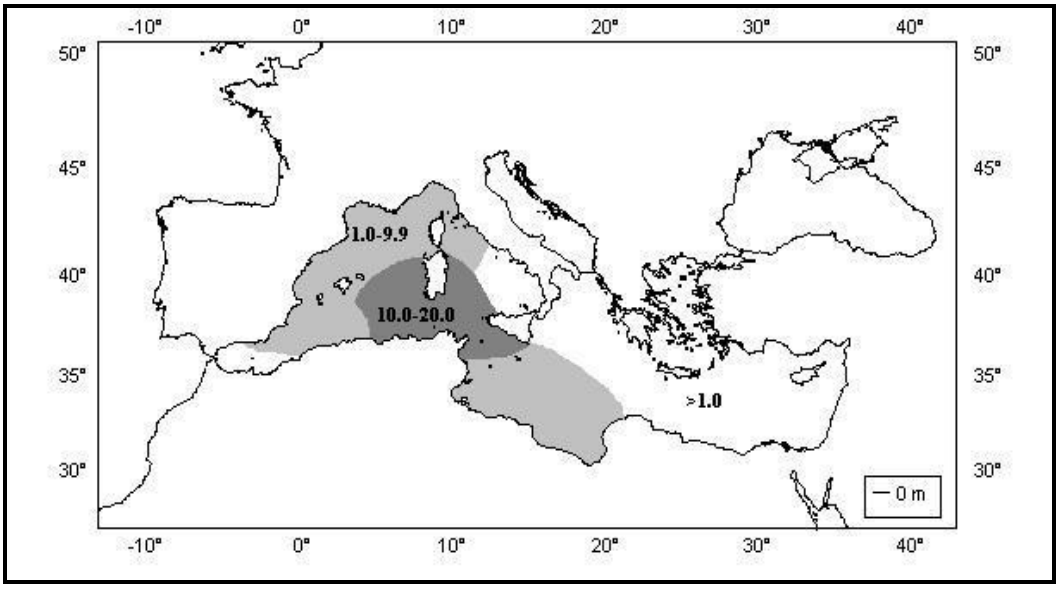

Figure 4.7. Relative abundance (%) of *G. truncatulinoides* in the surface sediments of the Mediterranean Sea (modified from Thunell, 1978).

The distribution of *G. truncatulinoides* is primarily concentrated in the western basin, particularly in the Balearic Basin (10-20%). Values decrease to <1.0% in the eastern basin (*figure 4.7*). The left and right morphotype of the species have been discussed together as the right coiling variety contributed to <1% of the faunal assemblage (Thunell, 1978). Figure 4.8 illustrates the ubiquitous distribution of *G. glutinata* between the two basins.

Identified as a polar-subpolar species in the cluster analysis, *G. glutinata* rarely exceeds 5% of the faunal assemblage (Thunell, 1978).

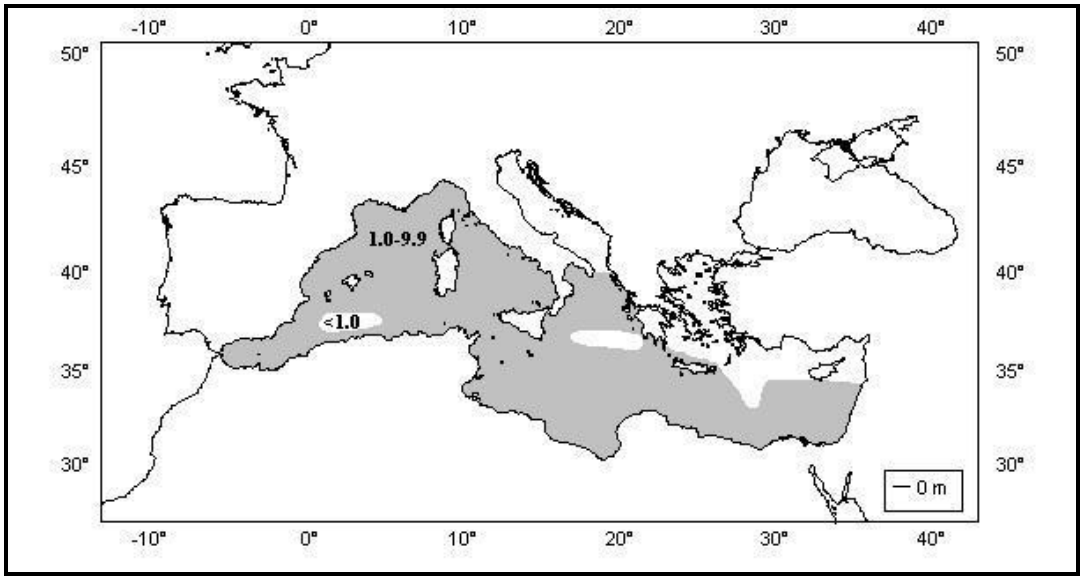

Figure 4.8. Relative abundance (%) of *G. glutinata* in the surface sediments of the Mediterranean Sea (modified from Thunell, 1978).

T. quinqueloba is a subpolar species with a present day optimum temperature of ~8 °C *(figure 4.2*). The highest abundance (1-10%) of *T. quinqueloba* is in the north western basin where winter surface temperatures drop to ~15°C (Pujol and Vergnaud Grazzini, 1995) The area of cooler AW inflow is also marked by an increase in abundance of this species (*figure 4.9*). However, temperature is not the only influencing factor as indicated by Kuroyanagi (2004), where a positive correlation with chlorophyll-a values and increased abundance of *T. quinqueloba* was observed in the seas around Japan.

O. universa is deemed a transitional spinose species (Bé, 1967) (*figure 4.2*). It is uniformly distributed throughout the Mediterranean Sea with the exception of regions characteristic of lower sea surface temperatures such as the north western region, the Adriatic and the Aegean Seas (*figure 4.10*). This correlates with the findings of Bé (1959) in the western north Atlantic Ocean where *O. universa*, existed in their highest abundances in the warmer temperature ranges south of the Gulf Stream.

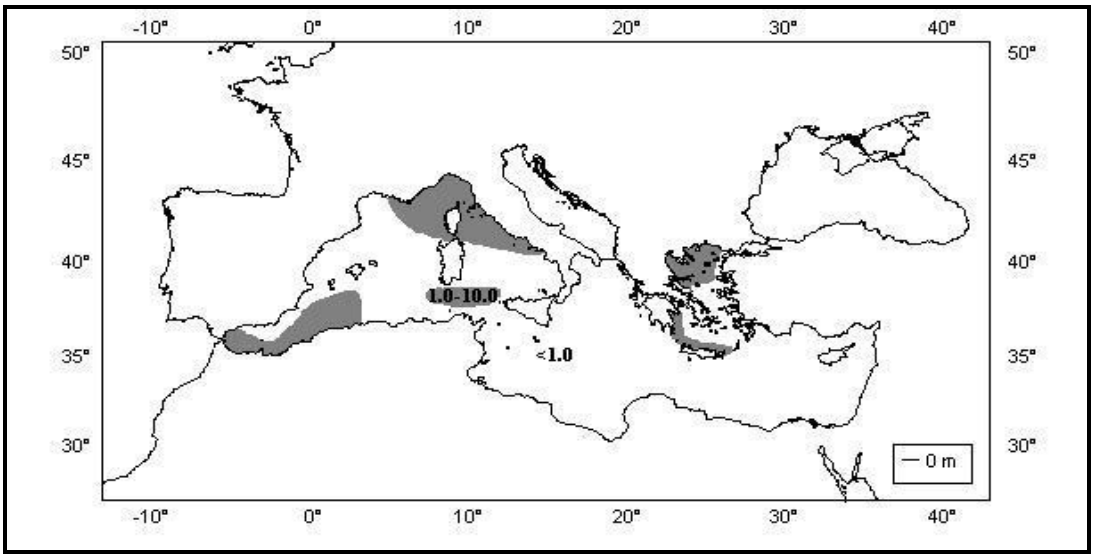

Figure 4.9. Relative abundance (%) of *T. quinqueloba* in the surface sediments of the Mediterranean Sea (modified from Thunell, 1978).

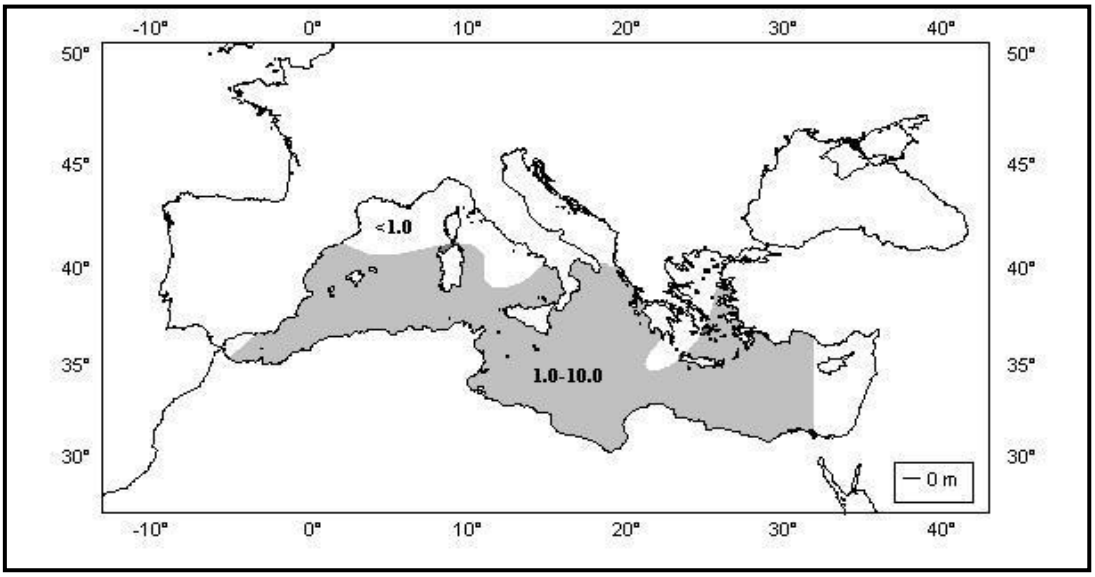

Figure 4.10. Relative abundance (%) of *O. universa* in the surface sediments of the Mediterranean Sea (modified from Thunell, 1978).

Identified as a tropical-subtropical species, *G. sacculifer* typically correlates with the temperature gradient in the Mediterranean Sea (*figure 4.11*). The highest abundances (5.0-10.0%) occur throughout the eastern basin, with significantly lower numbers existing in the western basin (<1.0%) correlating with lower temperatures in the north-western Mediterranean.

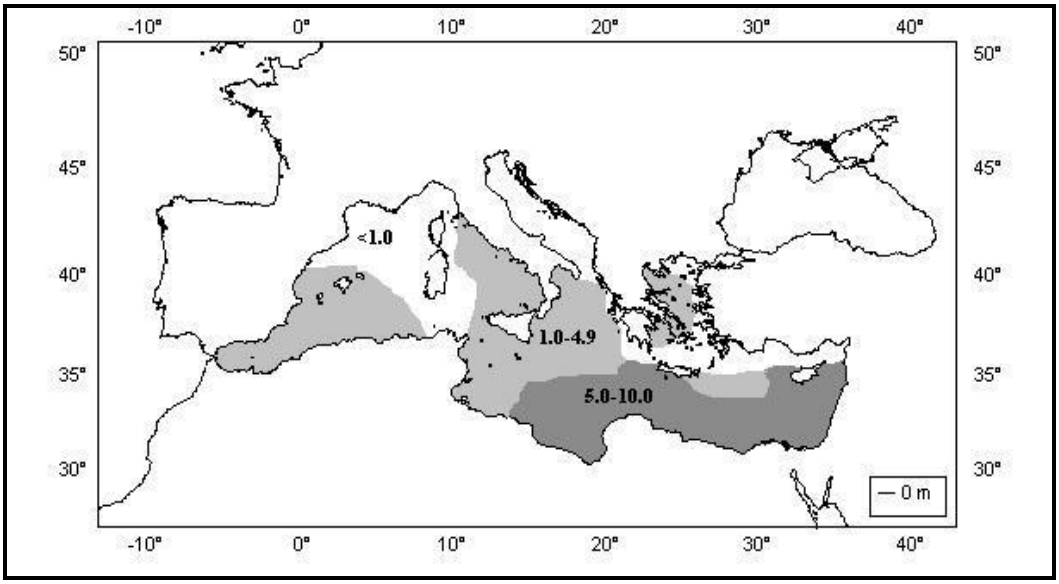

Figure 4.11. Relative abundance (%) of *G. sacculifer* in the surface sediments of the Mediterranean Sea (modified from Thunell, 1978).

Thunell (1978) also identified several minor species (*B. digitata, G. tenella, G. calida, G. siphonifera, H. pelagica*) many of which did not exceed 5% of the faunal assemblage and are therefore not presented here. These species together with *O. universa*, *G. rubescens* and *G. sacculifer* comprise the SPRUDTS Group (see Chapter 5, section 5.3), this was determined due to their low abundances and similar environmental parameters as indicated by multivariate cluster analysis carried out by Rohling et al, (1993).

4.3 Live Plankton Sampling

Both Thunell (1978) and Pujol and Vergnaud Grazzini (1995) utilised the same mesh sampleing size of >150µm, this provided us with the opportunity to make direct comparisons between both data The first study of the distribution of living planktonic foraminifera in the Mediterranean Sea was carried out by Cifelli (1974). Since then the most extensive research on the seasonality and distribution of live planktonic foraminifera was conducted by Pujol and Vergnaud Grazzini (1995). Much of the data obtained in the following sections is an overview of their results.

The distribution of live planktonic foraminifera was examined by Pujol and Vergnaud Grazzini (1995) across the entire Mediterranean Sea *(figure 4.12)* during two distinct seasons: late summer (September-October) and winter (February/March). At each

location planktonic foraminiferal densities (number of specimens/1000 m^3 of filtered water) were calculated to a depth of 350 m.

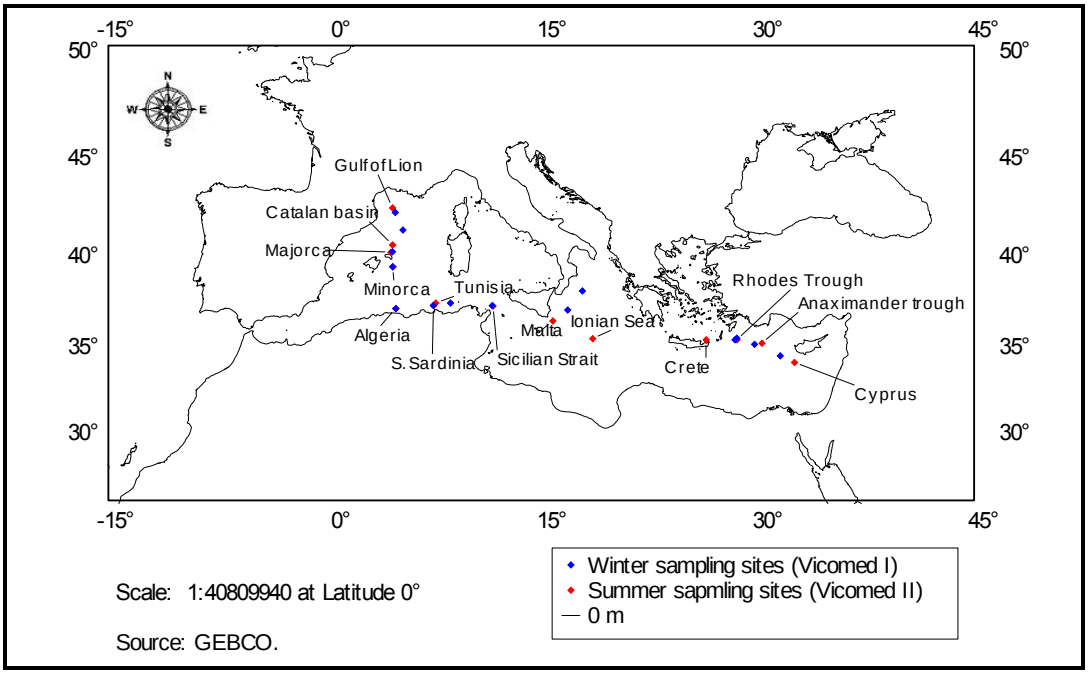

Figure 4.12. Distribution of sampling locations during Vicomed I, II (from Pujol and Vergnaud Grazzini (1995).

The results highlighted variation in species distribution between the western and eastern basins during the two seasons and at different depths. Overall distribution patterns identified a higher production in the winter than the summer, with a greater overall density occurring in the western basin. Late summer data recorded an area of peak production in the central and eastern basin reaching 1000-2000 specimens/1000m^3, while the western basin peak production occurred during the winter reaching ~ 3500 specimens/1000m^3 (Pujol and Vergnaud Grazzini, 1995).

4.3.1 Species Distribution

The distribution of species observed can be divided into summer and winter dominant species. However, distribution and abundance is not solely governed by temperature, but also by nutrient availability as indicated by depth distribution profiles (Pujol and Vergnaud Grazzini, 1995). The depth/density distribution of species varies throughout the western basin in response to variations in physiochemical and hydrographic features. The depth of the pycnocline, thermocline and deep chlorophyll maximum influence nutrient availability

thereby affecting primary production and can be observed throughout the water column in faunal density levels (Pujol and Vergnaud Grazzini, 1995). As this research focuses solely on the western basin the distribution of the individual species will focus in particular on this region. Eastern Mediterranean distribution will be addressed as a comparison for the increased temperature and salinity levels.

4.3.1.1 Late Summer

Late summer average production levels are low, with non spinose faunal densities averaging at ~200 specimens/1000m^3 of filtered water compared to average spinose species densities of ~600 specimens/1000m^3 of filtered water (Pujol and Vergnaud Grazzini, 1995). Spinose species (*G. bulloides, G. ruber* (pink/white)*, and G. sacculifer*) are typically more dominant in shallow depths (0-100m) compared to non-spinose faunal assemblages dominated by *G. truncatulinoides, G. glutinata* and *G. inflata* which exist in greatest densities below 100m at most of the western basin stations (Pujol and Vergnaud Grazzini, 1995). The reduction in late summer density levels correlates with the general oligotrophic nature of the basin during the season. The nutrient depleted surface layer (0-20m) is depicted by the reduction in species densities with the highest densities occurring between 50-100m below the base of the mixed layer in most of the western basin stations (Pujol and Vergnaud Grazzini, 1995).

Figure 4.13 illustrates the species that dominate the faunal assemblage during the late summer months: *G. ruber* (pink and white), *G. sacculifer, O. univers*a, and *G. glutinata. G. ruber* (pink) is restricted to the eastern basin with peak abundances (~3000/2200 specimens/1000m^3) occurring at the Strait of Sicily and the Rhodes trough respectively *(figure 4.13).* In contrast, *G. ruber* (white) is evident in both western and eastern basins albeit in lower abundances with a peak abundance of ~1200 specimens/1000m^3 occuring in the eastern basin at depths between 20-50m *(figure 4.13).*

O. universa is most abundant in the western basin, obtaining density levels of ~1400 specimens/1000m^3 of filtered water. A clear reduction in the number of specimens is recorded at the Sicilian Strait, where *O. universa* declines to near absence in stations eastward of the Sicilian Strait *(figure 4.13).* The subtropical nature of *O. universa* is indicated in its minimal winter abundance, while its reduction in numbers in the eastern

basin suggests its intolerance to the high summer temperatures and salinity levels in the region.

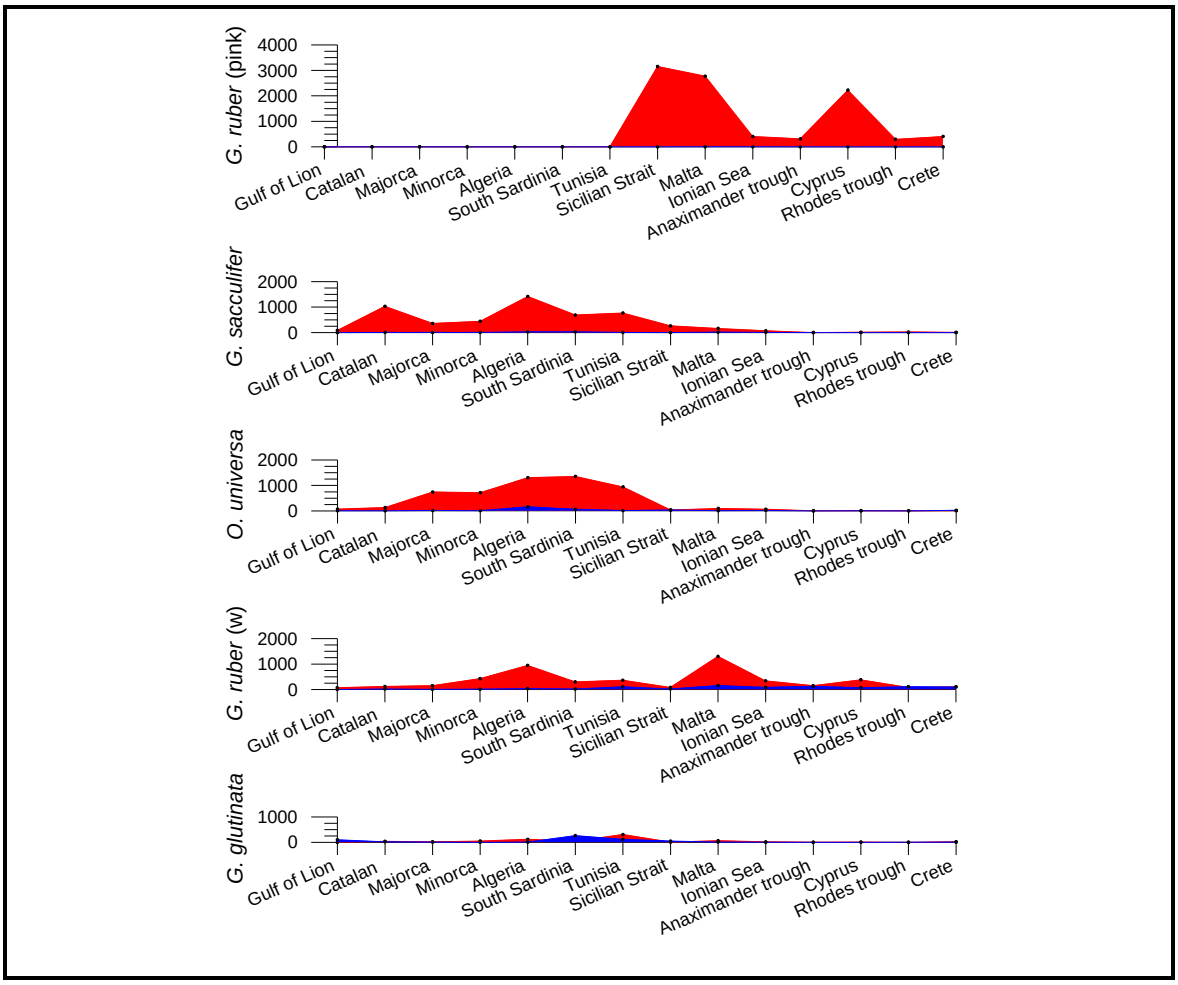

Figure 4.13. Dominant summer (red) species densities (number of specimens/1000m^3 of filtered water) for the depth interval 0-350m for each station. For comparison the blue shaded area represents winter density values (data from Pujol and Vergnaud Grazzini, 1995).

Summer distribution of *G. truncatulinoides* is confined to the western basin with two density peaks of ~600 specimens/1000m^3 of filtered water in the Catalan and Tunisian sub-basin *(figure 4.14)*. Maximum abundances of *G. truncatulinoides* were located at depths >100m with the exception the Tunisian station where maximum abundances were located in the mixed layer at ~ 25m. All species at the Tunisian station reach maximal peak abundances at this depth, possibly associated with the upwelling of nutrients from the MAW layer identified by a salinity minimum at 50m (Pujol and Vergnaud Grazzini, 1995). Maximum densities of *G. truncatulinoides* in the South Sardinian station below 100m indicates the impact of nutrient availability, where a deepening of the DCM (>70m) may

have contributed to phytoplankton blooms thereby affecting primary production (Pujol and Vergnaud Grazzini, 1995; Barale et al., 2008).

4.3.1.2 Winter

Species densities are significantly higher during winter with values reaching up to 8259 specimens/1000m^3 of filtered water (Pujol and Vergnaud Grazzini, 1995). Four faunal species, *N. pachyderma, G. truncatulinoides, G. inflata* and *G. bulloides* dominate the winter assemblage, with *G. siphonifera* occurring only at the Algerian and South Sardinian stations.

N. pachyderma (right coiling) dominates the faunal assemblage in the Gulf of Lion *(figure 4.14)* where it represents ~74% of the assemblage and ~43% in the Catalan sub basin (Pujol and Vergnaud Grazzini, 1995). This correlates well with the results from the surface sediments *(figure 4.5)*. In the Gulf of Lion *N. pachyderma* (right coiling) recorded the greatest increase between 25-50m where it peaked in abundance (~ 2100 specimens/1000m^3 of filtered water). This increase correlates with the depth of the deep chlorophyll maximum (DCM) that migrates to shallower depths of 40-50m during winter (Pujol and Vergnaud Grazzini, 1995). The DCM and the supply of nutrients by strong winter vertical mixing may be responsible for the peak of shallow species abundances, highlighting the effect of nutrient availability on primary production. Beyond the Catalan sub-basin *N. pachyderma* (right coiling) density values reduce to almost non existent *(figure 4.14)*.

Reaching peak abundances of 5487 specimens/1000m^3 of filtered water (Majorca), *G. truncatulinoides* is prolific throughout faunal assemblages in the western basin *(figure 4.15)*. Although not absent in the eastern basin, values significantly decrease reaching ~1000 specimens/1000m^3 of filtered water at the Malta station. This concurs with data obtained in the surface sediments *(figure 4.7)*. *G. truncatulinoides* dominates the winter assemblage by 64-80% at the two Balearic basin stations, with *G. inflata* and *G. bulloides* comprising the remainder *(figure 4.15)*. *G. truncatulinoides* is the most dominant species in the 3 southern stations in the western basin: Algeria, South Sardinia and Tunisia. Maximum densities are found on a west to east gradient for the southern stations, where peak density values recorded are ~ 3500, 2000 and 1000 specimens/1000m^3 respectively.

Maximum densities recorded in all 3 locations occur between 100-200m, in particular at 200m. (Pujol and Vergnaud Grazzini, 1995).

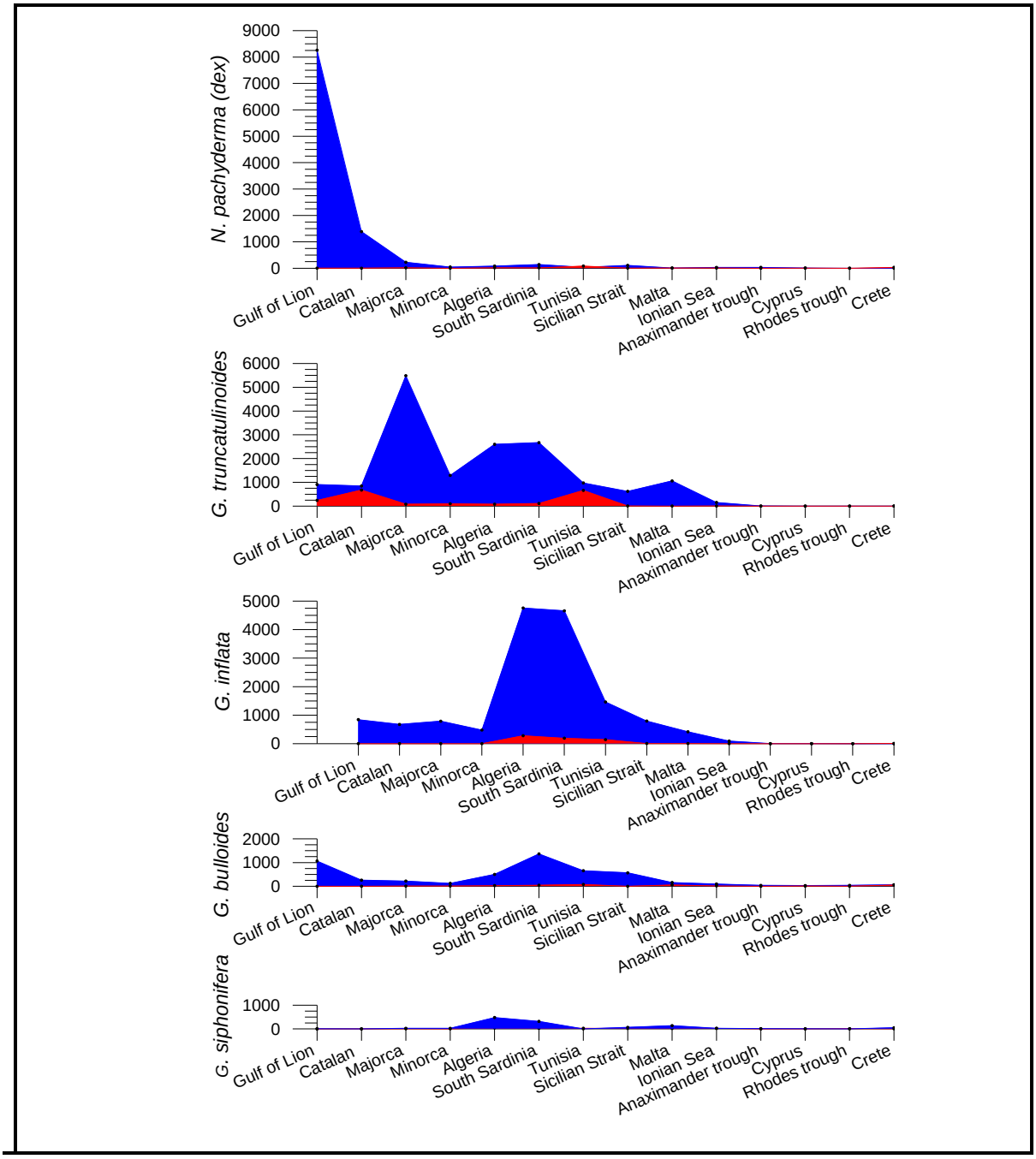

Figure 4.14. Dominant winter (blue) species densities (number of specimens/1000m^3 of filtered water) for the depth interval of 0-350m for each station. For comparison the red shaded area represents summer density values (data from Pujol and Vergnaud Grazzini, 1995).

G. inflata records densities of ~1000 specimens/1000m^3 of filtered water throughout the western basin with the exception of two significant density peaks in the Algerian and Southern Sardinian stations (5000 specimens/1000m^3, of filtered water) *(figure 4.14)*. Along the North African Coast (Algeria, South Sardinia and Tunisia) *G. inflata* dominates the winter assemblage (45-55%) peaking between 100-200m. At the Algerian station *G. inflata* records a density peak at 200m, correlating with that of *G. truncatulinoides*. The maximum density abundances in the southern stations occur below the mixed layer. The base of the mixed layer was identified at 100m at the Algerian and Tunisian station, reaching 200m at South Sardinia (Pujol and Vergnaud Grazzini, 1995). The permanent currents and jets along the North African and Algerian coasts provide a continuous nutrient supply during winter. Phytoplankton blooms in the photic zone provide the nutrients for the development of deeper dwelling non spinose species that can migrate throughout the water column when the pycnocline is erased (Pujol and Vergnaud Grazzini, 1995). East of the Strait of Sicily *G. inflata* densities reduce, correlating with the findings of Thunell (1978) *(figure 4.6)*.

G. bulloides peaks at two regions during winter, the Gulf of Lion and South Sardinia reaching ~1000 specimens/1000m^3 of filtered water *(figure 4.14)*. In the Gulf of Lion winter peak densities correlate with those of *N. pachyderma* (right coiling) and *G. truncatulinoides* at 50m. Winter atmospheric forces (Mistral) and fluvial inputs (Rhone/Ebro) influence the biological activity in the region, as phytoplankton growth is restricted until turbulent winter mixing declines (Barale et al., 2008). The presence of a phytoplankton bloom in calm high nutrient waters correlates with the high species densities in the western basin during winter (Barale et al., 2008).

Phytoplankton production correlates with planktonic foraminiferal density values, with peak values occurring when phytoplankton production is high. While environmental parameters such as temperature and salinity may affect species assemblages (winter/summer differences) the depth of the DCM and nutrient supply seem to govern their proliferation (Pujol and Vergnaud Grazzini, 1995; Barale et al., 2008). A summary of the species identified in both live and sediment studies is depicted in Table 4. 1 with Table 4.2 presenting a summary of the winter and summer distribution patterns of the main species identified by Pujol and Vergnaud Grazzini (1995), their associated regions and water depths of maximum abundances.

Species	Live Plankton Tows	Sediment Core Top
Globigerina bulloides	**Y**	**Y**
Globigerinella calida	**Y**	**Y**
Globigerinoides conglobatus	**Y**	N
Beela digitata	N	**Y**
Neogloboquadrina dutertrei	N	**Y**
Globigerina falconensis	N	**Y**
Globigerinita glutinata	**Y**	**Y**
Globorotalia hirsuta	**Y**	N
Globorotalia inflata	**Y**	**Y**
Neogloboquadrina pachyderma L	**Y**	**Y**
Neogloboquadrina pachyderma R	**Y**	**(ND)**
Hastigerina pelagica	**Y**	**Y**
Turborotalia quinqueloba	**Y**	**Y**
Globigerinoides ruber white	**Y**	**Y**
Globigerinoides ruber pink	**Y**	**(ND)**
Globoturborotalita rubescens	**Y**	N
Globigerinoides sacculifer	**Y**	**Y**
Globorotalia scitula	**Y**	N
Globigerinella siphonifera	**Y**	N
Globoturbotalia tenella	N	**Y**
Globigerinoides trilobus	**Y**	**(ND)**
Globorotalia truncatulinoides (sin + dex)	**Y (SIN)**	**Y (ND)**
Orbulina universa	**Y**	**Y**

Table 4.1. Variation in species identified from live plankton tows (Pujol and Vergnaud Grazzini, 1995) and fossilised surface sediment assemblages Y = yes, N = no, ND = not differentiated (Thunell, 1978).

Species	Winter area of dominance	% of faunal assemblage	Winter max. abundance Depth (m)	Late Summer area of dominance	% of faunal assemblage	Summer max. abundance Depth (m)
G. ruber (pink)	Levantine	>40%	20-50	Eastern Basin	>40%	20
G. ruber (white)	Levantine	>40%	20-100	**Ionian** **Levantine**	20-30% 20-30%	20-50 20-50
O. universa	-	-	-	**Balearic** African coast	>40% >40%	20-100 50-100
G.sacculifer	-	-	-	**N. African coast** Catalan	20-30% <20%	20-50 20-50
N. pachyderma (dex)	Provencal Catalan	>40 >40	**50**, 200-350	-	-	-
G. truncatulinoides	Balearic	>40	50-100	Pro – Cat Balearic N. African coast	<20 <20 <20	200 100 100-300
G. inflata	N. African coast	>40	100-200	Alboran	20-30	100-200
G. bulloides	Provencal Catalan Balearic N. African coast Ionian	<20 <20 <20 <20	20-50 20-200 20-100 50-200 200-300	Alboran (June)	>40	20-300

Table 4.2. Dominant winter and summer species distribution and their associated depth profile, areas highlighted in bold indicate species dominance in location (Pro=Provencal, Cat=Catalan sub-basins) (data from Pujol and Vergnaud Grazzini, 1995).

Chapter 5: Material and Methods

5.1 Introduction

This chapter provides a comprehensive overview of the materials and methods utilised during this research. The first part of this chapter will concentrate on the deep sea cores and refer directly to their localities and physical attributes. The second part of the chapter will concentrate on the methods employed in the laboratory, while addressing the application of accelerator mass spectrometry (AMS) ^{14}C dating and oxygen isotope stratigraphy.

5.2 Material

5.2.1 Deep Sea Cores

Sediments from four western Mediterranean deep sea cores were utilised for the purpose of this research chosen for their distinct location within 3 different sub-basins in the Western Mediterranean Sea. Core locations and details are summarised in *figure 5.1* and *Tables 5.1* and *5.2*.

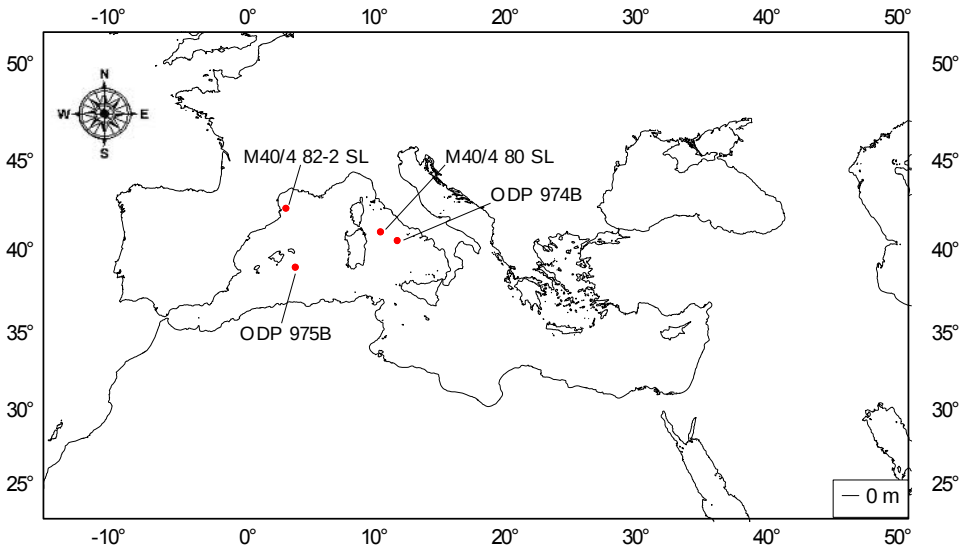

Figure 5.1. Map depicting the localities of the four western Mediterranean deep sea cores utilised in this research from the RV Meteor cruise (28 October 1997 - 10th February 1998) and the JOIDES Resolution cruise (3rd May – 2nd July, 1995).

Core Name	Cruise	Core Type	Region	Long.	Lat.	Core Length (metre)	Water Depth (mbsl)	AMS	O.I.A.
M40/4-82-2 SL	RV Meteor	Gravity	Gulf of Lion	03°46, 40.	42°18, 51.N	5.45	1079	Yes	No
ODP 975B	JOIDES Resolution	Advanced piston corer (APC)	Balearic Basin	04°30, 596.E	38°53, 786.N	317.1	2415.5	Yes	Yes
M40/4-80 SL	RV Meteor	Gravity	Tyrrhenian Sea	11°00, 22.E	40°57, 31.N	7.4	1881	Yes	No
ODP 974B	JOIDES Resolution	Advanced piston corer (APC)	Tyrrhenian Sea	12°08, 515E	40°21, 362.N	203.7	3453.9	Yes	No

Table 5.1. Core location and cruise information, including total core length and water depth (metres below sea level). AMS ^{14}C dating was carried out in the Beta Analytic Radiocarbon Dating Laboratory, Florida, USA and Oxygen isotope analysis (O.I.A) was carried out at the School of Ocean and Earth Sciences, Southampton, England.

5.2.1.1 Core Lithology

The predominant lithology of the four studied cores are represented in figure 5.2 and summarised in Table 5.2. The lithology of core M40/4 82-2 SL is dominated by nannofossil/foraminiferal ooze and exhibits slight bioturbation (Hieke et al., 1999). Similarly the lithology of the Balearic Basin core ODP 975B consists of nannofossil/calcareous clay, nannofossil/calcareous silty clay and nannofossil ooze, of which, nannofossils comprise the major component of the carbonate fraction with foraminifera and micrite comprising up to 30% of carbonate sediments (Comas et al., 1995). Bioturbation is common throughout the studied section but is especially prominent below 150 mbsf (beyond the depth of the studied interval in this research) (Comas et al., 1995). The lithology of core M40/4 80 SL is dominated by nannofossil/foraminiferal ooze and exhibits moderate bioturbation in the analysed section of the core (Hieke et al., 1999). As described in the Preliminary report of Leg 161, the predominant lithology of the studied section of core ODP 974B consists of nannofossil-rich clay to nannofossil-rich silty clay,

calcareous nannofossil ooze and ash particles and the sediments are locally bioturbated (Comas et al., 1995).

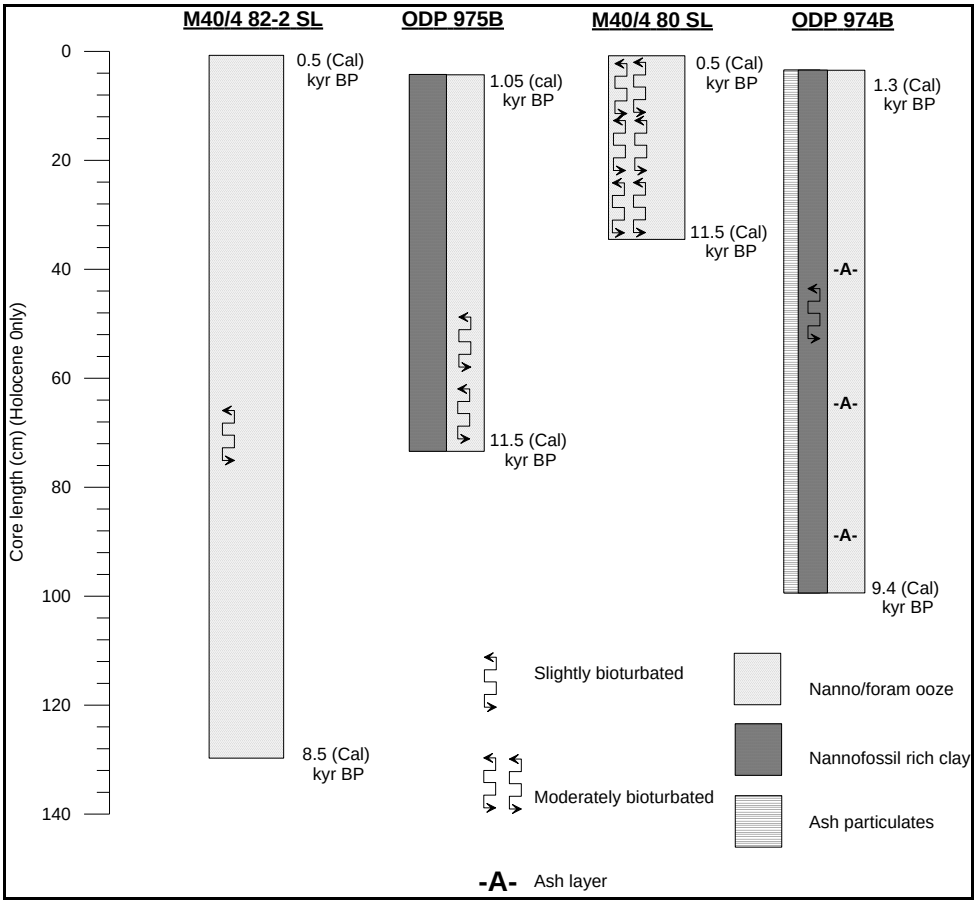

Figure 5.2. Schematic representation illustrating the prominent lithology and physical features of the studied sections of the four cores pertaining to this research.

The minimum resolution for sampling was set at 3cm with a maximum resolution of 1-2cm, this high resolution was justified in order to achieve a detailed record of foraminiferal response and to facilitate the observation of short term climatic events that may otherwise be unavailable at a lower resolution, thereby allowing the completion of our research aims. The highest resolution was obtained for the Gulf of Lion core where many samples have a 1 cm resolution; this was deemed appropriate as this core was to be extensively studied in order to reconstruct a palaeoenvironmental reconstruction as set out in our research aims.

Core	Interval analysed (cm)	Sampling Resolution (cm)	Bioturbation	Lithology
M40/4 82-2 SL	0-129.5	1-2	Moderate-slight	Nannofossil ooze
ODP 975B	0-72.5	3	Absent in first 50cm Minor (<30% of surface area) for remainder	Nannofossil ooze and calcareous clay Sediments were slightly disturbed during drilling
M40/4 80 SL	0-38.5	1-2	slight	Nannofossil ooze
ODP 974B	0-100	3	slight	Predominantly calcareous clay with nannofossil ooze and minor presence of volcanic ash

Table 5.2. Summary of sampling resolution, bioturbation and lithology of the studied sections in all cores pertaining to this research.

5.3 Methods

5.3.1 Foraminiferal analysis

5.3.1.1 Laboratory Procedures

Micropalaeontological analysis was undertaken in the laboratory in Mary Immaculate College, Limerick, Ireland. Following standard foraminiferal procedures, samples were placed on a weighed petri-dish and dried in an oven at <40°C overnight before weighing to obtain a dry sample weight. Low oven drying temperatures are used to decrease the chance of damage to the foraminiferal tests thereby preventing loss of sample quality, as increased temperatures can result in fragmentation and subsequently affect statistical analysis. Samples were then disaggregated in deionised water and wet sieved through a 63µm sieve using a gentle flow of deionised water. The use of deionised water prevents contamination of the sample by minerals that occur in natural water such as carbonates that may affect subsequent geochemical analysis. With this in mind all equipment that had direct contact with foraminifera during laboratory procedures were cleaned thoroughly with deionised water. The remaining sediment was placed in a weighed petri-dish and dried again in an oven at <40°C. The final weight of the dried sample is taken once the drying stage is

complete to obtain >63µm dry weight. Finally, the sample was dry sieved through 150µm sieve and stored in glass bottles. In line with the standard sieve size fraction as advised by the CLIMAP project members, the >150µm size fraction was used for foraminiferal analysis (Kucera et al., 2005). As most research associated with planktonic foraminifera in the Mediterranean Sea is carried out using this sieve size it allows for direct comparison between faunal results (Cacho et al., 1999; 2001; Sbaffi et al., 2001; 2004; Melki et al., 2009 and references therein).

5.3.2.2 Quantitative Foraminiferal Analysis

A random micro-splitter was used to divide samples into aliquots of ~300 planktonic foraminiferal specimens per sample. Statistically this ensured a 95% probability of not encountering an additional species comprising at least 1% of the faunal assemblage (Shaw, 1964). Using a fine tipped (00000) paintbrush and a stereo microscope (20 X objective lens) complete specimens were picked onto Cushman slides. Identification was accomplished using the taxonomy of Hemleben et al. (1989). Once identified, each sample was quantified and the planktonic foraminiferal abundances were presented as absolute and relative abundances of the sample.

Calcium carbonate is a soluble mineral particularly susceptible to water associated with increased carbon dioxide levels (Dickey, 1996). Dissolution in planktonic foraminifera occurs from the moment of death and as such is a source of concern for palaeoenvironmental research. The extent of dissolution is dependant on certain factors, such as the individual species robustness and the duration of exposure within the water column, this is significant for smaller foraminifera that have a longer exposure within the water column due to their slower rate of sinking (Dickey, 1996; Kucera, 2007). Calcite dissolution is reflective of the saturation of the water surrounding the shell. Saturation levels vary with depth but are also susceptible to micro-scale gradients reflecting organic matter re-mineralization and as a result calcite dissolution can occur at any depth. The depth at which calcium carbonate cannot be recorded in the sediment is where the rate of dissolution is greater than the rate of precipitation, this depth is known as the calcium carbonate depth (CCD) (Dickey, 1996; Kucera, 2007). The general global CCD is located between 3 and 5km (Walker, 2005) of which the deeper depth reflects that of the Atlantic (Dickey, 1996). Of the cores analysed only core ODP 974B is located in proximity to the

3km depth guideline of the CCD. However, the quality of the samples utilised in this research appears to be uncompromised by dissolution, this is indicated by the presence of pteropods (composed of aragonite) in many of the samples, as aragonite is more susceptible to dissolution than that of calcium carbonate (Dickey, 1996).

For the purpose of planktonic foraminiferal analyses, seven species were grouped together entitled the SPRUDTS group. The SPRUDTS-group is comprised of *G. sacculifer, H. pelagica, G. rubescens, O. universa, B. digitata, G. tenella and G. siphonifera* (Rohling et al., 1993). Clustering in multivariate analysis indicated that these minority species exist within similar environmental parameters and as such may be combined to represent a similar ecological environment (Rohling et al., 1993). *G. ruber* was separated into the pink and white varieties and the coiling variants of *N. pachyderma* and *G. truncatulinoides* were recorded separately.

Individual quantitative analysis was performed on both coiling types of *G. truncatulinoides* (sinistral and dextral) in order to fully represent the biostratigraphic potential of the species. Prior to faunal abundance analysis each sample was analysed for the presence of *G. truncatulinoides* (sinistral and dextral). In order to obtain a minimum of 100 specimens samples were either counted in full or split using a random microsplitter where required, 100 specimens were chosen as it was deemed the most appropriate number to be acquired for one species, this number would allow for a true representation of the species abundance while also providing an achievable target as faunal % varied downcore. The relative abundance of both coiling types was established as a percentage of the total *G. truncatulinoides* population providing a record of coiling variation in each core (See Appendix B for detailed counts).

5.4 Dating Techniques

5.4.1 Radiocarbon Dating

Living organisms contain a level of ^{14}C in equilibrium with that available in their immediately surrounding atmosphere. Upon death of the organism, ^{14}C are no longer replenished and begin to decay in a way that provides a method to produce an approximate age for the death of the organism (Wilson et al., 2005). Referred to as the half life, the rate of ^{14}C decay is 5730 years, the time taken for ^{14}C to deplete by half (Walker, 2005). Due to the short half life, radiocarbon dating can only be used reliably during the last 55 kyrs,

(spanning approximately 10 half lives) (Walker, 2005). Subsequently, as Holocene research is well within the confines of the dating time limit it is an appropriate dating technique for the purpose of this research (Bell and Walker, 2005).

Radiocarbon dating however, is based on certain assumptions and as such is liable to error. Three of these assumptions appear to cause the greatest concern, the first of which relates to the contamination of the sample material, secondly the assumption that global ^{14}C levels remained constant over time and finally that the distribution of this ^{14}C has been even (Walker, 2005). Sample contamination of deep sea sediment can occur through the addition of older or younger carbon as a result of bioturbation and/or laboratory processes (Pilcher, 2005). For example, the addition of 1% present day carbon to a 17.0 kyr old sample can reduce the age by 700 yrs, similarly the addition of 1% older carbon such as that introduced by river runoff or local bedrock can increase the age of a modern sample by ~ 80 yrs (Walker, 2005). The comparison of radiocarbon and dendrochronological dates highlighted significant variation between the calendar ages, where the radiocarbon dates presented a younger age than that indicated by dendrochronology (Renfrew, 1973). The source of this error has been attributed to variations in atmospheric ^{14}C activity (Walker, 2005). This variation in atmospheric ^{14}C activity is identified by cyclical and plateau patterns in ^{14}C levels that can lead to significant errors in dating. Radiocarbon levels are believed to have reached plateaus, identified at ~ 11.0, 11.5 and 12.0 cal kyr BP, therefore radiocarbon dates that fall within these plateau can have a calendar age range of up to several hundred years (Goslar et al., 2000; Walker, 2005).

In modern day ocean surface waters, ^{14}C is replenished through interactions between the atmosphere and the ocean. Over time surface waters sink to intermediate and deep water depths ceasing the replenishment of ^{14}C and initiating the process of ^{14}C decay. Referred to as the marine reservoir effect, this results in an apparent ageing of surface water from ~ 30 to 400 years to up to thousands of years in deep ocean waters (Walker, 2005). Subsequently, ages determined from proxies such as planktonic foraminifera need to be corrected for the age of the sea water. However, establishing an appropriate reservoir correction age (the difference between the ^{14}C age of the sea surface and that of the atmosphere (Siani et al., 2001) is a difficult task, as circulation patterns not only exhibit spatial but also temporal variation and as such poses a significant error in radiocarbon dating (Walker, 2005).

Radiocarbon dates can exhibit considerable variation (up to 3.5 kyrs) from actual calendar years (Bell and Walker, 2005). In response to this ^{14}C ages are converted into calendar years using a calibration package such as CALIB 5.0.1 (Stuvier et. al. 1998). CALIB 5.0.1 is based on a high resolution (10 cal yrs) calibration curve (INTCAL98) based primarily on dendrochronological comparisons between the age of wood as determined by dendrochronology and by radiocarbon methods (Walker, 2005). The INTCAL98 calibration curve extends beyond the Holocene and as such, is suitable for Holocene conversions of ^{14}C ages to calendar years. Despite the advantages of the INTCAL98 calibration curve, due to the errors outlined previously, ^{14}C dates are expressed as probabilities ranging from 68% (1σ) to 95.4% (2σ) probability.

5.4.1.1 Accelerator mass spectrometry (AMS) ^{14}C dating

Derived from the development of radiocarbon dating during the late 1940s, AMS was developed in the 1980s (Wilson et al., 2005). AMS dating is a more advanced process of radiocarbon dating. Mass spectrometers separate the carbon atoms 14, 12 and 13 respectively (^{14}C ^{12}C and ^{13}C) to assess the ratio of ^{14}C to that of ^{12}C or ^{13}C, the age can then be determined by comparing the measured ^{14}C ratio with that of a standard known ^{14}C content (Walker, 2005). This process presents a less time consuming method of establishing the age of death (hours rather than weeks) and can process samples less than 1 mg due to the processing mechanism that does not need to count individual carbon atoms, but establish the ratio between them (Walker, 2005; Wilson et al., 2005).

A total of 16 AMS ^{14}C dates were obtained by this research using >10mg of clean unbroken non-specific planktonic foraminifera from the >150μm size fraction. Radiocarbon dating is can also be based on monospecific planktonic foraminifera, however there was an insufficient amount of any one species evident in all cores for all samples non-specific species were chosen so as to achieve the required amount for each dating sample. Five additional AMS^{14}C dates were acquired for core ODP 975B, based on ~10mg of the >125μm size fraction of the planktonic foraminiferal species *G. bulloides* (Jimenez-Espejo et al., 2007). Each AMS^{14}C date was converted into calendar years using the computer software CALIB 5.0.1 (Stuvier et al. 1998), using the Marine04 calibration curve dataset and a standard global ocean reservoir age (400 yrs) (Siani et al., 2001; Hughen et al., 2004). All AMS ^{14}C dates employed by this research are expressed using the 2σ calibration. As a

consequence of the reservoir effect, the application of a marine dataset is necessary to account for the variations in ^{14}C activity. Siani et al (2001) determined the regional average marine reservoir affect in the Mediterranean to be 390+/- 80 with local reservoir age (ΔR) of 35±70 yrs. Recent studies however, have suggested that significant variation has occurred in Mediterranean surface waters over time (Melki et al., 2009) and as such this research has applied the standard global ocean reservoir age (400 yrs), with no ΔR correction, as incorporated by the Marine04 calibration curve dataset (Hughen *et al*., 2004).

5.4.2 Oxygen Isotope analysis

Oxygen exists as three naturally occurring isotopes, oxygen 16, 17 and 18 (^{16}O, ^{17}O and ^{18}O). These three isotopes are incorporated into water molecules and it is the variation between the ratios of these isotopes that provide the basis for palaeoclimatic reconstruction, in particular the ratio between oxygen ^{18}O and ^{16}O (Walker, 2005). Variance in the oxygen isotope ratios from ice and deep sea cores is temperature dependent and can be used as a proxy for reconstructing climate change. During colder periods of the Earth's history (glacials) $H_2{}^{16}O$ is preferentially evaporated from the oceans, due to its lighter weight, and becomes trapped in the continental ice sheets, leaving the oceans enriched in water molecules with the slightly heavier ^{18}O *(figure 5.3)*. In contrast, during an interglacial ^{16}O is returned to the ocean by melting of the continental ice and as such the ratio of ^{18}O to ^{16}O increases *(figure 5.3)*. As a result of glacial/interglacial cycles can be determined by studying downcore variations in the oxygen isotope signal of past ocean water recorded in biogenic material.

Organisms such as foraminifera record the isotopic ratio of seawater in their carbonate shells. The ratio of oxygen isotopes are expressed in isotopic curves that can be correlated on a global scale to the orbitally tuned isotopic SPECMAP timescale, as established by Imbrie et al. (1984). However correlating between isotopic profiles is also open to sources of error. This error can manifest itself primarily in variable sedimentation rates between cores with subsequent differences in resolution, post depositional effects such as bioturbation and reworking by sea floor currents and/or dissolution effects to the calcareous foraminiferal test presenting a bias of only the more durable species (Walker, 2005). An additional source of error can also result due to the re-crystallization of the test on the ocean floor, which results in significant differences in the isotopic values of the

surface waters (Schrag, 1999). The re-crystallization structure is only evident under a Scanning Electron Microscope (SEM), subsequently samples that have been processed using a binocular microscope may have been entirely re crystallized and as such contain a combination of surface and bottom water isotopes. Pearson (2001) observed a recorded temperature 15°C warmer than that of crystallized samples from the same time frame, this raises a considerable level of doubt regarding samples that may have been processed without prior knowledge of crystallization. In additional to environmental forcings correlation between isotopic profiles are also subject to interpretation, where errors may arise between actual marine oxygen isotope stage (MIS) boundaries and subdivisions that exist, such as MIS 5 that has 5 substages (Walker, 2005).. Despite the possible source errors, oxygen isotope analysis provides a unique global stratigraphic correlation tool (Walker, 2005). All isotopic measurements are established using a mass spectrometer and calculated relative to an internationally accepted standard (Vienna Pee Dee Belemnite) V-PDB. The results are expressed as parts per mille (δ).

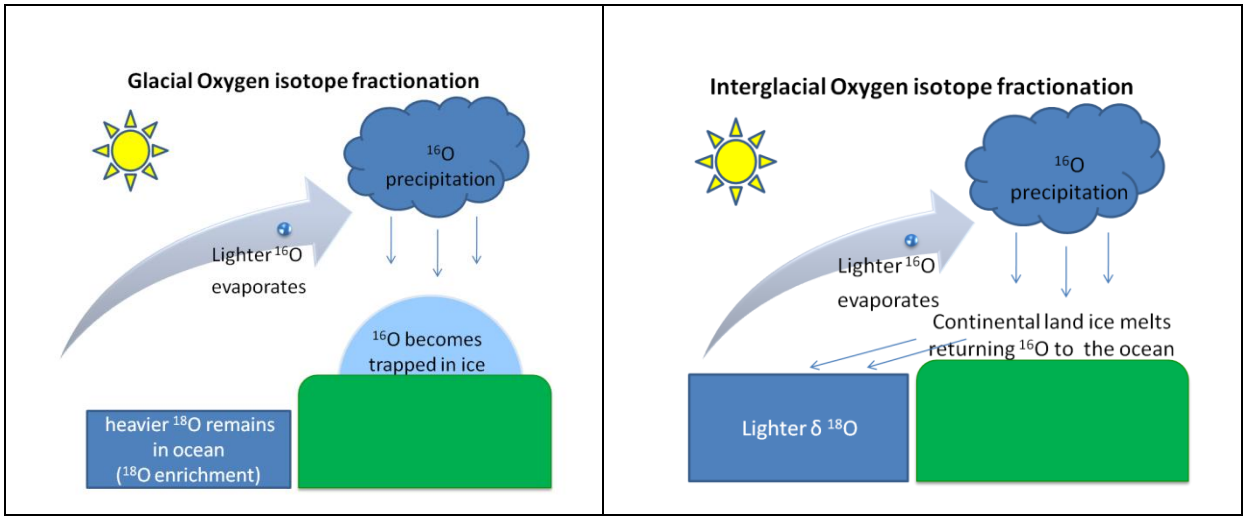

Figure 5.3. Schematic representation of isotopic fractionation of ^{16}O and ^{18}O during glacial and interglacial periods and its affect on marine oxygen isotopic ratios.

Of the four cores utilized in this research, oxygen isotopes were available for core ODP 975B. Performed at the School of Ocean and Earth Sciences, Southampton, England, the analyses was based on ~ 25 specimens (per sample) of *N. pachyderma* (dextral) from >150µm size fraction. The resultant age model for this core is based on peak-to-peak correlation with the oxygen isotope record of core MD95-2043 (Alboran Sea). Oxygen isotopic measurements for core MD95-2043 were deduced from analysis of ~25-30

specimens of the planktonic foraminiferal species *G. bulloides,* from the 300-355 µm size range, and were calibrated to the V-PDB standard (Cacho et al., 1999).

5.5 Artificial Neural Networks (ANNs)

ANNs are a form of artificial intelligence that has the capacity to 'learn' the relationship between different variables. For this research we utilised the learned relationship between planktonic foraminiferal abundance and SST in order to reconstruct SST down core. The applicability of the ANNs relies on the assumption that such a relationship exists between the variables for example planktonic foraminiferal assemblages and SST (Hayes et al., 2005). By observing the present day relationship between the variable (SST) and faunal abundances it can then be applied to fossil assemblages. The most significant disadvantage regarding ANNs is that the calibration equation does not define the contribution of individual variables to the resulting estimate. Advantageously however, the ANN calibration datasets are not as dependant on size of the calibration dataset and allow for the extrapolation of variables (i.e. SST) outside the range of the calibration dataset (Kucera, 2003).

This research utilises the calibration dataset established by Hayes et al. (2005) that presented the relationship between planktonic foraminiferal faunal assemblages and SSTs. It was particularity suited to this research as the calibration dataset is based in the same locations as this research. The calibration dataset is composed of 23 planktonic foraminiferal species (>150µm size fraction) from 145 Mediterranean Sea and 129 North Atlantic Ocean core tops (Hayes et al., 2005). North Atlantic Ocean core tops were analysed in order to provide comparable analogues for glacial Mediterranean Sea planktonic foraminiferal assemblages (Hayes *et al*., 2005). However, North Atlantic cores were utilised with caution to avoid the over-representation of a particular environmental variable, and as such only selected cores were applied in the training of the dataset. In order to reduce the error of over-representation of a particular environmental variable or the lumping together of cryptic species core sample locations included were chosen that represented a non biased faunal distribution pattern within a specific spatial range (Hayes et al., 2005).

Annual, winter (January-March) and summer (July-September) SST data from the World Ocean Atlas (WOA, Vol. 2) was also extracted from a depth of 10m in association with the core top locations (Hayes et al., 2005). The ANN produced prediction errors

ranging between 1.1 and 0.5 °C with winter reconstructions showing the lowest error rate (Hayes et al., 2005).

5.6 Mapping Tools

Maps depicting core locations were created using the download mapping software package PanMap. PanMap mapping software package is operated by the Alfred Wegener Institute for Polar and Marine Research and the Centre for Marine Environmental Sciences and available to download from the PANGAEA website at the following link: http://www.PANGAEA.de/Software/PanMap. PanMap is a global mapping tool that facilitates numerous geographic layers for different resolutions and purposes. Maps created using this package were based on a primary imported Global Bathymetric Chart of the Ocean (GEBCO) layer. The software package facilities the input of latitude and longitude values to represent point locations, as is done in this research to represent geographical locations and the deep sea core locations

Chapter 6: Chronological Framework

The chronological framework for this research is based on a total of 21 AMS ^{14}C dates for all four cores (*Table 6.1*). Radiocarbon ages obtained by this research were determined by AMS at the Beta Analytic Radiocarbon Dating Laboratory on non specific planktonic foraminiferal assemblages (>150µm). Whole non specific species were sampled due to the high resolution of the cores, as we were working with less material there was no single species that was present to reach the required sample weight to process for AMS dating (>10µm).

No:	Core	Depth (cm)	Samples	^{14}C (yrs BP) Radiocarbon	Error (± yrs)	Mean Calendar Age (kyr BP)	Source
1	**M40/4 82-2 SL**	1.5	0-1cm,1-2cm, 2-3cm (Section 6)	820	40	429.5	*1*
2		56	24-25cm (Section 5)	3980	40	3978.5	*1*
3		68	36-37cm, 38-39cm (Section 5)	4620	40	4841.5	*1*
4		74	42-42cm, 44-45cm (Section 5)	4770	40	5042	*1*
5		97	68-69cm (Section 5)	5980	40	6387.5	*1*
6	**ODP 975B**	9.0	8-10cm	2455	27	2099.5	*2*
7		29.5	29-30cm	5070	40	5427	*1*
8		37	36-38cm	6160	50	6593	*1*
9		51	50-52cm	7070	37	7549.5	*2*
10		91	90-92cm	13330	60	15283.5	*2*
11		131	130-132cm	15870	80	18790	*2*
12		190	45-47cm (Section 2)	19460	110	22610	*2*
13	**M40/4 80 SL**	0.5	0-1cm	1780	40	1329	*1*
14		10.5	10-11cm	5680	40	6082.5	*1*
15		20.5	20-21cm	8450	40	9089	*1*
16		40.5	40-41cm	11000	40	12580	*1*
17	**ODP 974B**	3.5	3-4cm	1680	40	1229.5	*1*
18		33.5	33-34cm	2490	40	2161	*1*
19		57.5	57-58cm	3730	40	3673.5	*1*
20		69.5	69-70cm	5040	40	5398	*1*
21		87.5	87-88cm	7350	40	7814	*1*

Table 6.1. AMS ^{14}C dating control points for all four cores. AMS ^{14}C dates are sourced from *(1)* this research and *(2)* Jimenez-Espejo et al., (2007).

All AMS ^{14}C dates were calibrated (cal) using the calibration program Calib 5.0.1 (Stuvier et al., 1998) using the Marine 04 calibration data set (Hughen et al., 2004). All ages are calibrated to 2 sigma (95% probability), which includes the universal marine reservoir age correction of ~400 yrs (Siani et al., 2001; Melki et al., 2009). (See Chapter 5 section 5.3.1).

Utilising AMS dating control points, a calendar age-depth plot was constructed for each core *(figure 6.1)*.

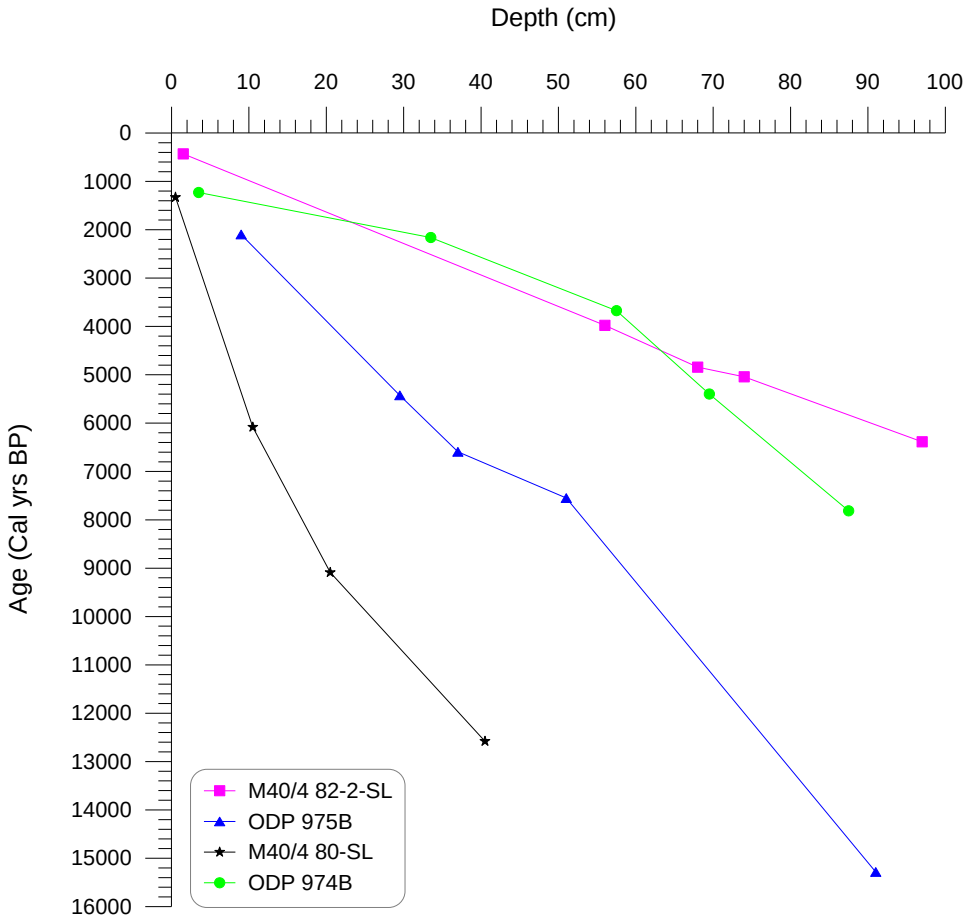

Figure 6.1. Age/depth profile as established using AMS ^{14}C dating.

Sedimentation rates between the cores varied, with an average sedimentation rate of 13.07, 15.95,7.36 and 2.88 cm/kyr for cores ODP 974B, M40/4 82-2 SL, ODP 975B and M40/4 80-SL respectively.

M40/4 82-2SL	Sed. Rate (cm/kyr)	ODP 975B	Sed. Rate (cm/kyr)	M40/4 80SL	Sed. Rate (cm/kyr)	ODP 974B	Sed. Rate (cm/kyr)
0-1.5cm	3.49	0-9cm	4.29	0-0.5cm	0.38	0-3.5cm	2.85
2-56cm	15.36	10-29.5cm	6.16	1-10.5cm	2.10	4-33.5cm	31.21
57-68cm	13.90	30-36.5cm	6	11-20.5cm	3.33	34-57.5cm	15.87
69-74cm	29.93	37-51cm	15.6	21-40.5cm	5.73	58-69.5cm	6.96
75-97cm	17.09	52-91cm	60			70-87cm	7.45

Table 6.2. Variations in core sedimentation rates (cm/kyr) as determined between each C^{14} AMS age control poin.t

Chapter 7: Variation in the coiling direction of the Planktonic Foraminiferal Species *Globorotalia truncatulinoides* in the Western Mediterranean Sea during the Holocene

7.1 Introduction

Planktonic foraminifera with trochospiral shells are present in two coiling varieties, as a sinistral (left) and a dextral (right) variant. Foraminifera are determined sinistrally coiled, if, when viewed from the dorsal side up the test chambers are added in an anticlockwise direction and dextrally coiled if the chambers are added in a clockwise direction (Bolli, 1950). Some foraminifera follow a distinct coiling preference and others exhibit both coiling variants and show distinct shifts in coiling direction. One such planktonic foraminiferal species, *Globorotalia truncatulinoides* exhibits morphological asymmetry through the presence of both sinistrally and dextrally coiled specimens *(figure 7.1)*.

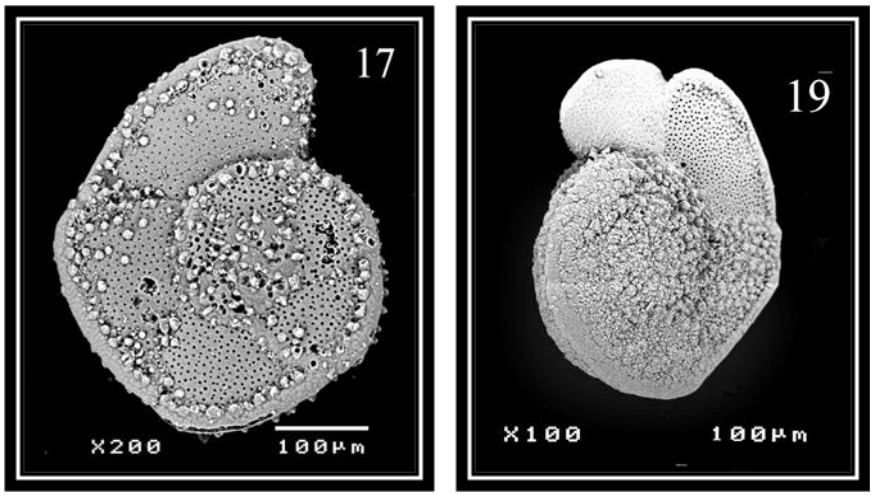

Figure 7.1. SEM images of the planktonic foraminiferal species *G. truncatulinoides*. Image 17 illustrates the dorsal view of the dextral (right) coiling variant and image 19 illustrates the dorsal view of the sinistral (left) coiling variant (from Hayes, 1999).

Initial studies observing the variation between dextrally and sinistrally coiled *G. truncatulinoides* highlighted the species' potential as a biostratigraphic tool (Bolli, 1950, 1951; Ericson, 1954, 1961; Herman, 1972). The exact reason for coiling direction change is not yet fully understood. Earlier studies focused on environmental forcing, having observed that the distribution between coiling varieties of *G. truncatulinoides* follows distinct environmental conditions (Ericson, 1954; Theide, 1971; Cifilli 1965; Herman, 1972; Lohmann and Schweitzer, 1990; Wilke et al., 2009). Recent work on other species

(Darling and Wade, 2008) indicates a genetic component but it could not yet be shown in fact (de Vargas et al., 2001; Ujiié et al., 2010).

This chapter presents the coiling variation of *G. truncatulinoides* in four western Mediterranean Sea cores during the Holocene, with the objective to assess the applicability of this species as a biostratigraphic tool within the western Mediterranean Sea *(figure 7.2)*. An observed change in the coiling pattern of *G. truncatulinoides* would provide a biostratigraphic marker that is easily attainable to researchers without the initial expense or time consumption of AMS dating methods. In addition this research will also address the palaeoecological changes as defined by present day ecological habitats from both the sinistral and dextral variants of *G. truncatulinoides*. Subsequent downcore analysis of coiling variation could determine if this ecological distinction prevailed throughout the Holocene.

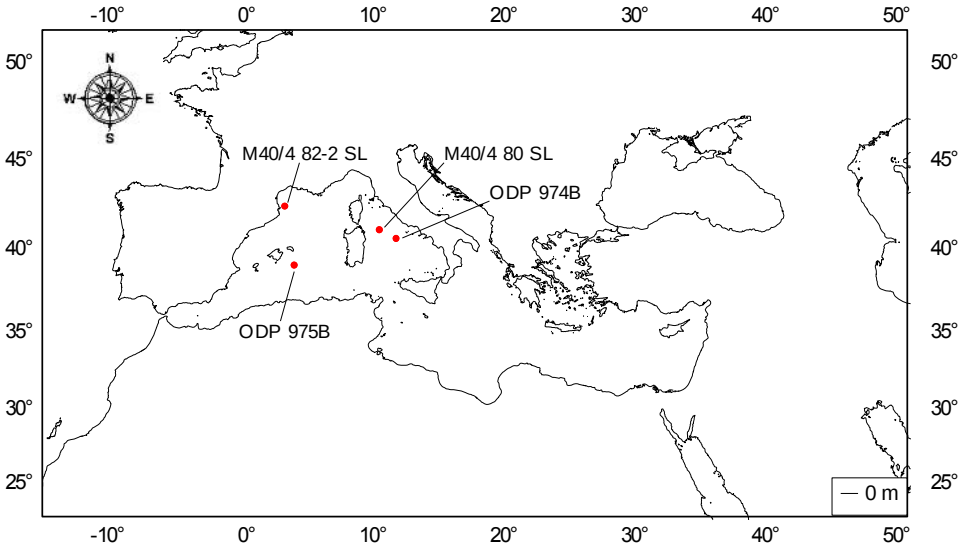

Figure 7.2. Map illustrating the locations of the 4 western Mediterranean Sea Cores (see chapter 5 for core details).

Understanding the distribution of sinistrally and dextrally coiled variants, with respect to environmental conditions, has become the focus of many studies (Lohmann and Schweitzer., 1990; Le Grand, 2004; Wilke et al., 2009; Ujjié et al., 2010). In order to fully understand the significance of *G. truncatulinoides* and its coiling patterns in the western Mediterranean Sea it is necessary to understand the modern day habitat preferences of the species in the present day oceans. The following literature will provide the present day

characteristics and features of *G. truncatulinoides* including its life cycle patterns, cryptic diversity and distribution.

7.1.2 *G. truncatulinoides*

7.1.2.1 Life Cycle

Extending to a depth of > 800m, *G. truncatulinoides* exhibits a yearly life cycle with different life stages recorded at different seasons and water depths *(figure 7.3)* (Hemleben et al., 1989; Lohmann and Schweitzer., 1990; Pujol and Vergnaud Grazzini, 1995; Wilke et al., 2009).

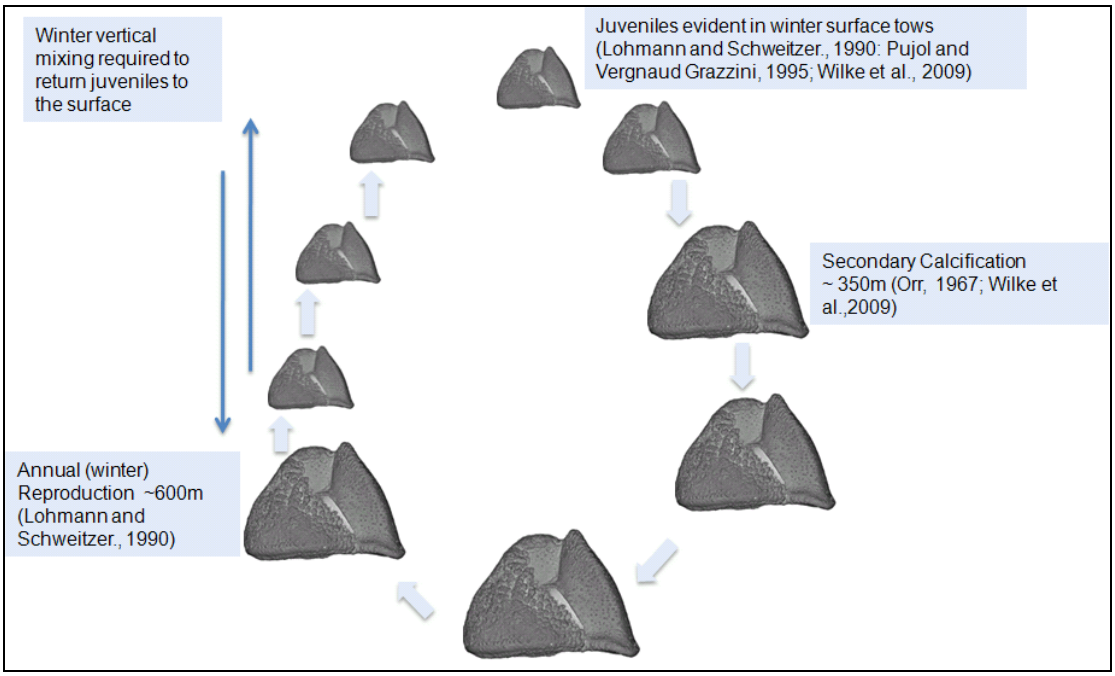

Figure 7.3. Schematic representation of the life cycle of *G. truncatulinoides* and associated water depth distribution. The light blue arrows represent the life sequence of *G. truncatulinoides* and the dark blue vertical arrows signify the vertical mixing of the water column to return juveniles to the surface waters.

Reproduction of the species is believed to occur during the winter at depth, where vertical mixing of the water column is required for the migration of juveniles to surface waters (Lohmann and Schweitzer., 1990). *G. truncatulinoides* continues its life cycle by migrating down through the water column, adding an additional calcite layer (secondary crust) (Bé and Lott, 1964) at ~350m depth when reaching cooler waters below the thermocline (Orr, 1967; Lohmann and Schweitzer, 1990; Wilke et al., 2009). Le Grand (2004) suggests that 30% of the test calcification of *G. truncatulinoides* occurs in surface layers and 70% in the thermocline.

7.1.2.2 Genetic Diversity within G. truncatulinoides

An understanding of cryptic diversity in planktonic foraminiferal species is vital when interpreting palaeoenvironments, as different cryptic species within morphospecies may represent different habitats. Recent research undertaken in the North Atlantic Ocean, observed a reduction in the prediction error rate (>20%) of the artificial neural networks (ANNs) with a greater awareness of cryptic diversity (Kucera and Darling, 2002). Genetic analysis on numerous species of planktonic foraminifera has suggested that cryptic diversity is common in this group (de Vargas et al., 2001; Kucera and Darling, 2002; Darling and Wade, 2008). Of particular importance to this research, *G. truncatulinoides* has recently been discovered to represent a complex of 5 genetically different types (Types 1–4) (de Vargas et al., 2001) and type 5 (Ujiié and Lipps, 2009). Types 1-4 were identified from genetic data obtained from plankton tows in the Atlantic Ocean and the Mediterranean Sea *(figure 7.4)* (de Vargas et al., 2001). The initial temporal events relating to the cladogenesis of *G. truncatulinoides* types 1-4 was established by de Vargas (2001), identifying a differentiation between warm and cold morphotypes at ~300 ka. Further differentiation was established by Renaud and Schmidt (2003) who indicated the emergence of 2 warm morphotypes (types 1 and 2) at ~ 170 ka and 2 cold morphotypes (types 3 and 4) at ~120 ka *(figure 7.5)*. Type 5 is present in the northwest Pacific Ocean and exists entirely as a dextral coiling variant *(figure 7.4)* (Ujiié and Lipps, 2009). Type 2 and type 5 are the only genetic types that contain the right coiling variant, Type 5 has an environmental preference similar to that of type 2, where the genetic divergence is 3.9% compared to 8.0% with type 1. Type 5 has to date, only been identified in oligotrophic subtropical areas in the central water of the North West Pacific Ocean (Ujiié and Lipps, 2009).

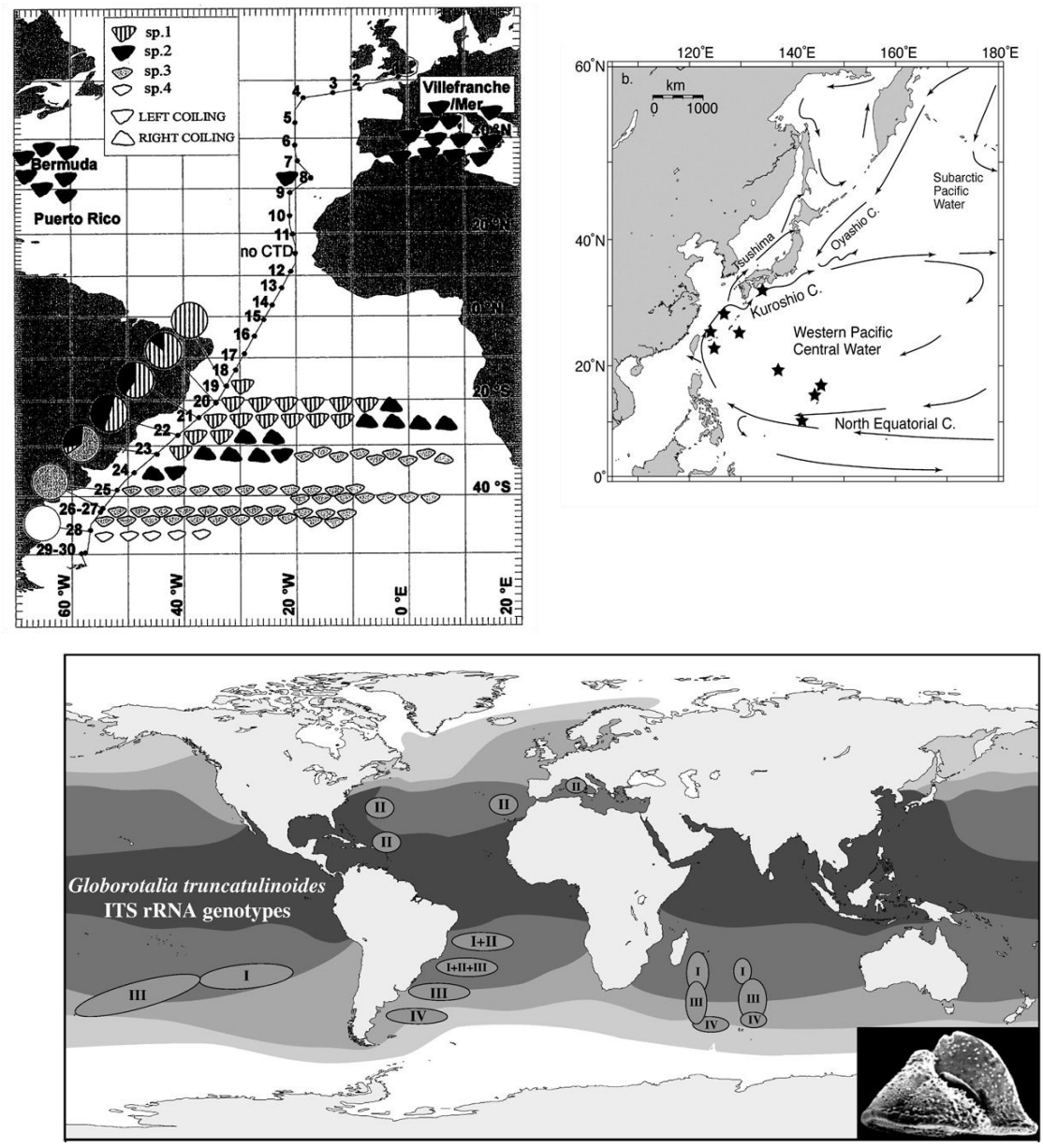

Figure7.4. represents the geographic distribution of the genetic variants of *G. truncatulinoides*. The top left picture represents geographic distributions of the four *G. truncatulinoides* genotypes. Each symbol is representative of a single genotype. The ratio of different genotypes is represented by pie charts for each location (from de Vargas et al., 2001). The top right represents the sampling sites (stars) indicating the location of *G. truncatulinoides* (type 5) and associated surface currents in the NW Pacific (from Ujiié and Lipps, 2009). The bottom picture represents the geographical distributions of *G. truncatulinoides* type 1- 4. Note the presence of type 2 only in the North Atlantic Ocean and the Mediterranean Sea, in contrast to the southern oceans where a combination of types 1-4 exist (shaded areas represent biogeographic regions of foraminiferal distribution-see Ch4 fig. 4.2) (From Darling and Wade, 2008).

While all 5 genetic types of *G. truncatulinoides* exist in the southern hemisphere, type 2 is the only morphotype that exists in the Northern Hemisphere *(figure 7.4)* (de Vargas et al., 2001; Darling and Wade, 2008; Ujiié and Lipps, 2009). Consequently the remainder of this discussion will focus on regions where only type 2 has been identified in order to ensure

correct ecological comparisons are made, as types 1, 3 and 4 are known to have independent ecological preferences to type 2 (de Vargas et al., 2001, Renaud and Schmidt, 2003).

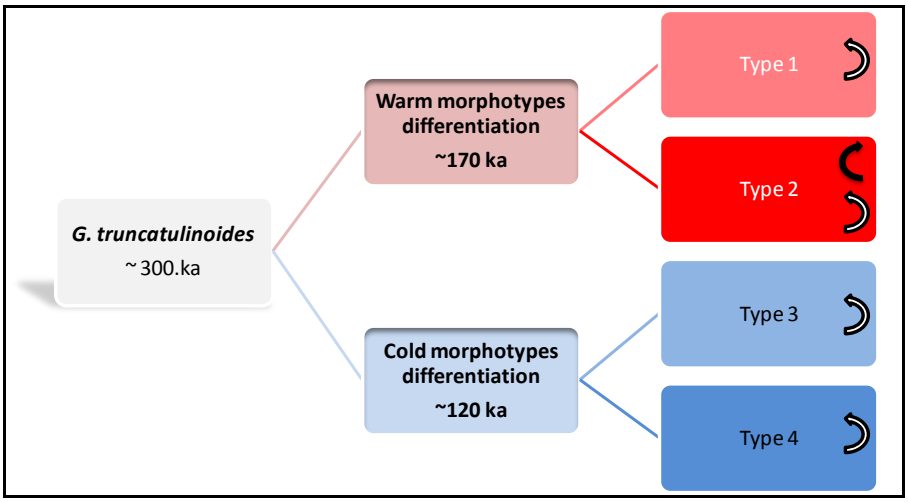

Figure 7.5. Schematic representation of the temporal divergence of *G. truncatulinoides* genetic types 1-4. Direction of arrows for each of the 4 morphotypes indicates the associated coiling variety, note only type 2 contains both coiling variants (de Vargas et al., 2001; Renaud and Schmidt, 2003).

7.1.2.2.1 Distribution of G. truncatulinoides (Type 2)

Under present day conditions, populations of *G. truncatulinoides* in the western Mediterranean Sea are dominated by the left coiling variety (Thunnel, 1978; Pujol and Vergnaud Grazzini, 1995). In particular, the species is abundant during the winter season, where optimum water column conditions with high nutrient availability promote juvenile growth and (Pujol and Vergnaud Grazzini, 1995) *(figure 7.6)*. Hydrographic conditions in the western Mediterranean basin, with winter SSTs ranging between ~12.6°C (Gulf of Lion) and ~14.8°C (of the North African coast), are associated with turbulent mixing of the water column, supporting nutrient advection into the surface waters (Pujol and Vergnaud Grazzini, 1995). The concurrent shoaling of the DCM to ~40-50m accompanies the peak abundances of *G. truncatulinoides* at this time. Similar abundances are also observed at ~300m. These depths correlate with areas of high nutrient availability (Pujol and Vergnaud Grazzini, 1995).

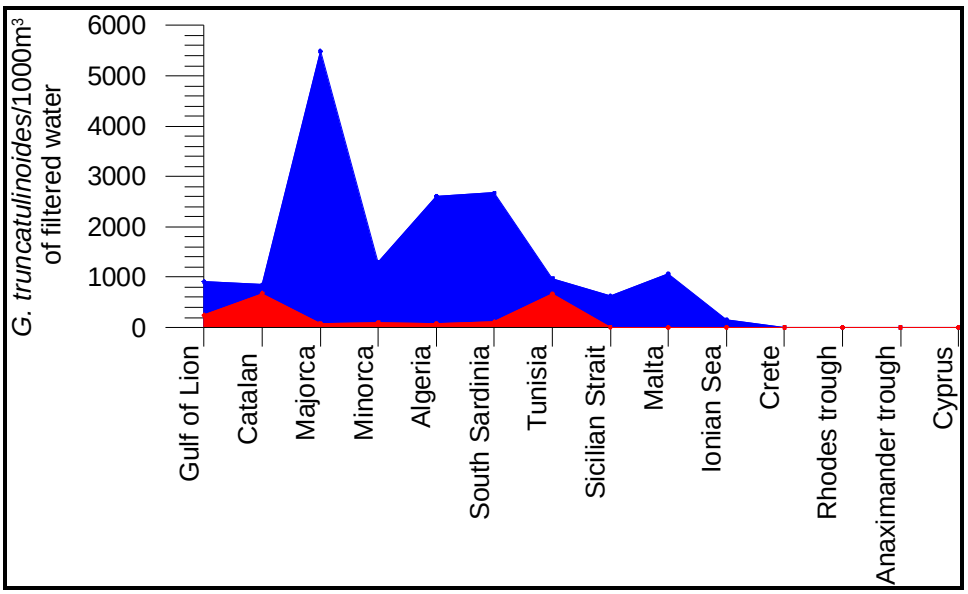

Figure 7.6. Present day abundance of *G. truncatulinoides* per 1000m^3 of filtered water in the Mediterranean Sea during 2 sampling seasons. The shaded blue area represents late winter (February) plankton tows and the shaded red area represents late summer (September) tows (see chapter 4 figure 4.12 for map illustrating sampling locations. Core M40/4 82-2 SL corresponds to the Gulf of Lion sampling station and ODP 975B corresponds closest to the Majorcan and Minorca stations (data from Pujol and Vergnaud Grazzini, 1995).

In contrast, during summer, when SSTs are higher (between ~21°C - ~24.5°C) the abundance of *G. truncatulinoides* is low *(figure 7.6)* (Pujol and Vergnaud Grazzini, 1995). The presence of a strong summer pycnocline (25-50m) results in a stratified water column which restricts the movement of nutrients to the surface mixed layer. As a consequence, maximum abundances of *G. truncatulinoides* are confined to deeper waters (~125m) (Pujol and Vergnaud Grazzini, 1995).

Based on plankton tows, sediment traps and surface sediments, a recent study concluded that winter cooling and convective overturn are the primary factors controlling the population of *G. truncatulinoides* off the northwest African coast (Wilke et al., 2009). During the winter months the surface waters are characterised by a chlorophyll maximum reflecting a phytoplankton bloom. This corresponds with maximum shell abundances (up to 11000/1000m^{-3}) of *G. truncatulinoides* (Wilke et al., 2009). In contrast, during spring and summer, when the seasonal thermocline has been re-established, surface waters are depleted of nutrients and the smaller populations of *G. truncatulinoides* are associated with the DCM below the mixed layer (Wilke et al., 2009). This relationship between seasonal stability of the water column (mixed or stratified) and associated nutrient enrichment, and peak abundances of *G. truncatulinoides* has also been observed in the North Atlantic Ocean (Bé, 1959; Lohmann and Schweitzer, 1990), the Bermuda Sea (Bé, 1960), the Western

North Atlantic (Tolderlund and Bé, 1971) and the Caribbean (Bé et al., 1971; Schmuker and Schiebel, 2002).

7.1.2.2.2 Coiling Distribution

As discussed previously, *G. truncatulinoides* (type 2) is represented by both sinistral and dextral coiling variants, the distribution of which has been discussed by several authors (Ericson et al., 1954; Bé et al., 1959; Bé and Hamlin, 1967; Cifelli, 1971; Thiede, 1971; Herman, 1972; Lohmann and Schweitzer, 1990; Wilke et al., 2009). Ericson et al. (1954) demonstrated that the North Atlantic Ocean could be subdivided into distinct zones based on the dominance of dextral or sinistral tests *(figure 7.7)*.

Three zones were identified corresponding to transitional waters in the northwest, subtropical waters in the central zone and tropical waters in the south *(figure 7.7)*. The authors concluded that in the absence of physical barriers, coiling preference was governed by the presence of ecological and/or environmental factors. Herman (1972) suggested that the distribution reflects the prevailing oceanic currents, noting that the sinistral variety broadly corresponds to the path of the warmer Gulf Stream and the North Atlantic current, while the dextral variety favours the cooler Northeast Atlantic water mass. The emphasis on SST as a controlling factor on coiling variation is further highlighted in 2 sediment cores in the eastern Mediterranean Sea. Postglacial sediments contained sinistrally coiled *G. truncatulinoides* whereas the dextral variety appears to be confined to the glacial sediments (Herman, 1972).

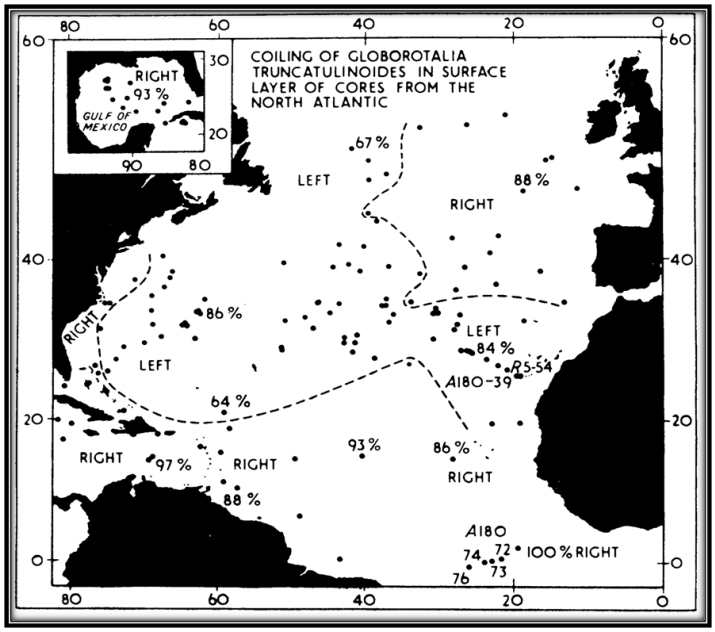

Figure 7.7 Graph depicting the representation of the coiling preference of *G. truncatulinoides* in the North Atlantic Ocean. The northeast and southerly regions are dominated by the dextral coiling variant with the central region dominated by the sinistral coiling variant (from Ericson et al., 1954).

7.3 Chronological Framework

In order to determine the applicability of *G. truncatulinoides* as a biostratigraphic tool, the time stratigraphic framework of this research (see chapter 6), was largely focused on the species coiling direction change. Samples in each core representing intervals of significant coiling direction change such as the peak abundances of the dextral coiling variant were processed for AMS dates. Additional AMS ^{14}C dates were acquired in close proximity to the coiling change events of the sinistral and dextral varieties in order to provide an accurate temporal representation of the biostratigraphic event. A total of 21 AMS ^{14}C dates were applied to establish the chronological framework for this research, 5 for core M40/4 82-2 SL, 7 in core ODP 975B, 5 in core M40/4 80 SL and 4 in core ODP 974B.

7.4 Results

7.4.1 Distribution of *G. truncatulinoides*

Relative abundance variations of *G. truncatulinoides* in all 4cores indicate a similar pattern, this pattern can be divided into distinctive phases of Holocene abundance based on the appearance and disappearance of the species *(figure 7.8)*. to allow for correct interpretation of the faunal abundance variation a 95% confidence interval has been established for the percentage values relating to *G. truncatulinoides* sinistral and dextral in this chapter. The

faunal abundance confidence intervals are presented in figures 7.9 A and B and indicate that the faunal abundance values are true representations of a mid Holocene dextral peak in abundance. The earliest, Phase 1 (~11.2 – 8.6 cal kyr BP) present only in two cores (ODP 975B and M40/4 80 SL) is characterised by a small peak in the relative abundance values where *G. truncatulinoides* contributes ~ 6% of the faunal assemblage *(figure 7.8)*.

In contrast, phase 2 (8.6 – 5.1 cal kyr BP) present in all four cores, identifies with the early Holocene disappearance of *G. truncatulinoides* from where it remains almost absent in all cores during this timeframe (*figure 7.8)*.

The mid to late Holocene is represented by Phase 3 (5.2 cal kyr BP – Present) marking the reappearance of both sinistral and dextral *G. truncatulinoides* and the onset of a significant increase in abundances of *G. truncatulinoides* where the relative contribution to the faunal assemblage ranges between 5 and 14%. This faunal contribution in Phase 3 is primarily dominated by the sinistral coiling variety, however, at ~4.4 cal kyr BP a faunal abundance peak (between 2 and 8%) in the dextral coiling variety is observed at all locations *(figure 7.8)*.

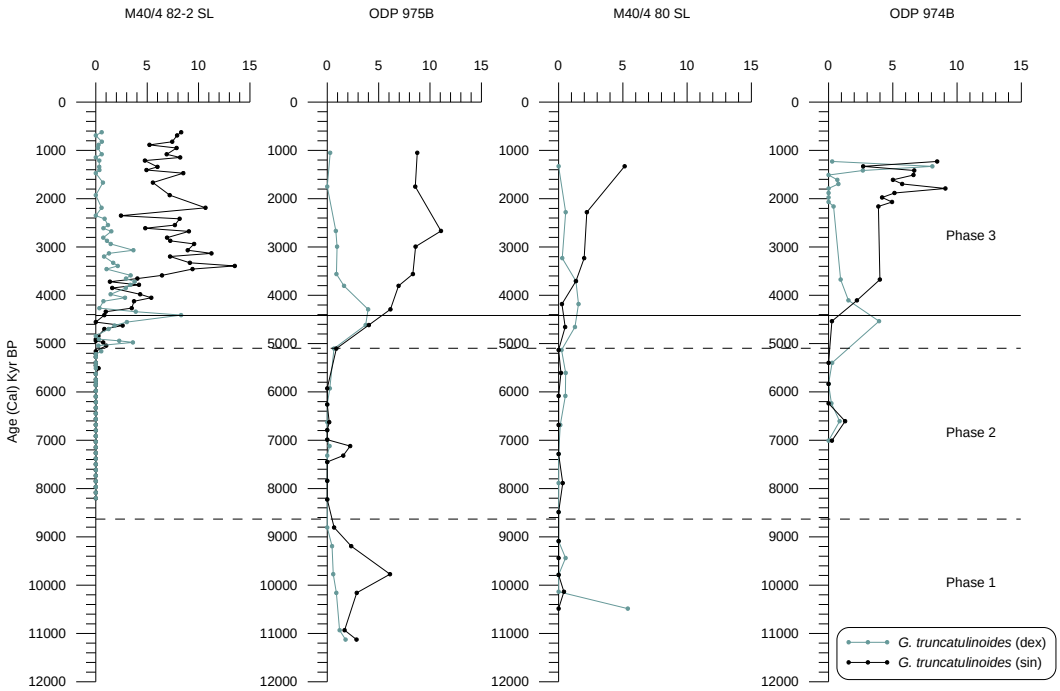

Figure 7.8 The relative faunal abundances of *G. truncatulinoides* (sinistral and dextral). The solid black line represents the faunal peak of *G. truncatulinoides* (dextral). The dashed lines indicate the 3 phases of abundance distribution: 1, 2 and 3 (see text).

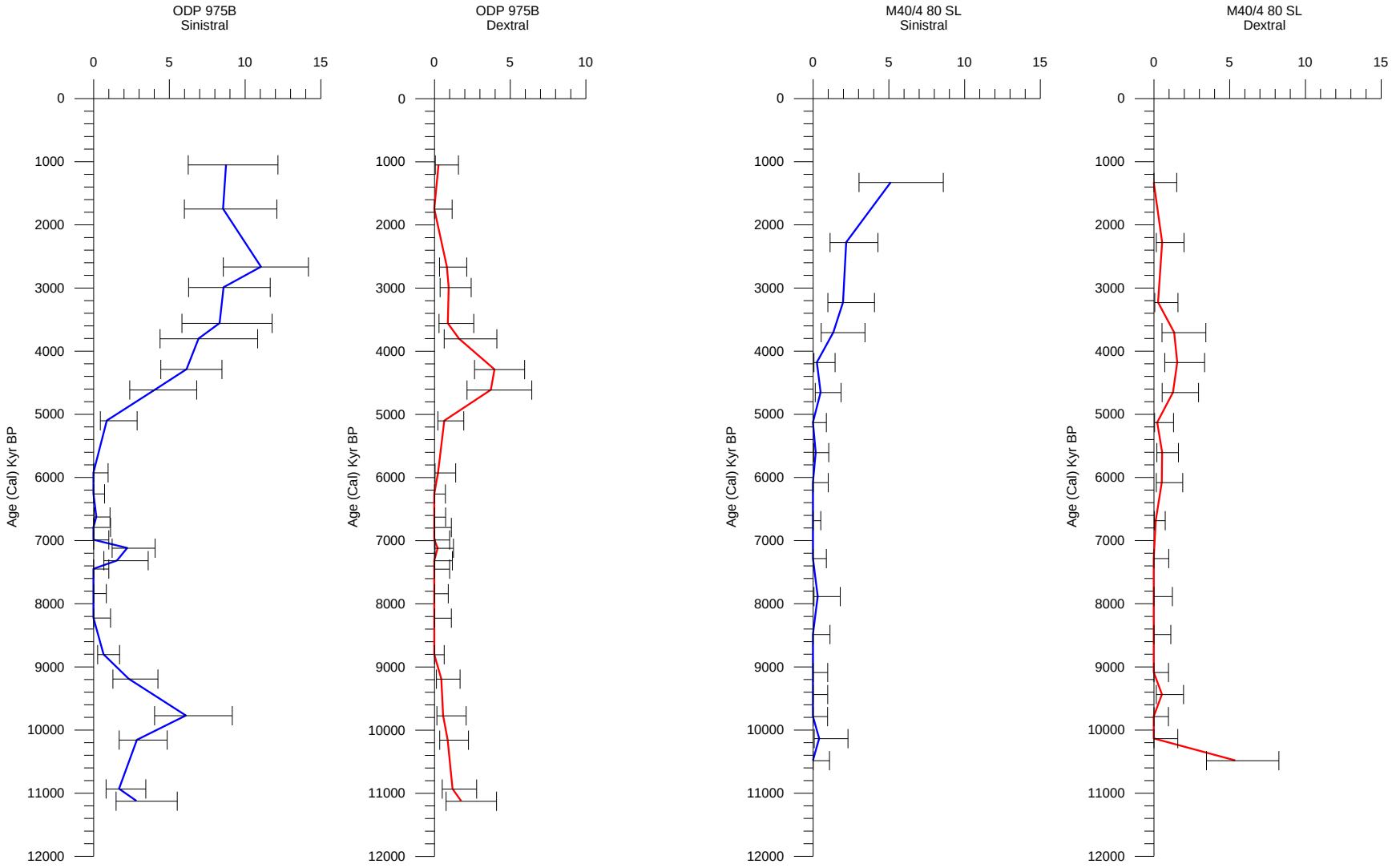

Figure 7.9A. Plotted 95% confidence intervals for the faunal abundance of *G. truncatulinoides* sinistral and dextral for core M40/4 80 SL and ODP 975B.

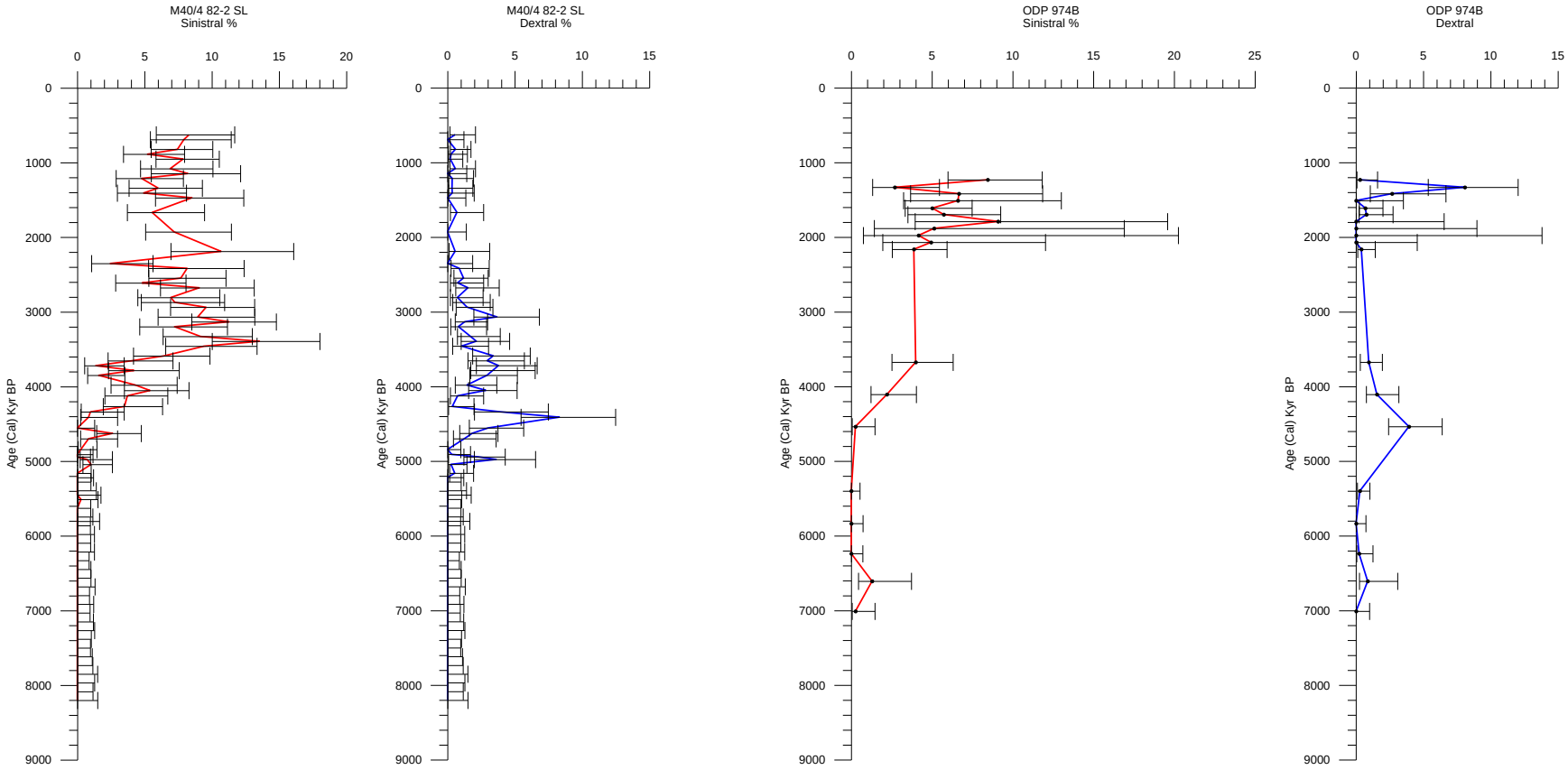

Figure 7.9B. Plotted 95% confidence intervals for the faunal abundance of *G. truncatulinoides* sinistral and dextral for core M40/4 82-2 SL and ODP 974B.

Further investigation into the observed pattern between sinistrally and dextrally coiled *G. truncatulinoides*, reveals elevated relative percentages (based on counts of >10 specimens, see chapter 5) of dextral *G. truncatulinoides* in each core ranging between 5.4 – 4.4 cal kyr BP accounting for ~80% of the *G. truncatulinoides* population *(figure 7.10)*. This *G. truncatulinoides* dextral peak occurs in all cores at ~ 5.0 cal kyr BP (5.4 – 5.2 cal kyr BP). 95% confidence interval bars plotted on the graph show that despite the associated percentage range there is still an obvious pattern of dextral dominance.

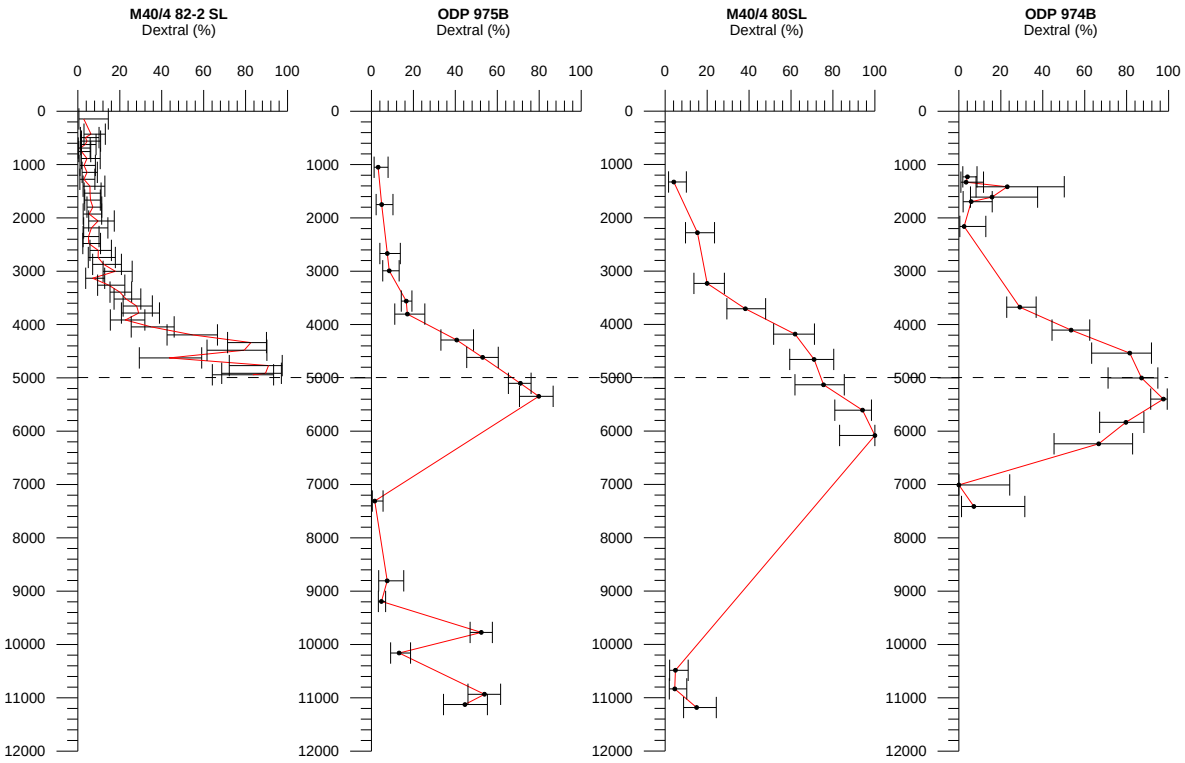

Figure 7.10. Graph representing the relative dextral coiling abundance of the total *G. truncatulinoides* population in 4 western Mediterranean Sea cores. The dashed line represents the interval of peak dextral coiling abundance, recorded in samples with a minimum of 10 *G. truncatulinoides* specimens.

7.4.2. Sea Surface Temperature Variability

ANN SST reconstructions are based on percentage data from a range of planktonic foraminiferal species including *G. truncatulinoides*. However, the calibration dataset did not distinguish between the two coiling varieties and as such the resulting SST reconstruction is independent of coiling direction. It is important to note that only SST variations >2°C have been considered as significant due to the error (between 0.5 and 1.1°C) associated with ANN SST reconstructions

It is immediately clear, that although a similar trend exists between the cores, the Gulf of Lion record displays the coldest Holocene SSTs (Holocene annual mean = 15.64ºC), while the Balearic basin and the Tyrrhenian Sea are marginally warmer (Holocene annual mean = 17.63ºC and ~18ºC respectively). An early to mid Holocene mean Annual SST reduction is observed in all cores between ~8.0 and 5.0 cal kyr BP *(figures 7.11 and 7.12)*. Corresponding to minimal abundances of *G. truncatulinoides*, this decrease in SST is more pronounced in Gulf of Lion record (~3.5ºC) compared to the Tyrrhenian Sea (between 1.5 and 2.5ºC) and the Balearic basin (~1 ºC) records, however Summer SST in the Balearic basin indicate a 2°C SST reduction at this time. A mid-late Holocene warming records the highest SSTs, peaking at ~ 2.0 cal kyr BP in the Gulf of Lion at ~ 17.5ºC, the Balearic basin shows an earlier warming at ~ 2.6 cal kyr BP however this falls within the error associated with ANN SST reconstruction and as such is subject to debate. The Tyrrhenian Sea core M40/4 80 SL also indicates a mid to late Holocene warming (>2°C) reaching maximum SST at ~ 2.0 cal kyr BP.

Both the sinistral and dextral coiling varieties of *G. truncatulinoides* appear to indicate different responses to the variability in SSTs. The initiation of the mid Holocene warm period coincides with peak abundances (>70%) of dextrally coiled *G. truncatulinoides* with respect to the total population of the species. However as SSTs continue to increase the dominance of the dextral variant is replaced by the sinistral variant. This pattern is also reflected in the faunal assemblages indicating that the sinistrally coiled *G. truncatulinoides* in particular, may demonstrate a potential correlation with SST.

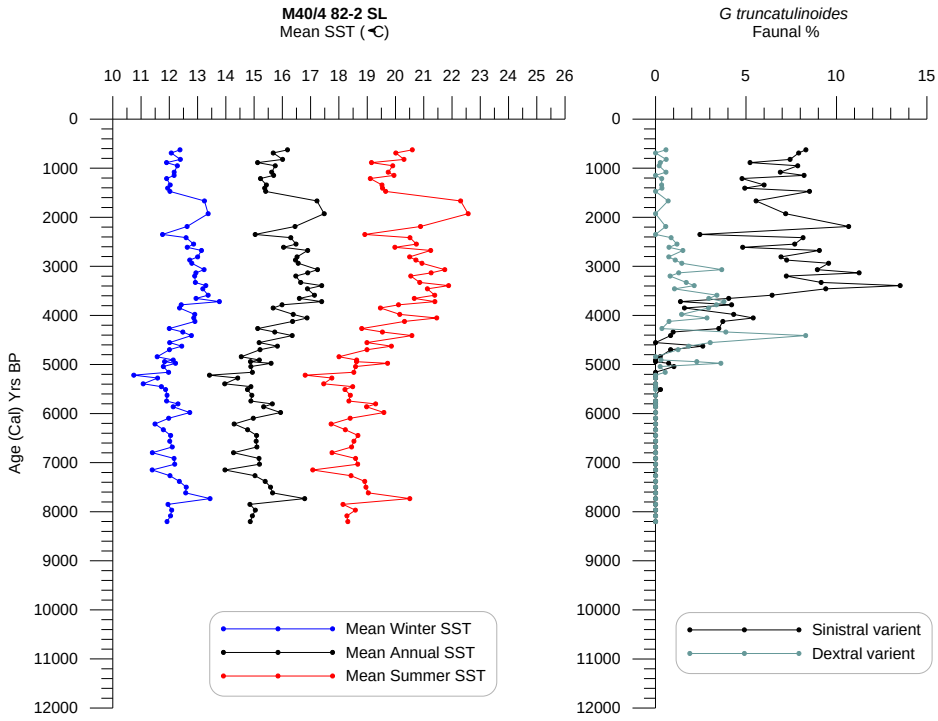

Figure 7.11A Graph illustrating the mean winter, annual and summer SSTs reconstructed using the ANN and corresponding *G. truncatulinoides* (sinistral and dextral) faunal abundance values for the Gulf of Lion.

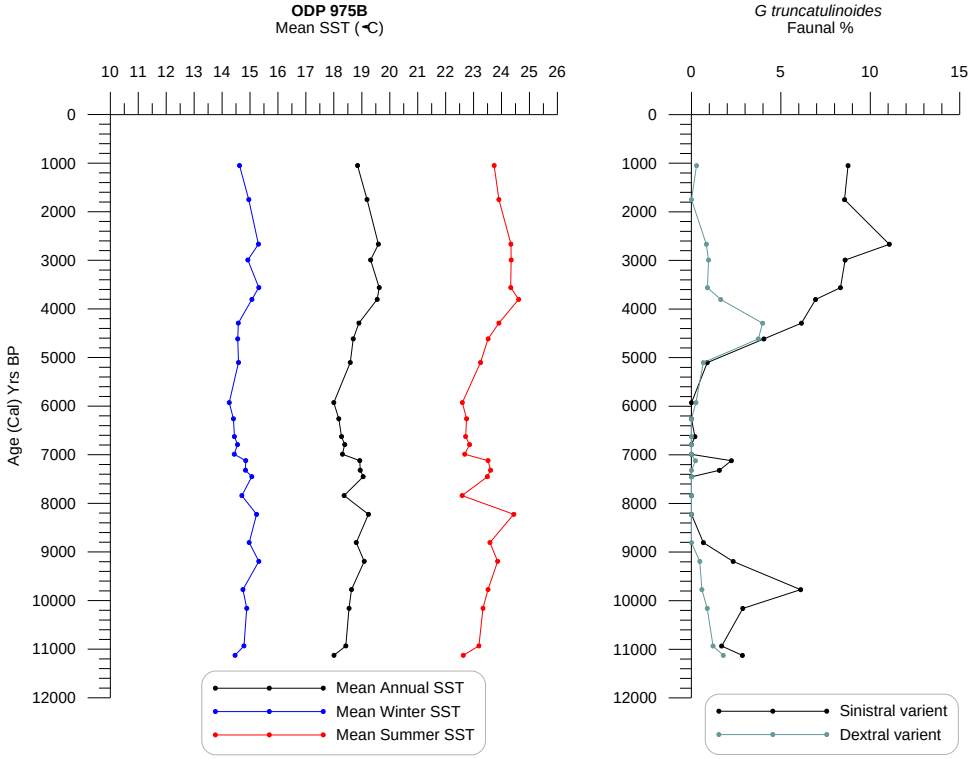

Figure 7.11B. Graph illustrating the mean winter, annual and summer SSTs reconstructed using the ANN and corresponding *G. truncatulinoides* (sinistral and dextral) faunal abundance values for the Balearic basin.

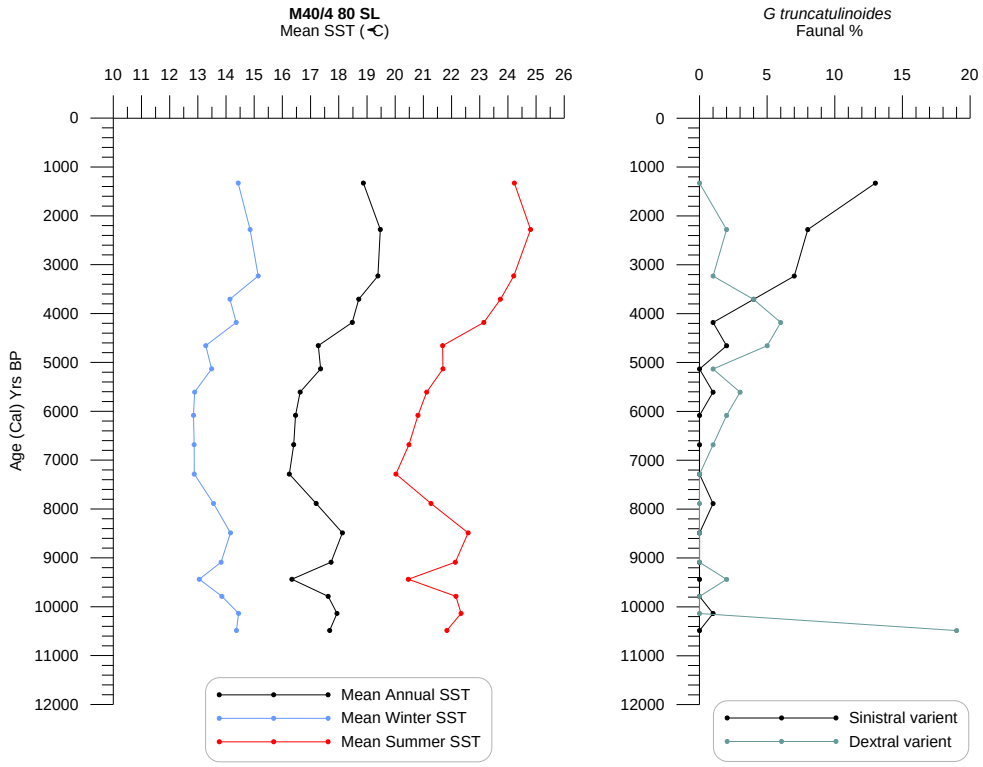

Figure 7.12A. Graph illustrating the mean winter, annual and summer SSTs reconstructed using the ANN and corresponding *G. truncatulinoides* (sinistral and dextral) faunal abundance values for Tyrrhenian Sea core M40/4 80 SL.

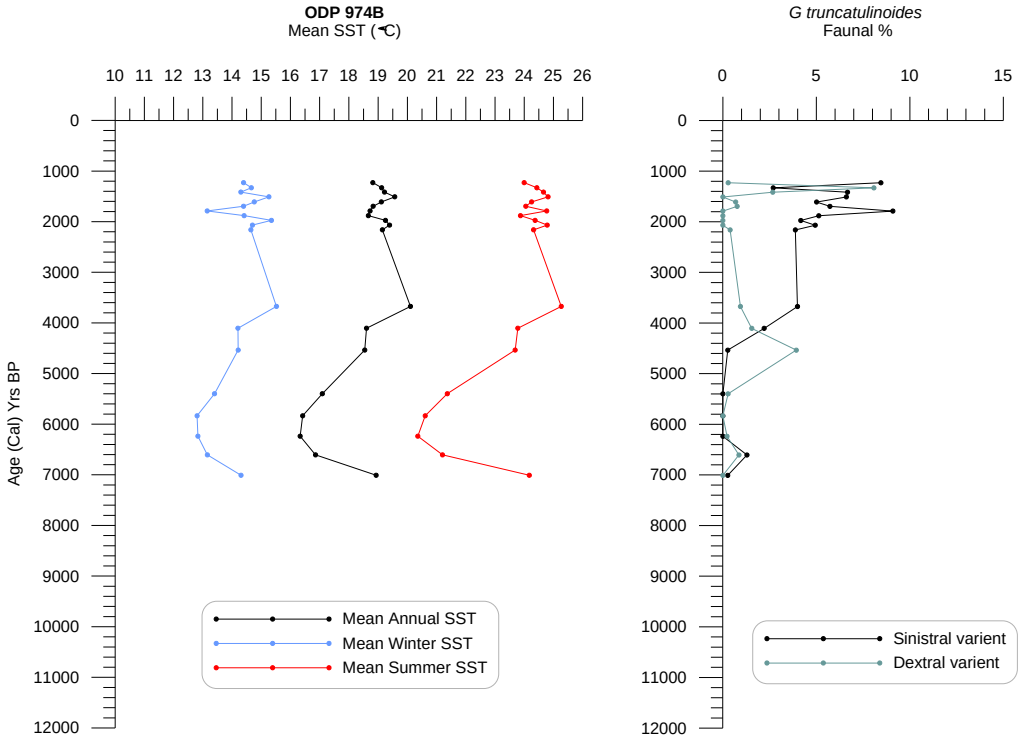

Figure 7.12B. Graph illustrating the mean winter, annual and summer SSTs reconstructed using the ANN and corresponding *G. truncatulinoides* (sinistral and dextral) faunal abundance values for Tyrrhenian Sea core ODP 974B.

7.5 Discussion

7.5.1 Applicability as a Biostratigraphic Tool

Previous research assessing the applicability of *G. truncatulinoides* as a biostratigraphic tool is dated to the mid-late 20th century (Ericson et al., 1954; 1961; Herman, 1972), this research was limited by the lack of advances in dating techniques to chronologically constrain their findings and low sampling resolutions. Nevertheless, their research paved the way in highlighting the biostratigraphic potential of *G. truncatulinoides*. Ericson et al. (1954; 1961) demonstrated the potential of *G. truncatulinoides* as a biostratigraphic tool by recognising synchronised alterations between the dominance of dextrally and sinistrally coiled specimens in Atlantic Ocean deep sea sediment cores *(figure7.14).*

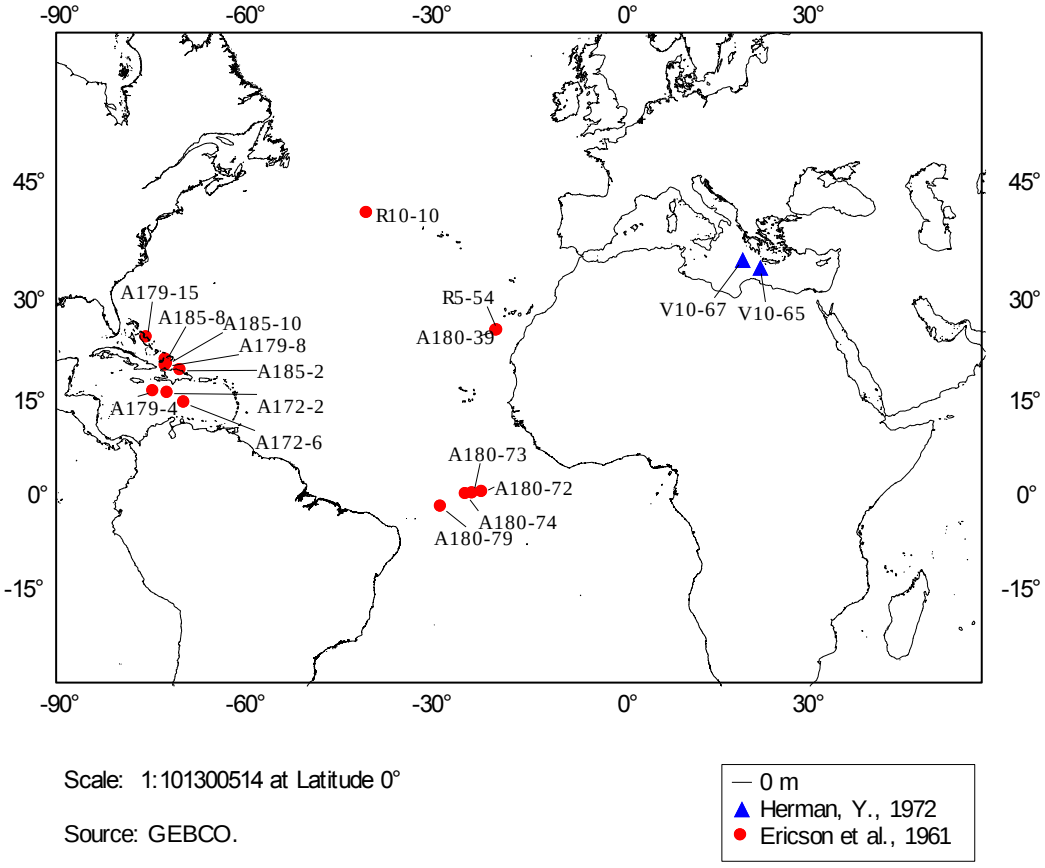

Figure 7.13. Location of cores analysed for coiling direction ratios of *G. truncatulinoides* in the Atlantic Ocean and eastern Mediterranean basin (Ericson et al., 1961; Herman, 1972).

Ericson et al. (1954; 1961) observed that the investigated North Atlantic cores exhibited a dominance of dextrally coiled *G. truncatulinoides*, with temporal shifts to sinistral dominance *(figure 7.14)*. Despite the lack of dating to determine the timing of these changes, the pattern of coiling direction appeared correlated among the cores (Ericson et

al., 1954, 1961). The lack of chronology however, makes correlation difficult over large spatial scales, particularly in the Atlantic Ocean *(figure 7.14)*. In a similar study, Herman (1972) determined the coiling variations from two eastern Mediterranean Sea cores *(figures 7.13)*. The addition of six radiocarbon dates allowed for correlation between the cores displaying a temporal synchronicity between coiling direction dominance between the two eastern Mediterranean cores. Despite the low sampling resolution a consistent pattern in the coiling variation is observed, with the cooler glacial periods dominated by the dextral variety with the sinistral variety dominating the warmer interglacial.

This research offers adequate chronological constraints for the assessment of the synchronicity of coiling shifts in these areas based on a much higher sampling resolution. The results demonstrate a distinct change from the dominance of dextral to sinistrally coiled tests within the Holocene. The timing of this event occurs in the Balearic basin and the Tyrrhenian Sea at ~5.4 cal kyr BP. The exception occurs in the Gulf of Lion core where the alternation between dextral dominance over sinistral dominance occurs ~1000 years later. Despite this local variation, the concurrent nature of coiling change between the other cores, highlights the potential of *G. truncatulinoide*s as a biostratigraphic tool in the Mediterranean Sea.

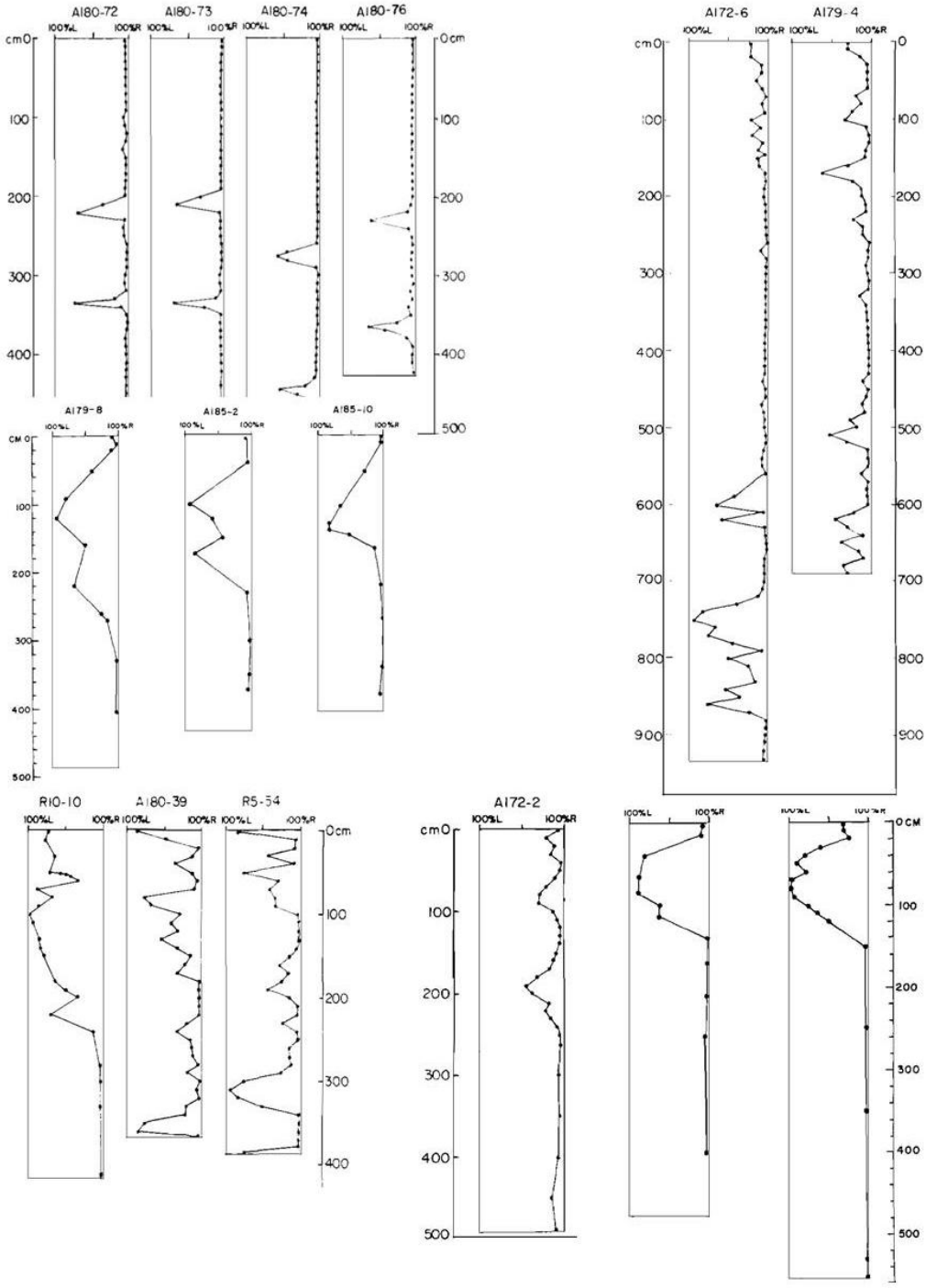

Figure 7.14 Graphs illustrating the downcore coiling variation of *G. truncatulinoides* in the Atlantic Ocean (Ericson et al., 1961), see figure 7.13 for core locations.

7.5.2 SST and Coiling in G. truncatulinoides

To determine the extent of SST control over coiling ratio, the relative abundance of both variants of *G. truncatulinoides* were plotted against the mean annual SST in the investigated western Mediterranean cores during the Holocene. As the abundance of sinistral and dextral variants are combined to derive the ANN SST it is only possible to plot the percentage of sinistral/dextral against the total *G. truncatulinoides* population rather than the total faunal abundance to determine if a correlation exists (***figure 7.15***). The results indicate a poor correlation with SST and coiling direction, indicating that coiling variation is affected by a different environmental variable

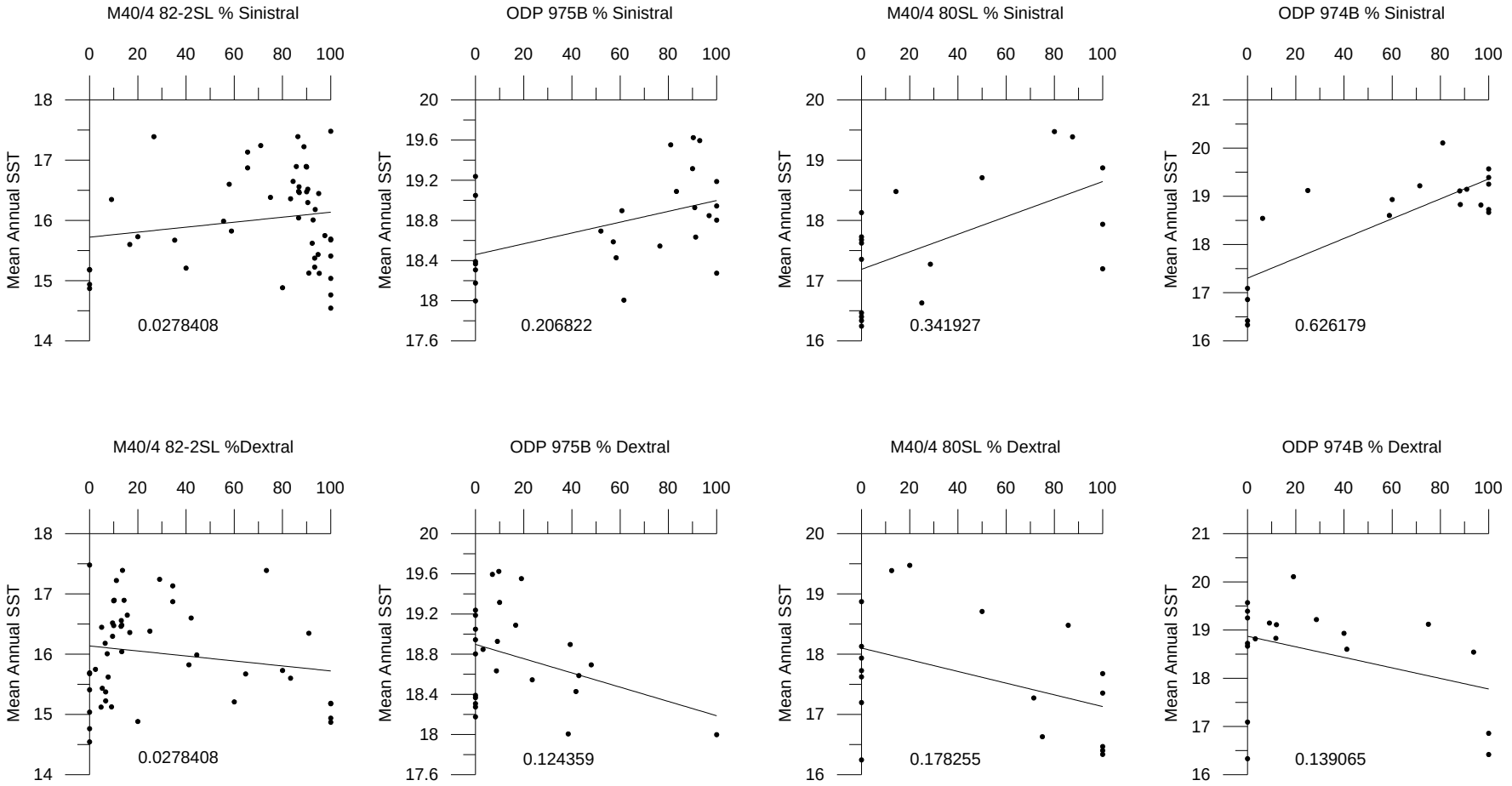

Figure 7.15 Linear plot representing the R Squared value between Mean Annual SST and *G. truncatulinoides* sinistral as a % of the total faunal abundance of *G. truncatulinoides* sinistral and dextral, whereby the closer to 1 the greater the correlation.

A study by Theide (1971) suggested that water depth was a potential factor controlling the variation between dextral and sinistral variants. Based on surface sediments along a 300km transect off the coast of Portugal, Thiede (1971) observed an increase in the proportion of sinistrally coiled *G. truncatulinoides* with increasing depth. The implications of this were also discussed in a study undertaken by Lohmann and Schweitzer (1990). These authors suggested that, rather than water depth, the depth of the thermocline determined the coiling direction of *G. truncatulinoides*. Based on plankton tows from the North Atlantic Ocean, their data suggests that the sinistral coiling variant is sensitive to a shallowing thermocline. A reduction in the number of sinistrally coiled tests was observed between Bermuda, (where the thermocline is ~800m) and the Rio Grande Rise (where the thermocline is ~600m) in contrast, the number of dextrally coiled tests remains unaffected. The Sierra Leone Rise records a thermocline depth of ~300m; here there is an absence of sinistrally coiling tests and the number of dextrally coiling tests is reduced (Lohmann and Schweitzer, 1990).

Based on their findings, and the complex life cycle of *G. truncatulinoides*, Lohmann and Schweitzer (1990) suggest that production of the species requires a deep thermocline, that is seasonally broken down to allow the migration of juveniles to surface waters. Simultaneous nutrient enrichment of the surface waters allows maximum abundances of *G. truncatulinoides* to develop at this time, where the sinistrally coiled variety dominates. During spring, once convective overturning ceases, abundances of *G. truncatulinoides* decline in the surface waters, however, those that remain are dextrally coiled. Lohmann and Schweitzer (1990) explain this by preferential removal of sinistrally coiled specimens associated with the re-establishment of a thermocline leaving a residual population of the dextrally coiled variety. This suggests that dextrally coiled *G. truncatulinoides* have more tolerance to stratified waters than their sinistrally coiled counterparts.

These findings are in agreement with a recent study in Bermuda, where sinistrally coiled *G. truncatulinoides* was absent at a site location with a relatively shallower thermocline of ~ 150m and only the dextrally coiled variant remained (Ujjié et al., 2010). A study undertaken at 4 sampling sites in the Sargasso Sea obtained *G. truncatulinoides* sinistral and dextral samples up to 1000m depth (Ujiié et al., 2010). The authors observed that hydrographic differences existed between the habitat of the present day sinistral and dextral coiling variants of type 2 *G. truncatulinoides*. *G. truncatulinoides* sinistral was

found deeper (down to 600m) between 400-200m depth in the central water mass synchronous with a mixed layer that extends down to 400m (Ujiié et al., 2010). In contrast the dextral variant was observed at shallower depths, located within the top 200m of the subtropical gyre associated with a thermocline at ~150m. The hydrographic features of the water masses are reflected in the abundances of the coiling variants of the 4 stations studied, one station showed a complete absence of the sinistral variant with only the dextral variant present, this station was associated with a relatively stable thermocline (*figure 7.16)*. The first station was dominated by the sinistral variant associated with a deep mixed layer *(figure 7.16)* total specimen quantities however, suggest that the dextral variant is most abundant associated with a relatively week thermocline as in station 3 *(figure 7.16)* (Ujiié et al., 2010).

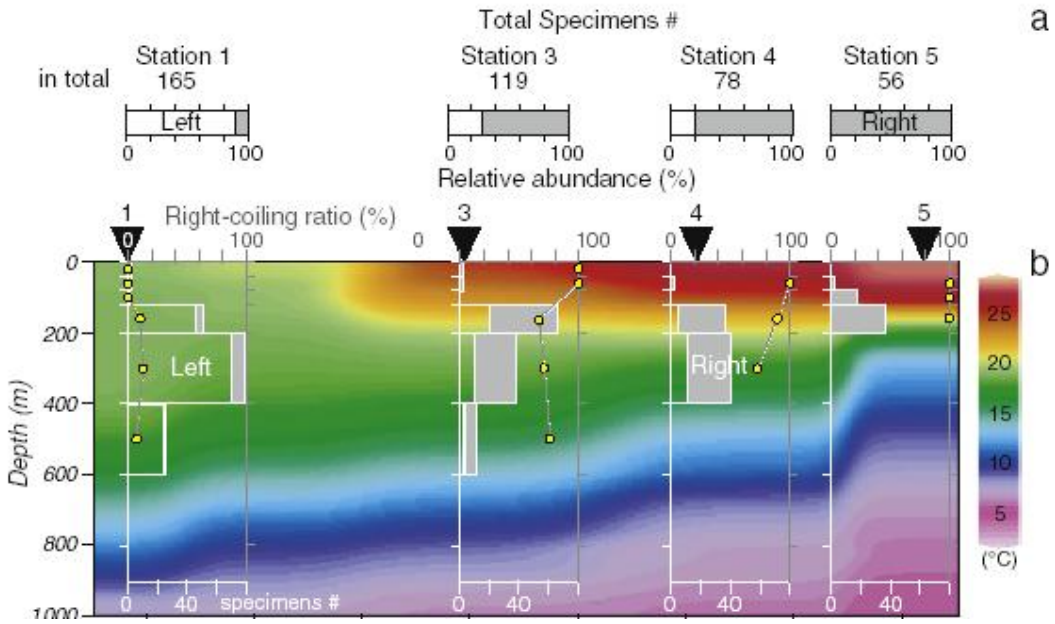

Figure 7.16. Graph depicting the findings of Ujiié et al. (2010) for each of the 4 studied stations, where **(a)** represents the relative abundance of *G. truncatulinoides* sinistral and dextral indicated by the open and shaded columns respectively. The total number of specimens in the study are indicated above each coloum, **(b)** represents the depth profile percentage of sinistral and dextral variants**.** The ratio of the dextral coiling variant to the total *G. truncatulinoides* population is indicated by the grey linear plot with yellow circles (from Ujiié et al., 2010).

Using these examples as guidelines it can be assumed that the:

a) The occurrence of *G. truncatulinoides* is governed by the stability of the water column (mixed or stratified). Winter convective overturning facilitates the transference of both nutrients and juvenile populations of

G. truncatulinoides into the surface waters where maximum abundances of the species develop.

b) The observed variation in coiling, appears to be related to the depth/presence of the thermocline. Dominant dextral populations tend to coincide with overall lower abundances of *G. truncatulinoides* possibly a residual population associated with increased stratification of the water column. The effects of SSTs are a potential secondary factor.

7.5 3 Significance of *G. truncatulinoides* in the western Mediterranean Sea

As shown in figure 7.9, a similarity in the abundance and coiling direction of *G. truncatulinoides* exists in the western Mediterranean Sea throughout the Holocene, suggesting that the hydrographic conditions affected the entire basin. The abundance of *G. truncatulinoides* is associated with 3 phases *(figure 7.3)* with each phase suggestive of different environmental conditions.

7.5.3.1 Phase 1 (~11.2-8.6 cal kyr BP)

As highlighted in section 7.3.1, Phase 1 is represented only in two cores and is characterised by low numbers of *G. truncatulinoides* which peak at ~ 9.0 cal kyr BP in the Balearic Basin and slightly earlier in the Tyrrhenian Sea (*figure 7.3*). Both coiling variants exist, but the sinistral variant dominates the faunal assemblage. Based on the modern day habitats of *G. truncatulinoides*, its presence in Phase 1 suggests seasonal mixing in the water column. However, the relatively low abundances and the presence of the dextral coiling variant may imply weakened vertical mixing associated with the formation of a shallow thermocline.

7.4.3.2 Phase 2 (8.6 – 5.1 cal kyr BP)

This early to mid Holocene phase is characterised by the near absence of *G. truncatulinoides* from the faunal record *(figure 7.3)*. The absence of *G. truncatulinoides* is attributed to enhanced stratification of the water column at this time. Under such conditions the migration of juvenile specimens and the advection of nutrients into the surface waters would be prohibited. The strong water stratification in the western Mediterranean Sea at this time could have developed due to the combined result of

postglacial sea level rise (and subsequent reduction in sea surface salinities) and increased precipitation (and subsequent river runoff). Melki et al. (2009) recorded a reduction in sea surface salinities (~2‰) in the Gulf of Lion at this time, which they explained as a result of freshwater input into the western basin, possibly due to increased river runoff. This is reinforced by Ali et al. (2008) who identified a period of extreme precipitation between ~7.2 – 5.0 cal kyr BP in southern France. The deposition of Sapropel 1 in the eastern basin between ~9.0 – 6.0 cal kyr BP provides further evidence of increased precipitation across the Mediterranean Sea (Rohling and Gieskes, 1989; Kallel et al., 1997). Associated with the increased intensity of the African monsoon, the deposition of sapropels has been correlated to periods of high river discharge from the Nile. The deposition of S1 in conjunction with the African Humid period lends weight to this theory (Rossignal-Strick et al., 1982; Rossignal-Strick, 1983; 1985; Kallel et al., 1997). During this time vegetational changes on the Iberian Peninsula (maximum development of deciduous forests) provide evidence of a more oceanic/moist climate (Fletcher and Sanchez-Gona, 2008). At ~7.2 cal kyr BP, a minor increase in the number of *G. truncatulinoides* suggests a temporary interruption to the prolonged period of water stratification. Associated with presence of the last redox event (LRE) in the Algero-Balearic basin, Jimnez-Espejo et al. (2007) suggest this event could represent intensification in the western Mediterranean thermohaline circulation.

7.4.3.3 Phase 3 (5.1 cal kyr BP - Present)

This phase marks the onset of a significant increase in the abundances of *G. truncatulinoides*, particularly in the Balearic basin *(figure 7.3)*. The start of this phase broadly corresponds with the end of the African Humid Period which marks the transition from a more humid climate to the semi-arid climate that exists in the Mediterranean region today (Jalut et al, 2000). Modern day hydrographic conditions in the western Mediterranean Sea support the development of deep vertical mixing, in particular in the north-western basin associated with WMDW formation, this subsequently provides the means for *G. truncatulinoides* to complete its life cycle thereby contributing to the proliferation of the species.

The presence and absence of *G. truncatulinoides* during the Holocene in the western Mediterranean Sea suggests a sequence of hydrological events. The early Holocene

presence of *G. truncatulinoides* indicates the initial presence of vertical mixing of the water column in the western basin, the subsequent decline and absence suggests a stabilisation of the water column associated with sea level rise, enhanced precipitation and sapropel formation. The initial rise in the dextral coiling variant at the onset of Phase 3 suggests a weakly stratified water column, following a period of prolonged stratification. As absolute abundances of *G. truncatulinoides* increase so too does the dominance of the sinistral variety. Modern conditions of the western basin take hold and the basin becomes more evaporative. This hydrological feature, including the presence of strong local winds encourages the development of seasonal mixing of the water column, similar to modern day conditions where *G. truncatulinoides* dominates the winter assemblage.

7.5 Conclusions

Downcore analysis of *G. truncatulinoides* in the western Mediterranean Sea has revealed three phases of abundance, each phase indicative of individual environmental conditions. A consideration of the ecological preferences of the coiling variants presents a more in-depth picture of Holocene environments in the western Mediterranean Sea. Previous studies indicate that the distribution of *G. truncatulinoides,* in particular the sinistral variant of Type 2, is especially susceptible to changes in the water column stratification, while both coiling variants require deep vertical mixing to complete its life cycle (Lohmann and Schweitzer, 1990; Cléroux et al., 2009; Ujiié et al., 2010). Based on this and supporting evidence from additional marine and terrestrial proxies (Jalut et al., 2000; Ali et al., 2008; Melki et al., 2009; Rohling et al., 2009) it is concluded that the early-mid Holocene absence of *G. truncatulinoides* is associated with a stratified water column likely the result of post glacial sea level rise and increased river runoff.

A mid Holocene peak in the dextral variant was synchronous across all cores (4.4 cal kyr BP in the faunal abundance record) this phenomenon provides us with a local biostratigraphic marker in the western Mediterranean Sea, while also indicating a weakly stratified water column as suggested by present day ecological preferences of the dextral variant. The present day conditions of the western Mediterranean Sea are associated with an evaporative basin and the presence of strong local winds that encourage deep vertical mixing, particularly in the Gulf of Lion where *G. truncatulinoides* sinistral dominates the winter assemblage. The dominance of this coiling variant during the mid to late Holocene represents the onset of vertical mixing and modern hydrological conditions.

Chapter 8: Holocene Planktonic Foraminiferal Ecozonation in the Western Mediterranean Sea

8.1 Introduction

The enclosed nature of the Mediterranean Sea has provided a particularly apt environment for recording climatic events. Consequently there has been an increasing interest in millennial/centennial climate variability in the Mediterranean Sea during the Holocene. Climatic changes experienced in the Northern Hemisphere recorded in the GRIP and GISP ice cores exhibit synchronicity with climatic changes in the Mediterranean Sea (Rohling and De Rijk, 1999; Cacho et al., 2001; 2002; Pérez Folgado et al., 2003; Sprovieri et al., 2003). The study of these climatic events is based on the palaeoenvironmental analysis of marine sediments (Cacho et al., 1999; 2000; Melki et al., 2009 and references therein). In order to fully utilise their findings, it is essential that these marine records can be correlated to an independent timescale, as such, the establishment of a reliable biostratigraphy can provide a valuable tool.

Biostratigraphic research in the western Mediterranean Sea previously focused upon the Alboran Sea (Pujol and Vergnaud Grazzini., 1989; Pérez-Folgado et al., 2003), the Tyrrhenian Sea (Jorissen et al., 1993; Capotondi et al., 1999; Sbaffi et al., 2001; 2004) and the Sicilian (Sprovieri et al., 2003) and Sardinian channels (Budillion et al., 2009). This research aims to address this geographical constraint by providing the first Holocene biostratigraphic zonation for the Gulf of Lion and the Balearic basin in the north western and central western Mediterranean basin respectively. Although the Holocene timeframe lies well within the scope of radiocarbon dating, establishing a biostratigraphic framework within a basin-wide or local scale provides an accessible and time efficient tool for researchers to determine the temporal progression of core samples in an environment where radiocarbon dating facilities may not be readily available, such as upon marine research vessels.

8.2 Chronological Framework

For the purpose of this chapter, cores from the Gulf of Lion (M40/4 82-2 SL) and the Balearic Basin (ODP 975B) were studied *(figure 8.1)*. AMS ^{14}C dates were available for both cores (Chapter 6, *Table 6.1*). The average sedimentation rates are significantly higher in the Gulf of Lion core M40/4 82-2 SL at ~16.1 cm/kyr, with the Balearic basin core ODP 975B indicating an average Holocene sedimentation rate of 10.6 cm/kyr.

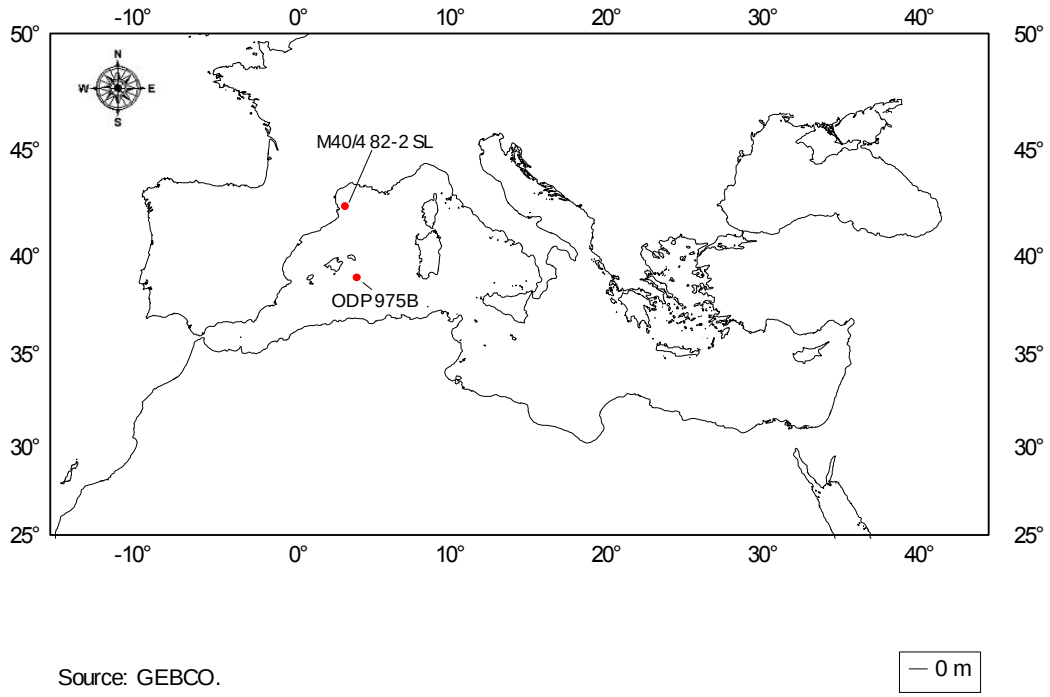

Figure.8.1. Location of cores M40/4 82-2 SL (Gulf of Lion) and ODP 975B (Balearic Basin) on which the proposed biozonations are based.

8.3 Results

8.3.1 Planktonic Foraminiferal Ecozonation

A total number of fourteen planktonic foraminiferal species or groups of species were observed in the faunal record of both cores and are listed as follows: *N. pachyderma* (dextral and sinistral), *G. bulloides*, *G. inflata*, *G. ruber* (white and pink), *G. truncatulinoides* (sinistral and dextral), *G. scitula*, *T. quinqueloba*, and the SPRUDTS group (*G. sacculifer*, *H. pelagica*, *G. rubescens*, *O. universa*, *B. digitata*, *G. tenella*, and *G. siphonifera*). Because the majority of planktonic foraminiferal species are sensitive indicators of environmental parameters, variations of these species in downcore sediments in the timescale of Quaternary climate change represent an ecological rather than an evolutionary response to environmental parameters (Bé, 1959; Bé and Hamlin, 1962; Pujol and Vergnaud Grazzini, 1995; Schiebel et al., 2005). Subsequently, zones representing a specific faunal assemblage of planktonic foraminifera can be associated with their specific environmental parameters and as such, can be established as an ecozone (EZ).

This research identifies 3 EZs *(figure 8.2),* established by the appearance or disappearance of specific taxa (Capotondi et al., 1999; Sbaffi et al., 2001, 2004). Each EZ

has been calibrated against age in cal kyr BP. 3 EZs have been established based on the disappearance or appearance of a species, in particular those of *G. scitula* and the *G. truncatulinoides* (sinistral and dextral) Although clear faunal patterns exist between both cores, as indicated by a corresponding EZ boundaries the relative abundance of certain species differs dramatically, for example *G. ruber* reaches peak abundances (35%) in core ODP 975B compared to ~ <10% in M40/4 82-2 SL *(figure 8.3)* highlighting the different ecological environments associated with the spatial distribution of the cores.

8.3.1.1 Ecozone 3 (~11.2-8.6 cal kyr BP)

Due to the temporal resolution of core M40/4 82-2 SL (extends only to 8.2 cal kyr BP) subsequently EZ3 only applied to core ODP 975B. EZ3 is dominated by *G. ruber* (~30%), *G. inflata* (~25%) and *G. bulloides* (~20%) while the SPRUDTS group, *G. truncatulinoides*, *G. glutinata*, and *G. scitula* contribute only 2-10% *(figure 8.2)*. The base of EZ3 is marked by the disappearance *G. scitula* and *G. truncatulinoides*.

8.3.1.2 Ecozone 2 (~8.6-5.1 cal kyr BP)

The onset of ecozone 2 is marked by the absence of *G. truncatulinoides* (sinistral and dextral). Faunal patterns evident in both cores include maximum mid Holocene abundances of *N. pachyderma* where abundances reach up to 60% in core M40/4 82-2 SL. *G. truncatulinoides* remains absent for the duration of the ecozone with the exception of a minor abundance (2.5%) peak at 7.1 cal kyr BP.

8.3.1.3 Ecozone 1 (~5.1-present)

The EZ2-1 boundary is marked by the reappearance of *G. truncatulinoides* (sin and dex) (*figure 8.2*) representing the onset of modern hydrographic conditions in the Gulf of Lion associated with deep vertical mixing. Minimum abundances of *N. pachyderma* (23%) occur in core M40/4 82-2 SL during EZ1 and reaches abundances as low as 3% in core ODP 975B, this *N. pachyderma* minimum coincides with peak abundances in *G. inflata* at ~3.5 cal kyr BP *(figure 8.2)*. An abrupt decline of *G. inflata* is evident in the late stage of EZ1 at ~ 2.2 cal kyr BP from where average abundances remain at ~6% *(figure 8.2)*.

The faunal abundance in EZ1 highlights the modern distribution patterns as identified by Pujol and Vergnaud Grazzini, (1995), with *G. ruber* dominating the assemblage in the

Balearic Basin core (~24%) associated with *G. bulloides* and *G. inflata* and low abundances of *N. pachyderma* and *G. truncatulinoides* (*figure 8.2*)

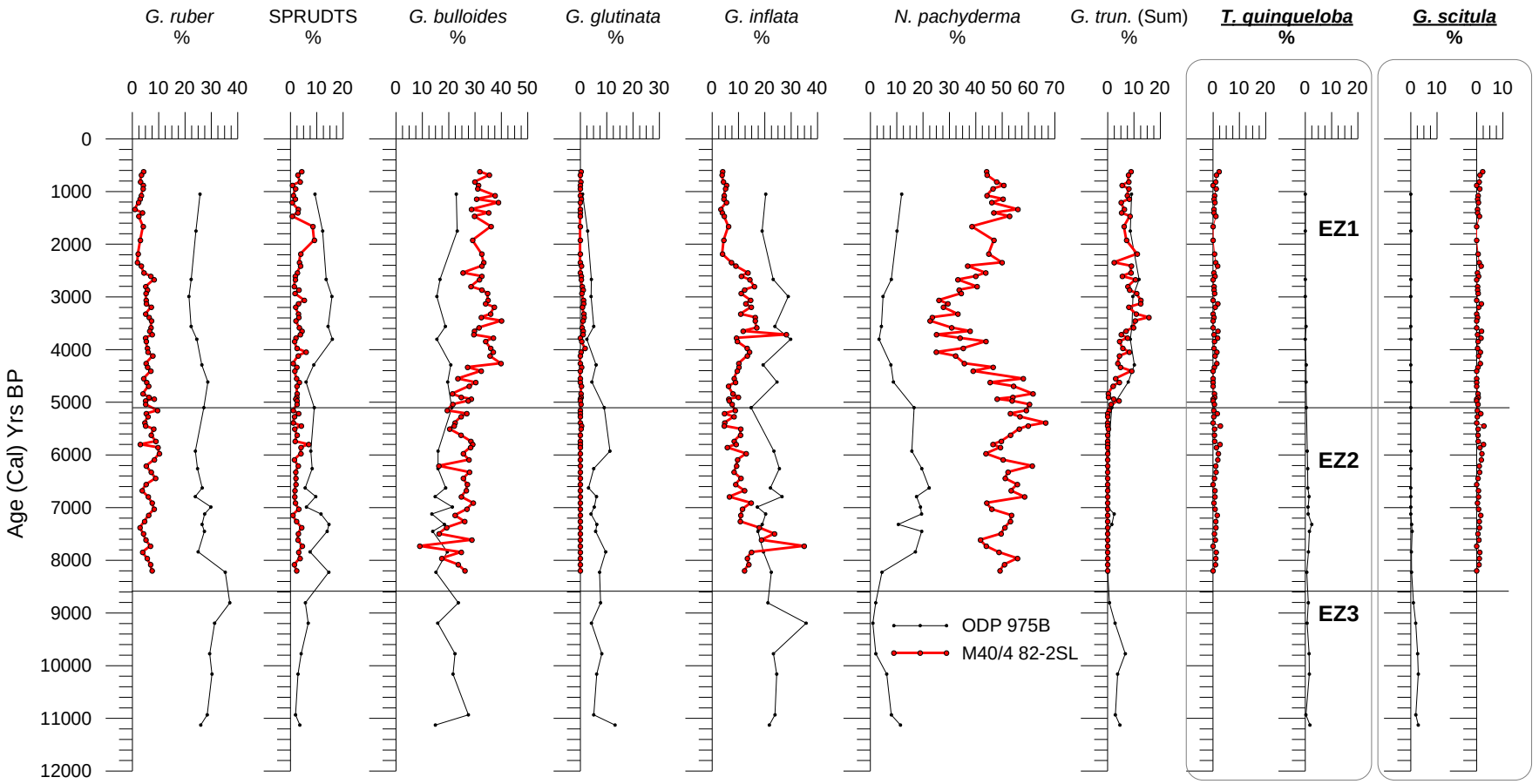

Figure 8.2. The relative abundance of the major species present in cores M40/4 82-2 SL and ODP 975B. The solid black lime represents the boundaries for EZ3, EZ2 and EZ1. *T quinqueloba* and *G. scitula* are plotted on individual graphs bounded by grey rectangle to allow for clearer visual representation).

Table 8.1 provides a summary of the dominating faunal characteristics for each biozone.

EZ	ODP 975B Age (Cal Kyr BP)	Faunal Characteristics
EZ1	~5.1-Present	Onset: Re-appearance of *G. truncatulinoides*(sin and dex) Early increase in *G. inflata* and decline in *N. pachyderma*
EZ2	~8.6-5.1	Onset: Marked by absence *G. truncatulinoides* and *G. Scitula.* Maximum abundances of *N. pachyderma* associated with decreasing *G. inflata* and increasing *G. bulloides* abundances.
EZ3	~11.2-8.6	Base of EZ determined by absence of *G. scitula* and *G. truncatulinoides.* Assemblage dominated by *G. ruber*, *G. inflata*, and *G. bulloides.* Presence of *G. truncatulinoides* (dominated by dextral variant)

Table 8. 1. Summary of ecozonation and faunal responses for the Gulf of Lion (M40/4 82-2 SL) and the Balearic Basin (ODP 975B).

8.3.2 SST Variability

Mean summer, winter and annual SST reconstructions based on planktonic foraminiferal assemblage variation were generated for each core using ANN *(figure 8.3)*. Despite the uncertainties associated with ANN SST reconstruction, variations in SST greater than 2°C are recognised in the record that are greater than the ANN SST reconstruction error. Variations in SST trends mirror changes in the relative faunal abundance record which identify the establishment of three EZs outlined in section (8.3.1) *(figures 8.2 and 8.3)*.

Each EZ is associated with either an increasing or decreasing SST trend which is particularly evident in EZ1 *(figure 8.3)*. Although similar SST patterns exist, the SST ranges vary between the two locations. Average annual, summer and winter SST for core M40/4 82-2 SL are ~ 16, 20 and 12°C respectively, whereas core ODP 975B presents an overall higher SST range with an average annual, summer and winter SST of ~ 15, 23 and 19°C respectively *(figure 8.3)*.

The oldest ecozone (EZ3), recognised only in core ODP 975B is marked by a relatively stable SST with average summer, winter and annual SSTs at 23, 15 and 19°C respectively

EZ3 presents the first comparable biozone between both cores. EZ2 indicates general declining trend in core M40/4 82-2 SL where an annual SST decrease of 4°C occurs from the early stage to the base of the ecozone, whereas core ODP 975B indicates a more conservative annual SST decrease of ~1°C *(figure 8.3)*.

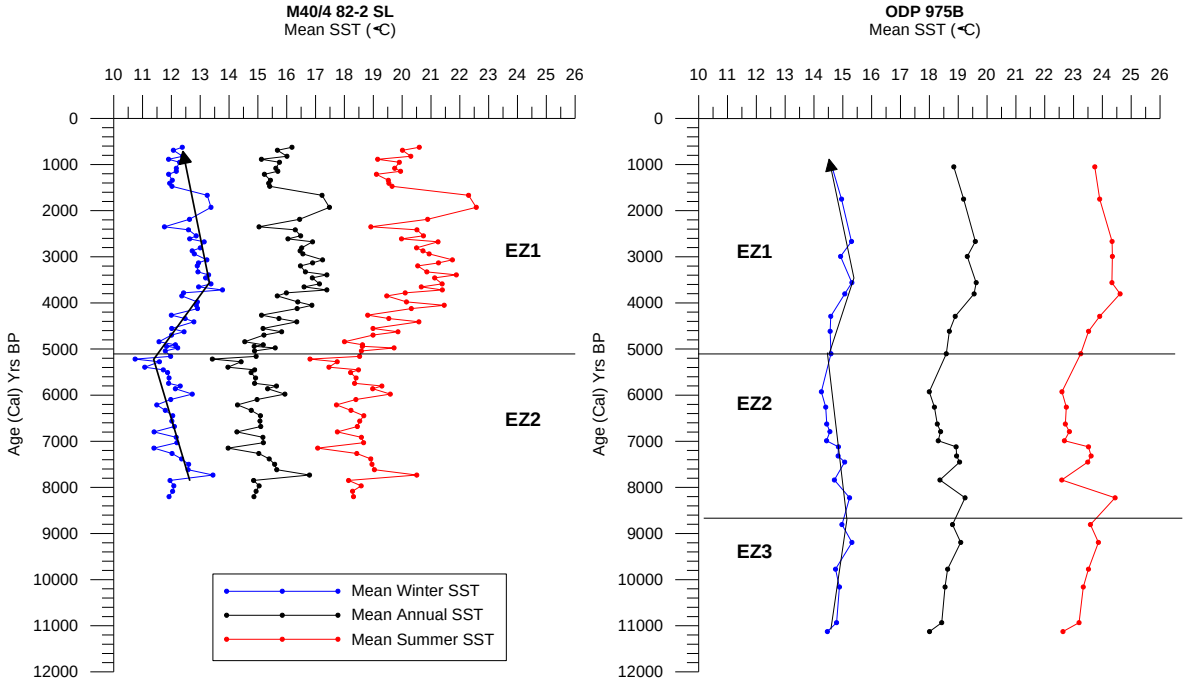

Figure 8.3. Graphs illustrating the mean summer, winter and annual SSTs (as determined by ANN) for cores M40/4 82-2 SL (A) and ODP 975B (B). Black arrow represents the main SST trend associated with each ecozone. Solid black line depict the boundaries between the ecozones as defined by relative faunal abundances (see figure 8.2).

In contrast, an increasing SST trend is observed in both cores throughout the first half of EZ1 with the highest temperatures occurring at ~3.8 cal kyr BP *(figure 8.3)*. The second phase of EZ1 indicates a general cooling trend in both cores, however, core M40/4 82-2 SL records a temporary SST increase (annual SST increase of 2.5°C) at ~ 1.8 cal kyr BP followed by a gradual SST increase to the present day (12, 21, 16°C winter, summer and annual respectively). Although some similar trends are evident between the 2 cores (BZ3 and 2), the SST signal indicates greater variability in core M40/4 82-2 SL, this is likely the result of the higher resolution of the core.

8.4 Discussion

8.4.1 Comparison with other faunal ecozonation in the western Mediterranean Sea

Of the previous ecozonations in the western Mediterranean Sea (Pujol and Vergnaud Grazzini., 1989; Jorissen et al., 1993, Capotondi et al., 1999, Sbaffi et al., 2001; 2004, Pérez-Folgado et al., 2003; Budillion et al., 2009), only 3 of the studies are directly comparable to this research. The size fraction, on which planktonic foraminiferal analyses is based, can differ between studies and as such has proved problematic when attempting to correlate faunal data. Specifically, smaller species such as *T. quinqueloba* and *G. glutinata* may be over-represented in the smaller size fractions (< 125 µm). Capotondi (1999) established foraminiferal ecozones for the late quaternary in the central Mediterranean Sea based on >63µm sample size, subsequently the faunal assemblage was dominated by *T quinqueloba* reaching abundances up to 90% in a Northern Tyrrhenian Sea core (ET 91-18). Species such as *N. pachyderma*, *G. inflata*, *G. ruber* and *G. truncatulinoides* comprised maximum abundances of ~14, 6, 5 and 1% respectively. However despite the variance in faunal composition some similar trends exist, a peak in *N. pachyderma* is evident at ~ 6.0 cal kyr BP similar that observed in this research, in addition *G. truncatulinoides* indicates a reappearance after 6.0 cal kyr BP following a period of absence precluded by an abundance peak at ~ 9.7 cal kyr BP similar to that identified in EZ3 in core ODP975B. This research utilises the >150 µm size fraction, as using the smaller size fraction could result in an under representation of some significant species such as *G. truncatulinoides* as evident where *G. truncatulinoides* comprised maximum abundances of ~ 1% in research undertaken by Capotondi (1999) and as this species was of particular importance to this research the more commonly used size fraction (as used by CLIMAP) was most suited for this study. However, while faunal shifts do occur that correlate with this research, the significantly reduced faunal abundances mean that direct species comparison is limited. Previous studies that utilise the same size fraction as this research (>150 µm) (Pujol and Vergnaud Grazzini. 1989; Pérez-Folgado et al., 2003; Sbaffi et al., 2001, 2004) provide the most comparable data with this research. Figure 8.4 illustrates the location of the deep sea cores on which these authors based their ecozonation. It is significant to note that the entire central western Mediterranean region is under-represented with respect to planktonic foraminiferal biozonation.

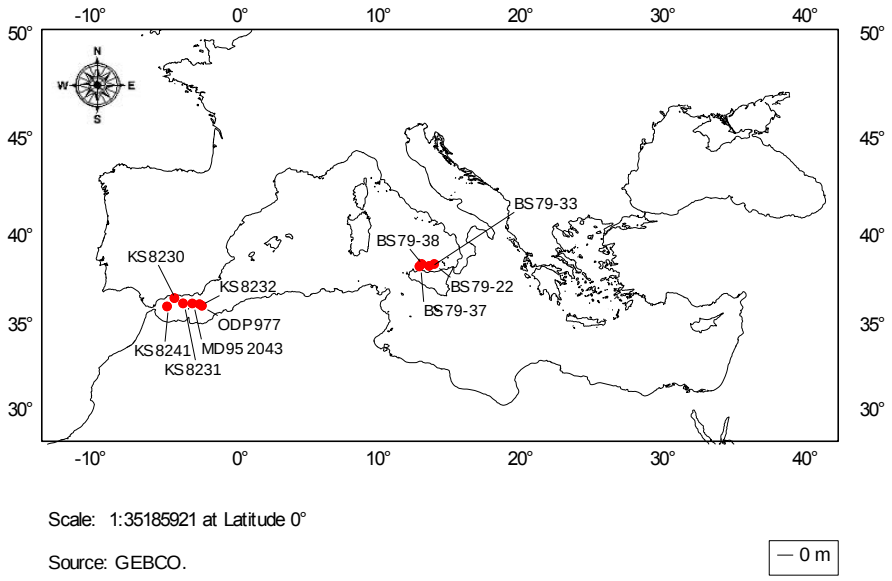

Figure 8.4. Localities of the deep sea cores on which previously defined biozones are based. The cores refer to studies undertaken in the Alboran Sea (Pujol and Vergnaud Grazzini., 1989; Pérez-Folgado et al., 2003) and the Tyrrhenian Sea (Sbaffi et al., 2001, 2004).

The first biozonation in the western Mediterranean basin was established in the Alboran Sea (Pujol and Vergnaud Grazzini (1989). Five zones of faunal succession were recognised during the Holocene with the boundaries represented by abrupt increases/decreases of planktonic foraminifera termed *bioevents* (Pujol and Vergnaud Grazzini, 1989) *(Table 8.2 and figure 8.5).* These bioevents were later identified and correlated with a second study in the Alboran Sea (Pérez Folagado et al., 2003) *(figure 8.5, Table 8.2).* However, data obtained from the current research indicate that these bioevents seem to be confined to the Alboran Sea. Of the nine main bioevents identified during the Holocene, only one can be correlated with this research, however, this could be due to a variation in sedimentation rates between the cores and/or spatial hydrographic differences. Bioevent Ra identified by an increase in *G. ruber* (white) at ~8.9 cal kyr BP (Pujol and Vergnaud Grazzini, 1989; Pérez Folagado et al., 2003) *(Table 8.2),* may correspond to a similar increase in *G. ruber* (white) identified in core ODP 975B at ~ 8.8 cal kyr BP.

Bioevent	Faunal Response	Age (centred at-cal kyr BP)
Pm[1]	*N. pachyderma* (dex) minimum	7.7
P1[1]	*N. pachyderma* (dex) increase	8.8
P2[1]	*N. pachyderma* (dex) increase	11.8
I[1]	*G. inflata* increase	7.7
BO[1]	*G. bulloides* increase	5.6
RO[1]	*G. ruber* alba post glacial max.	7.7
Ra[1]	*G. ruber* alba increase	9.5
Sc1[2]	*G. scitula* increase	10.8
Q1[1]	*T. quinqueloba* increase	9.7

Table 8.2. Main Holocene bioevents identified by ([1]) Pujol and Vergnaud Grazzini, (1989) and ([2]) Pérez Folgado et al., (2003) and the corresponding faunal response. Ages are those established and calibrated by Pérez Folgado et al. (2003).

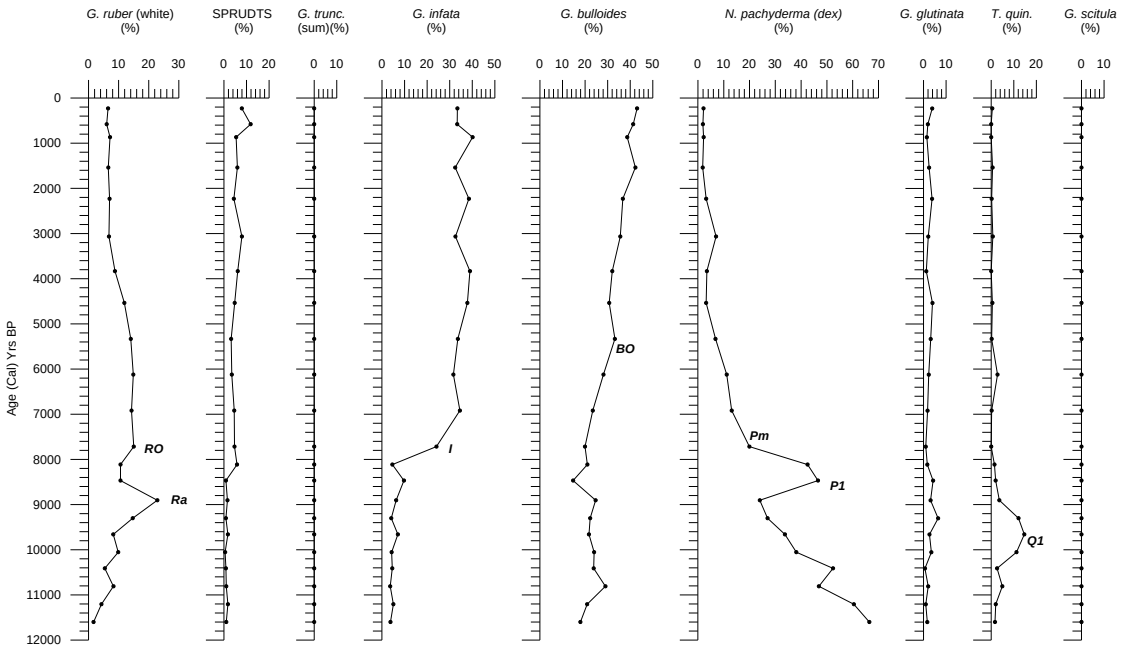

Figure 8.5. Planktonic foraminiferal variation, recorded in core ODP 977, and associated bioevents as established by Pujol and Vergnaud Grazzini (1989) (data from Pérez-Folgado et al., 2003).

Significant faunal variations exist between the Alboran Sea studies and this research. These differences include the absence of *G. truncatulinoides* and the minimal (<10%) abundances of *N. pachyderma* (dextral) from ~5.0 cal kyr BP to the present in the

Alboran Sea record *(figure 8.5)*. In contrast, this research identifies an increase in *N. pachyderma* (dextral) and a significant presence of *G. truncatulinoides* (~10%) from the mid Holocene to the present.

Work by Sbaffi et al. (2004) provides the most recent biozonation from the Tyrrhenian Sea *(Figure 8.6b)*. The high sedimentation rates of the cores utilised (BS7937 and BS7938) are similar to those of core M40/4 82-2 SL and as a consequence downcore faunal variation from both localities are well represented and directly comparable (*figure 8.6*). Sbaffi et al. (2004) presented a total of 8 *biozones*, based on the variation of planktonic foraminiferal assemblages during the last 25 cal kyr BP. Of particular relevance to this research are biozones 1-3, encompassing the last 12.0 cal kyr BP (*figure 8.6b*) that correspond to the temporal range of ecozone 1-3 (this research) (*figure 8.6a*). Corresponding to EZ3 from this research, biozone 3 (Sbaffi et al., 2004) (12.2-10.7 cal kyr BP) represents the termination of glacial conditions and the onset of the recent postglacial period. Sbaffi et al. (2004) define the end of the biozone by the final disappearance of cold species *T. quinqueloba* and *G. scitula* at ~11 cal kyr BP (*figure 8.6b*). This is in stark contrast with the findings of this research which records the disappearance of *G. scitula* at ~7.3 cal kyr BP while *T. quinqueloba* remains present in very low abundances until EZ1 in Core ODP 975B (*figure 8.6a*). *Biozone 2* (Sbaffi et al., 2004) is characterised by high frequencies of *N. pachyderma* (dextral) and a decrease in the abundance of *G. inflata (figure 8.6b)*. The boundary between *biozone 2* and *biozone 1* corresponds with an abrupt decrease in *N. pachyderma* (dextral) together with the re-appearance of *G. truncatulinoides (figure 8.6a)*. Finally, *biozone 1* (Sbaffi et al., 2004) represents the modern-day faunal assemblages in the Tyrrhenian Sea where ~80% of the faunal assemblage constitutes warm subtropical species. This *biozone* (6.3 cal kyr BP-sub recent) is subdivided into 3 subzones (1c, 1b and 1a), justified by faunal variations of *G. ruber* and *N. pachyderma* (dextral). Drawing on comparisons with this research, similar faunal trends are observed during *biozone 1* (Sbaffi et al., 204) for *G. inflata* and *N. pachyderma* (dextral). Minimum values of *G. inflata* evident in biozone 1b correlate with a significant decrease in core M40/4 82-2 SL and a declining trend in core ODP 975B *(figure 8.6)*. Frequencies of *N. pachyderma* (dextral) also record an increase during biozone 1b, corresponding to a similar increase observed by this research at this time *(figure 8.6)*. Overall, it appears that there are similarities between the faunal assemblages in the Tyrrhenian Sea and those recorded by

this research, however the main difference appears to be the timing of specific faunal events, in particular for the early to mid Holocene.

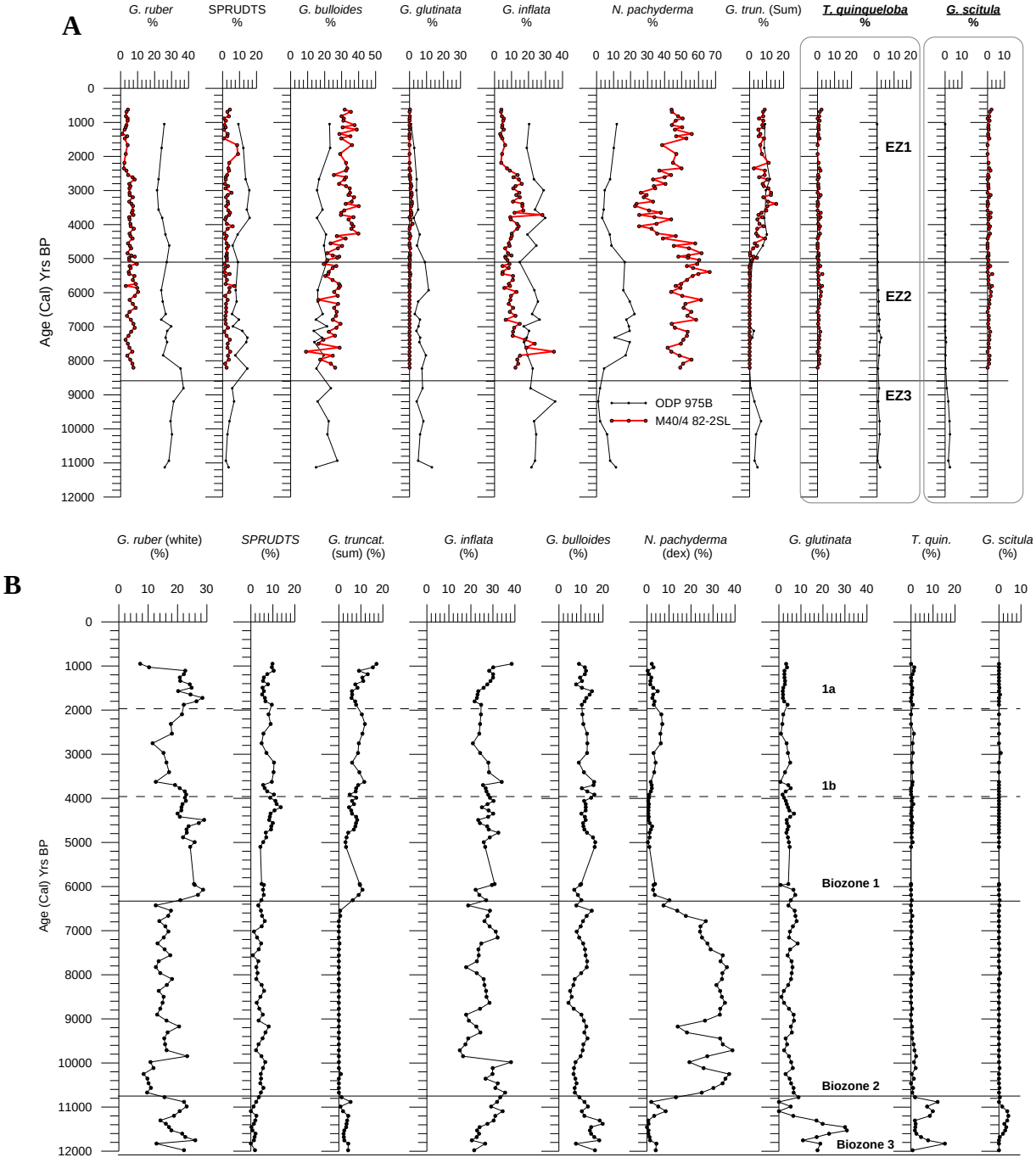

Figure 8.6. (A) Ecozonation of the Gulf of Lion (M40/4 82-2 SL) and the Balearic Basin (ODP 975B) (Solid black line represents the ecozone boundaries for ODP 975B, dashed line represents the onset of EZ2 in core M40/482-2SL, EZ2-1 boundary is represented in both cores by a solid black like at 5.1 cal kyr BP) (B) Biozonation of the Tyrrhenian Sea core BS7938 (data from Sbaffi et al., 2004).

This spatial unconformity concurs with research undertaken by Hayes et al. (1999) in which the authors state that basin-wide planktonic foraminiferal biostratigraphy must be treated with caution. While synchronicity may exist between certain species, other species distribution patterns are related to the climatic and hydrographical parameters in the region in which they developed. Indeed this is apparent between the cores utilised in this study. While faunal assemblages from both ODP 975B and M40/4 82-2 SL highlight a reasonable degree of similarity, both the temporal and sampling resolution would need to be further constrained to more accurately assess the biostratigraphical comparison.

8.5 Summary and Conclusions

Of the previous biozonation that has been proposed for the western Mediterranean Sea only partial correlation of planktonic foraminiferal frequency variations can be made with this research. In the absence of a biozonation for the central and north-western Mediterranean Sea, this research proposes a new biozonation for the region *(Table 8.1, figure 8.2).* Despite the degree of faunal correlation that exists between cores ODP 975B and M40/4 82-2 SL the exact regional validity of this scheme needs to be verified by further study. The correlation that exists between the two cores validates the usefulness of planktonic foraminiferal biostratigraphy as a palaeoenvironmental tool but on a local rather than regional scale.

Chapter 9: Early-Mid to Late Holocene Palaeoclimatic Reconstruction in the Gulf Of Lion

9.1 Introduction

The western Mediterranean Sea has been the target of intense research relating to Holocene climatic variability (Cacho et al., 2001; Sbaffi et al., 2004; Jimenes-Espejo et al., 2007). In particular, earlier studies have observed a relationship between the North Atlantic and the Mediterranean Sea, specifically associated with the occurrence and frequency of cold episodes (Bond et al., 1997). Since the atmospheric circulation over the North Atlantic influences the strength of the westerlies, it is anticipated that climate signals recorded in the western Mediterranean Sea would correlate to those observed in North Atlantic proxies (Rixen et al., 2005). However, most of the Mediterranean Sea studies have been confined to the Alboran (Cacho et al., 1999 and 2001; Perez-Folgado et al., 2003) and Tyrrhenian Seas (Sbaffi et al., 2001, 2004) few studies have concentrated on the Gulf of Lion. Situated at the site of WMDW formation, the sensitivity of the area to abrupt climate change has implications on the formation of deep water masses and ultimately the thermohaline circulation of the western basin (Rixen et al., 2005).

Figure 9.1. Map depicting the core location of M40/4 82-2 SL in the Gulf of Lion (Source Google Earth).

The most recent research undertaken in the Gulf of Lion used both planktonic and benthic foraminifera to investigate SST, salinity and primary productivity over the past 28 kyr (Melki et al., 2009). Melki et al, (2009) observed reduced SST in the Gulf of Lion during the early to mid Holocene coeval with a salinity reduction associated with the inflow of reduced salinity North Atlantic surface waters through the Strait of Gibraltar. In addition the authors suggested that the Mediterranean Sea remained a concentration basin during these low salinity periods. As a contribution to the palaeoclimatic reconstruction of the western Mediterranean Sea this research presents a high resolution micropalaeontological investigation into the climatic variability for core M40/4 82-2 SL in the Gulf of Lion, during the last 8.4 cal kyr BP (*figure 9.1*). This new data verifies and provides robustness to existing data. The chronological framework of this core is based on five AMS ^{14}C dates (*Chapter 6).* The resultant age-depth profile illustrates relatively high linear sedimentation rates (15.6 cm/kyr) for this core similar to those that have been recorded for other cores in the Gulf of Lion during the Holocene (Melki et al., 2009).

9.2 Results

9.2.1 Planktonic Foraminiferal Distribution

The pattern of planktonic foraminiferal abundances presents an increasing trend from the onset of the faunal record at ~8.4 cal kyr BP to the late Holocene (*figure 9.2*). Correlating with EZ2 (see Chapter 8), planktonic foraminiferal abundances are low at the onset of the record however, an increase is observed at ~5.0 cal kyr BP which continues into the late Holocene (EZ1) when peak abundances are recorded (*figure 9.2*).

Beginning at ~8.2 cal kyr BP, the relative abundance of the main planktonic foraminiferal species is presented in figure 9.3. The faunal assemblage is dominated primarily by cold indicator species *N. pachyderma* (dextral) (40-60%) and *G. bulloides* (20-30%). However, between 5.4 and 3.6 cal kyr BP a decrease in the frequency of *N. pachyderma* (dextral) coincides with an increase of *G. inflata* and *G. truncatulinoides* (*figure 9.3*). *G. glutinata*, *T. quinqueloba* and *G. scitula*, also cold indicator species (Bé, 1960; Sbaffi et al., 2004), comprise minimum abundances (<5%) in the faunal record (*figure 9.3*). Consistent with modern day distribution patterns in the Gulf of Lion, warm indicator species, such as *G. ruber* (white and pink) and the SPRUDTS-group, record low faunal abundances (<10%) throughout

the Holocene. A notable reduction (~5%) in *G. ruber* frequencies occur at ~ 3.0 cal kyr BP, while the SPRUDTS-group records a minor increase (~5%). (*figure 9.3*). The deeper dwelling transitional species such as *G. truncatulinoides* (sinistral and dextral) and *G. inflata* constitute an average of 4% and 10% respectively of the faunal assemblage. Peak abundances of *G. inflata* occur in ecozone 2, whilst the emergence of *G. truncatulinoides* only occurs midway through the record at ~5.1 cal kyr BP (*figure 9.3*).

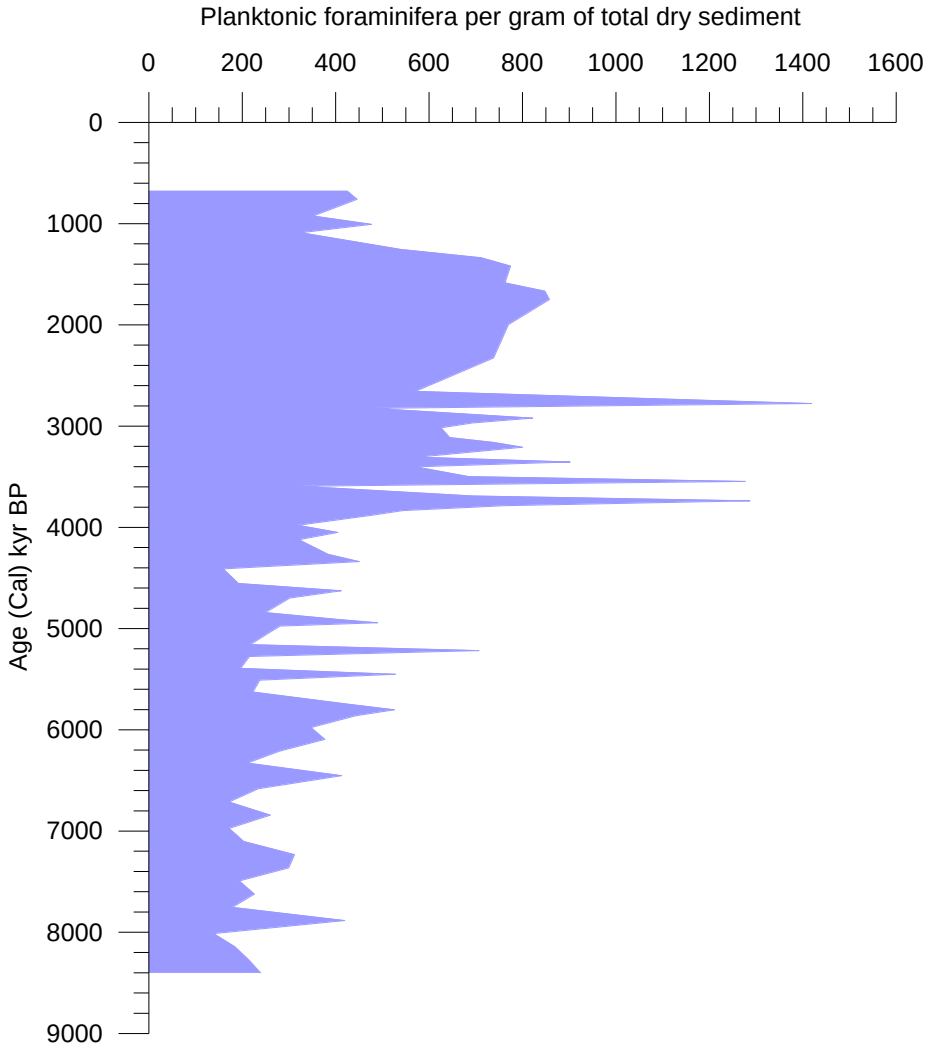

Figure 9.2. Graph depicting the Holocene planktonic foraminiferal abundance per gram of dry sediment for core M40/4 82-2 SL.

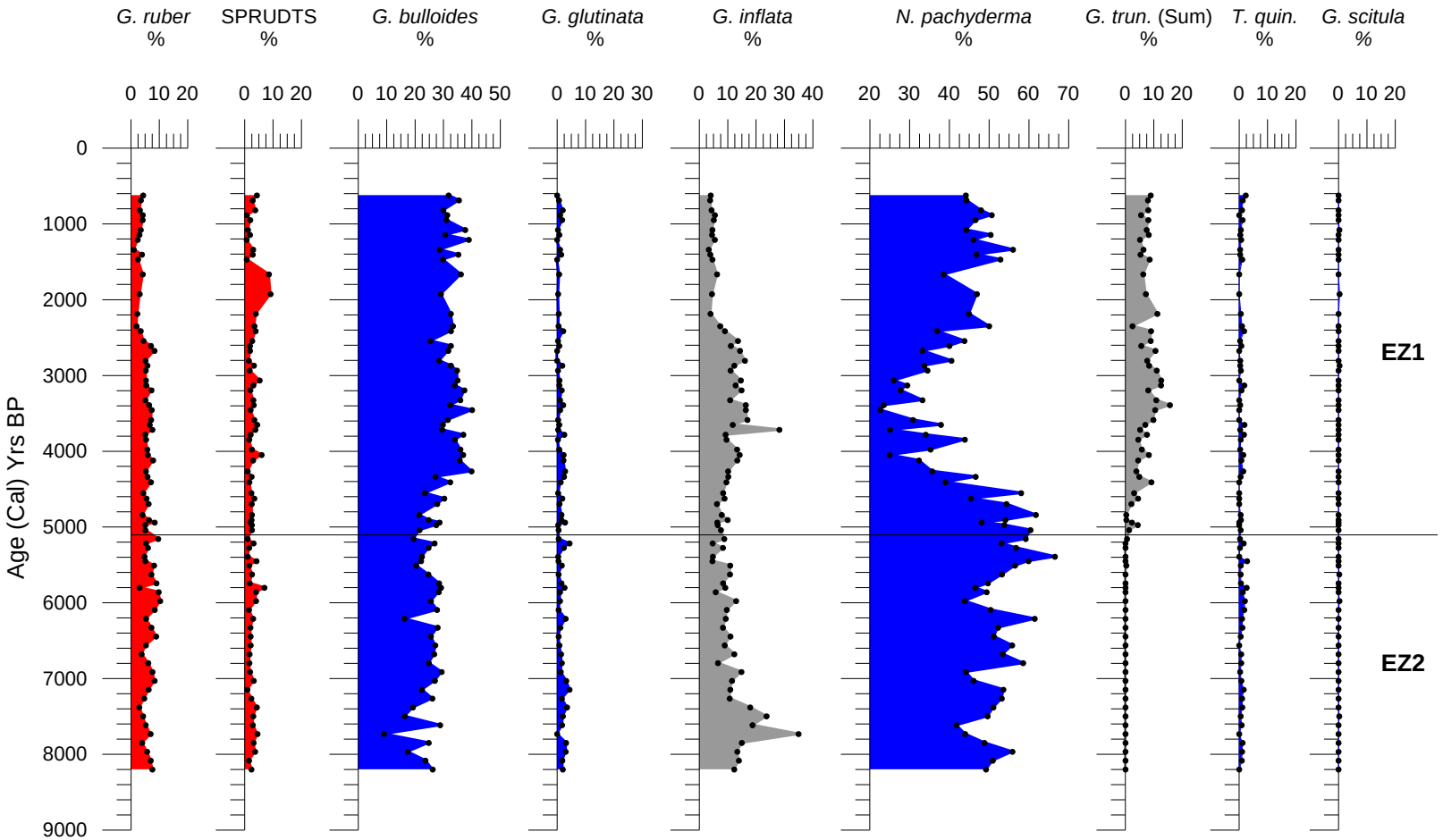

Figure 9.3. Graph illustrating the relative abundance of the main planktonic foraminiferal species for core M40/4 82-2 SL. Warm indicator species are shaded red, transitional species are shaded grey and cold species are shaded blue (Sbaffi et al., 2004). Solid black line represents ecozone boundaries identified in chapter 8.

9.2.2 Sea Surface temperature variability

Planktonic foraminiferal assemblages have proved a very useful proxy for reconstructing past SSTs in the Mediterranean Sea (González-Donoso et al., 2000; Kallel et al., 1997a,b, 2000; Hayes et al., 2005; Melki et al, 2009). Based on faunal assemblage data, SSTs are provided for core M40/4 82-2 SL using the ANN transfer function *(figure 9.4)*. Mean annual, summer and winter SSTs are presented producing average SST standard deviations of 0.34, 0.37 and 0.33 respectively. The error associated with ANN SSTs ranges between 1.1 and 0.5°C, this therefore must be taken into consideration when interpreting the data, however, the data presents SST variability that is greater than the associated error and as such can be interpreted as significant.

Overall a general warming trend is observed in core M40/4 82-2 SL, from the early/mid to late Holocene however, episodes of significant (≥2ºC) variation are superimposed on this trend (*figure 9.4*). For example, a cooling trend (~3.4°C) is observed between ~8-5.2 cal kyr BP which is punctuated by two short term cold events (CE1 and CE2 at 1.2 and 2.4 cal kyr BP respectively) (*figure 9.4*). These cold events represent the coldest (annual mean of 14 and 13°C respectively) SST recorded in the entire Holocene record. A subsequent warming culminates in annual SSTs of ~17°C at ~3.7 cal kyr BP. This is the most significant increase in Holocene SST in the Gulf of Lion during which the mean summer, winter and annual SSTs show increases of 5°C, 3°C and 4°C respectively. Two further cold events are observed at ~5.2 and ~7.2 cal kyr BP (CE3 and CE4). These events are separated by a significant warm episode in which the highest SSTs from the core are recorded (*figure 9.4*). Table 9.1 represents the associated SST variation for each of the Cold Events (CE) that represents the culmination of a cooling period, depicted in figure 9.4.

	Winter	Summer	Annual	Age
CE1	1.47	3.46	2.25	1211
CE2	2.01	2.48	2.35	2351
CE3	1.98	2.78	2.51	5218
CE4	2.05	3.43	2.82	7148

Table 9.1. Mean Winter Summer and Annual SST decrease associated with each CE and the associated age (cal) kyr BP of each CE.

Mean SSTs core M40/4 82-2 SL

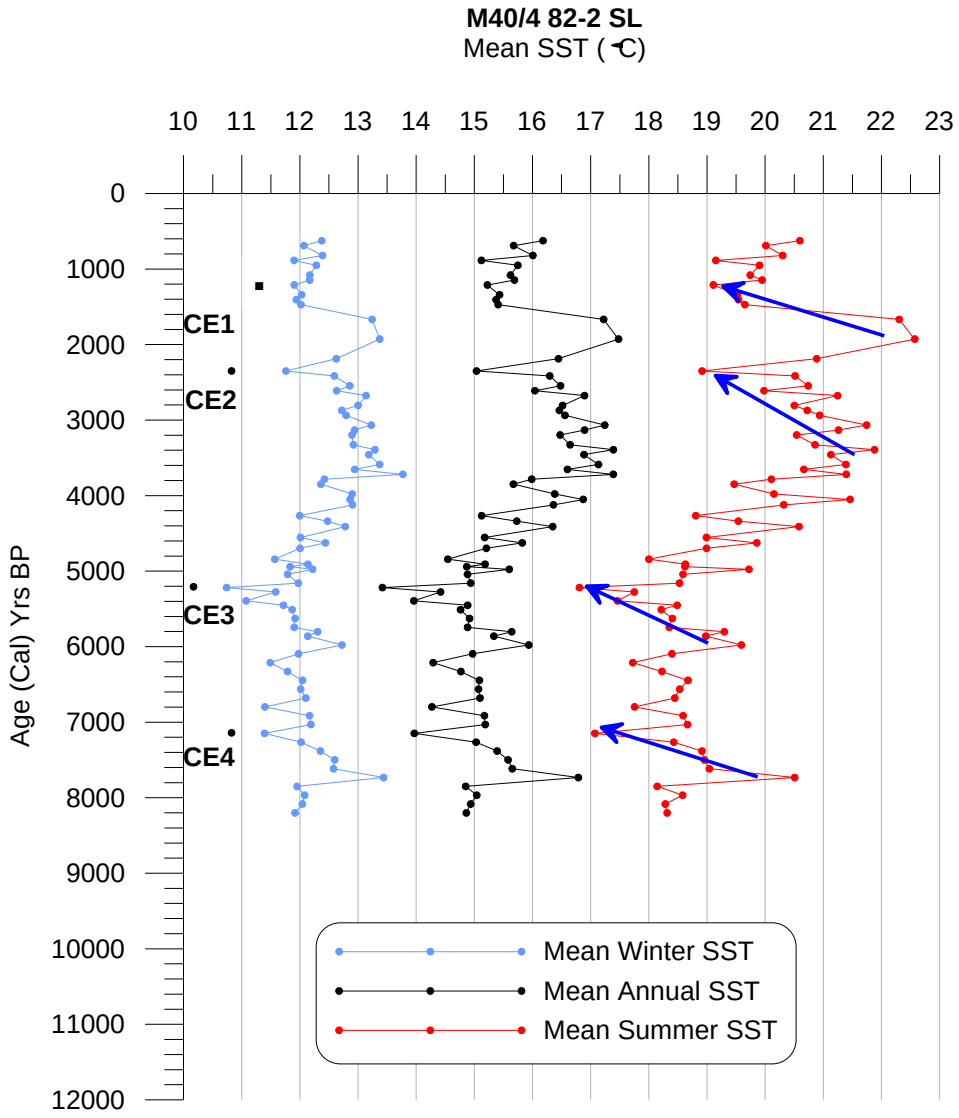

Figure 9.4. SST reconstruction of the Gulf of Lion core M40/4 82-2 SL based on ANN. The four cold events (CE1-4) were identified as SST minima subsequent to periods of significant cooling indicated by the blue arrows. (See Table 9.1 for timing of cold events).

9.3 Discussion

9.3.1 Palaeoclimatic variations in the Gulf of Lion

Our data indicates significant Holocene SST variation in the Gulf of Lion where respective decreases and increases in the mean annual SST are recorded up to 3 and 4°C. Chapter 2 outlined the atmospheric teleconnections existing between the North Atlantic Ocean and the western Mediterranean Sea with numerous research indicating correlations between the

two regions (Cacho et al., 1999; 2001; Emeis et al., 2000; Sbaffi et al., 2001; Bout-Roumazeilles et al., 2007; Frigola et al., 2007). Figure 9.5 compares the timing of cold events recorded in the North Atlantic Ocean with those observed in the Mediterranean Sea. Despite its unique hydrographic features, as the site of WMDW, core M40/4 82-2 SL records many of the climatic events recorded in the North Atlantic and the Mediterranean Sea. The timing of the four CE in our record implied by our age model is within the uncertainty comparable with other cooling events identified in the Balearic basin (Frigola et al., 2007), the Tyrrhenian and Alboran Seas (Cacho et al., 2001; Sbaffi et al., 2001) and the North Atlantic (Bond et al., 1997) (*figure 9.5*).

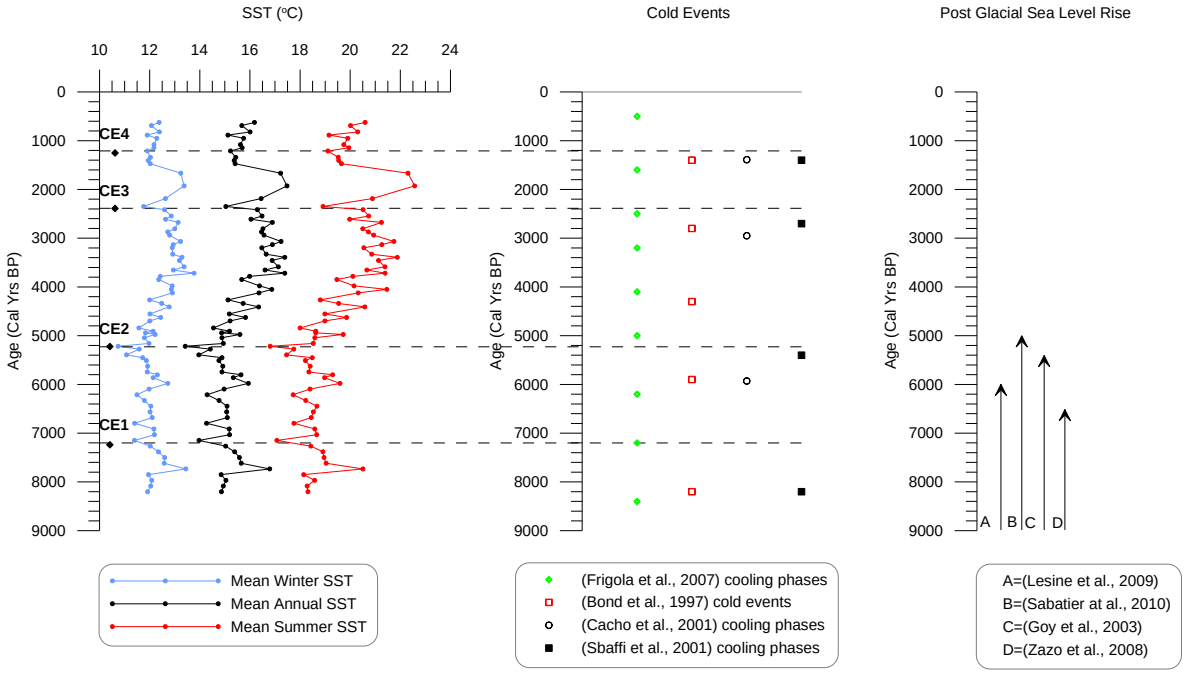

Figure 9.5. The first graph represents the reconstructed SST in the Gulf of Lion and associated cooling events (CE1-4). For comparison, the middle graph represents North Atlantic Ocean and western Mediterranean Sea cooling events based on four separate studies, dashed line represents the correlation between this research and previous studies. The final graph illustrates the maximum post glacial sea level rise before stabilisation.

The onset of the record core M40/4 82-2 SL records a mean annual SST of 15°C, followed by a rapid increase to almost 17°C by ~7.9 cal kyr BP. It is possible that the initial low SSTs may be related to the 8.2 Event recorded in numerous North Atlantic and Mediterranean Sea proxies (Bond et al., 1997; Emeis et al., 2000: Cacho et al; 2001; Sbaffi et al., 2001; Mayewski et al., 2004; Frigola et al., 2007). However, as the core does not extend beyond 8.2 cal kyr BP it is not possible to conclude that a cooling event occurred. Cacho et al. (2001) observed a Holocene thermal maximum between 10.0-9.0 cal kyr BP in

the Alboran Sea while Sbaffi et al. (2001) observed a similar trend in the Tyrrhenian Sea between 8.9-8.4 cal kyr BP that was followed by a subsequent decline. The onset of core M40/4 82-2 SL records a decrease in SST, this may indicate a similar post Holocene thermal maximum decline in SSTs as was evident in the Alboran and Tyrrhenian Seas. The Holocene climatic trends can be associated with the faunal ecozone patterns as identified in chapter 8.

9.3.1.1 8.2-5.0 cal kyr BP

This phase represents the early to mid Holocene, in core M40/4 82-2SL, represented by a declining SST trend and encompassing cold events 1 and 2. The decline in SST is synchronous with post glacial sea level rise until ~5.0-6.0 cal kyr BP when water levels stabilised (*figure 9.6*) (Goy et al., 2003; Zazo et al., 2008; Lesine at al., 2009; Sabatier at al., 2010). The rise in sea level and SST decline is attributed to the influx of cooler meltwater into the Mediterranean from the North Atlantic Ocean, (Rohling et al., 1995; Perez Folgado et al., 2003; Jimenez Espejo et al., 2006). The increased influx of surface Atlantic water at this time is associated with a significant decrease in sea surface salinity in the Tyrrhenian Sea which is believed to have interrupted the thermohaline circulation of the Mediterranean Sea causing stratification of the water column and subsequent collapse of vertical mixing in the eastern basin, resulting in the formation of S1 (Kallel et al., 2004). Experimental flux forced circulation models in the Mediterranean Sea indicate that a decrease in excess evaporation, thereby reducing the salinity of MAW, resulted in the weakening and cessation of LIW. This subsequently resulted in the termination of deep water formation and vertical mixing in the eastern basin (Myers, 2002). The loss of salinity input via the LIW also resulted in weakened convection in the Gulf of Lion in the western Basin (Myers, 2002). In an experiment where excess evaporation is reduced by 20%, convection was significantly reduced in the western basin, limited to just the top 500-600m of the water column. Even the forcing of extreme cold winter events could not produce convection that was able to ventilate deep waters (Myers, 2002). Considering that a 60-80% decrease in excess evaporation recreates conditions closest to those suggested for S1 formation (Myers, 2002), it would suggest that during this time frame deep water functioning and vertical mixing would be absent within the western basin. The relatively high abundances (>50%) of *N. pachyderma* (dextral) during the early/mid to mid Holocene

is consistent with water column stratification since the species is associated with the presence of a DCM and a shallow pycnocline (Pujol and Vergnaud Grazzini, 1995). Myers (2002) suggests that pycnocline shoaling occurred in all experiments simulating decreased excess evaporation, resulting in productivity enhancements allowing for the development of *N. pachyderma* (dextral) (Rohling, 1994). In addition, the absence of *G. truncatulinoides* in the faunal record attributes to a possible collapse of deep vertical mixing and water stratification. Similarly, *G. inflata* which exists as a deep dwelling planktonic foraminiferal species that requires some degree of vertical mixing (Pujol and Vergnaud Grazzini, 1995) also shows a declining trend from ~8.0 - 5.0 cal kyr BP.

Evidence of reduced sea surface salinities (SSSs) in the western basin, coeval with S1 deposition, is present in proxies from the Tyrrhenian Sea (Kallel et al., 1997, 2004; Bernasconi and Pika-Biolzi, 2000; Di Donato et al., 2008) and the Gulf of Lion (Melki et al., 2009). Reconstructions suggest that SSSs decreased to ~35.5‰ in both basins during S1 deposition (Kallel et al., 2004; Melki et al., 2009). Indeed, isotopic differences in the analysis of the shallow dwelling species *G. ruber*, suggests that strong water column stratification was present in the Tyrrhenian Sea during S1 deposition (Bernasconi and Pika-Biolzi, 2000).

The end of the early-mid to mid Holocene phase is associated with numerous changes across the Mediterranean region, coinciding with the end of the humid period (between 5.5 and 6.0 cal kyr BP) (De Menocal et al., 2000; Lezine et al., 2009) while proxies in the Tyrrhenian Sea indicate a re-establishment of winter mixing (Di Donato et al., 2008). Around the same time (~5.4 cal kyr BP) data from both the Alboran and Tyrrhenian Seas indicate a cooling (Sbaffi et al., 2001; 2004) correlating with a similar event observed in the faunal record from core M40/4 82-2 SL (CE2). However, this cooling is associated with the climatic optimum and it has been suggested that the reconstructed SST (associated with the increase in *N. pachyderma*) is related to a change in the pycnocline position rather than a temperature change (Sbaffi et al., 2001). The end of this phase also indicates the stabilisation of sea level rise at ~5.0 cal kyr BP and coincides with a change in vegetation indicating the onset of arid conditions (Pirazzoli et al., 2005; Bout-Rousmazeilles et al., 2007; Zazo et al., 2008). The faunal record at this time supports the re-establishment of vertical mixing with an increase in both *G. truncatulinoides* and *G. inflata* and a decline in *N. pachyderma* (dextral).

9.3.1.2 (~5.0 Cal Kyr BP-Present)

This phase coincides with an early mid Holocene warming between ~5.1-3.5 (cal kyr BP), (*figure 9.5*). During this timeframe there is a significant change in the faunal record., Relative abundances of *N. pachyderma* (dextral) decline drastically to a Holocene minima of ~22%, while *G. bulloides*, *G. inflata* and *G. truncatulinoides* all record an increase (*figure 9.3*). Such faunal signals would suggest enhanced mixing within the water column and availability of nutrients possibly through upwelling processes. This is in agreement with the findings of Frigola et al. (2008) that present a phase of good functioning deepwater circulation during this time. Frigola et al. (2008) attribute this circulation pattern to drier conditions around the western Mediterranean Sea, similarly Jalut et al. (2009) suggests that this timeframe is marked by a transition from more temperate to arid conditions as identified in pollen proxies. An increase in surface salinities, as a result of reduced precipitation, would reduce stratification allowing convective overturning allowing the increase of species such as *G. truncatulinoides* that require vertical mixing to proliferate and *G. inflata*. Indeed Melki (2009) observed an increasing salinity trend after 5.0 kyr cal BP (37.5‰) until ~1.0 cal kyr BP, similar faunal patterns also exist between this research, figure 9.6 presents the faunal assemblage observed between both cores, where both abundances and faunal patterns correlate. Mean Annual SST curve is plotted against both faunal abundance curves, as the faunal pattern of Melki et al., (2009) is similar to that of this research the SST pattern correlated with the authors data. The timing also corresponds with overall increased absolute abundances of planktonic foraminifera possibly a result of enhanced nutrient levels due to the break down of water column stratification and increasing SSTs.

The late Holocene is marked by a general increasing SST trend (*figure 9.5*). The onset of this phase is associated with a cooling SST trend that culminates with a CE2 at ~2.4 cal kyr BP. This event is synchronous with the cooling events in the Tyrrhenian and Alboran Seas (*figure 9.5*) and corresponds with a significant reduction in *G. inflata* and *G. ruber* and a minor increase in *T. quinqueloba* (*figure 9.3*). The reduction of *G. ruber* to almost absent from the faunal record suggests a significant cooling and/or reduction in salinity however, as the abundances remained relatively low and not absent during the reduced salinity period corresponding to S1, it is likely that SST was the most significant factor for reduced faunal abundances. This final phase however, is represented by the

highest absolute planktonic foraminiferal abundances, similar to that as identified by Melki et al. (2009).

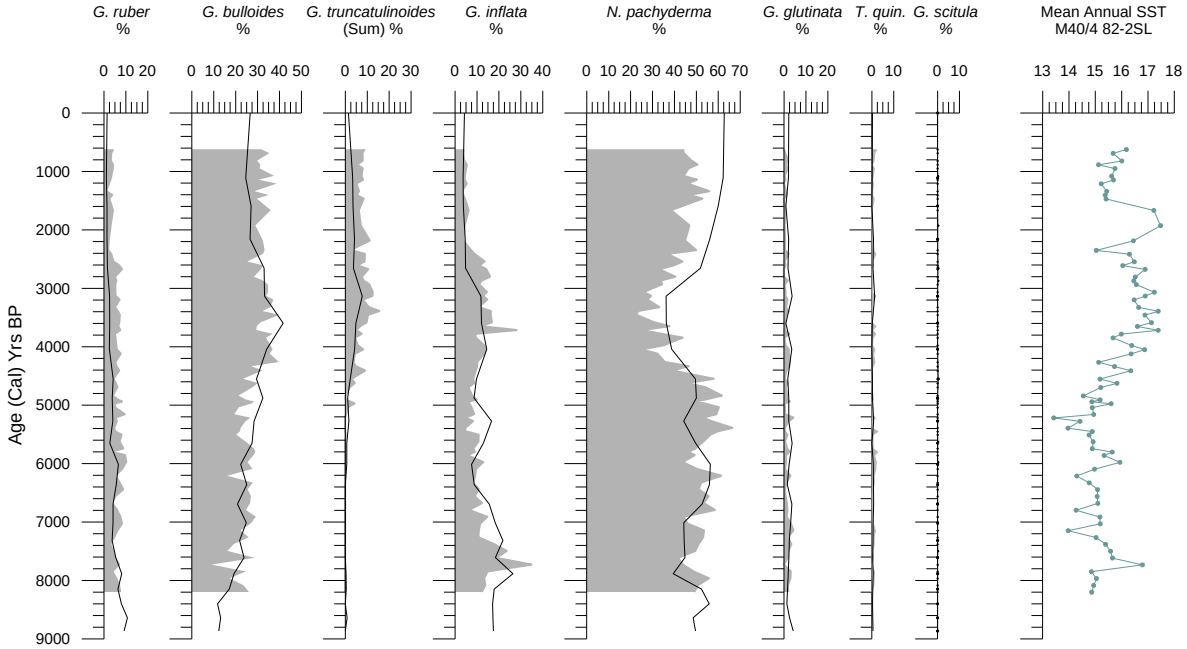

Figure 9.6. Faunal comparisons between this research (shaded area) and that of core MD99-2346 located in the Gulf of Lion (Melki et al., 2009). Mean Annual SST curve as established by this research is plotted against both faunal abundance curves.

A late Holocene decline in planktonic abundances occurs in core M40/4 82-2SL at ~2.6 cal kyr BP that correlates with a similar decline in planktonic foraminiferal abundances identified by Melki et al. (2009). Subsequent to the SST increase between ~2.2-1.8 cal kyr BP a cooling event (CE1) is observed at ~ 1.2 cal kyr BP that is identified in almost all other cold event proxies in *figure 8.6*. Mayewski et al., (2004) identified a similar increase in summer SST by almost 4°C between ~ 2.4-1.9 cal kyr BP. The increased SST possibly as a result of increased solar insolation may also have been the driving force for high lake level stands at ~2.6 cal kyr BP identified at Lake Ledro in notheastern Italy (Magny et al., 2009a). Finally the faunal assemblage in this phase is representative of modern conditions and can be explained by the different phases of the WMDW formation as outlined in Pujol and Vergnaud-Grazzini (1995)

9.4 Conclusion

Although not all of the climatic events indicated in figure 9.5 are evident in our data, in particular the more prominent 8.2 event core M40/4 82-2 SL highlights four cooling events

at ~7.2, 5.2 2.4 and 1.2 cal kyr BP, which can be correlated to cooling to cooling events recorded in a range of proxies. The lack of correlation with all of the events recognised in earlier studies may be due to the temporal extent of our core and/or variations in sampling resolution. It is possible that the lower SST represented at 8.2 cal kyr BP in our data may represent the well known 8.2 Event, however as temporal resolution of the core does not extend beyond that it is impossible to determine if the SST represents a short term cooling event or another climatic trend. The faunal composition of the early/mid-mid Holocene suggests a reduction or possible termination of deep water ventilation associated with a SST decrease culminating with minimum SST at ~5.2 cal kyr BP. The hydrological condition of the western Mediterranean basin during this time were subject to increased precipitation in addition to post glacial sea level rise resulting in reduced salinities and hydrological conditions conducive to reduced vertical mixing and enhanced water column stratification (Bernasconi and Pika-Biolzi, 2000; Kallel et al., 2004; Ali et al., 2008; Di Donato et al., 2008). The absence of *G. truncatulinoides* in the faunal record during this time further suggests the presence of a stratified water column. The faunal composition and subsequent reconstructed SST during the mid-late Holocene suggests a re-establishment of deep water convection in the Gulf of Lion and an increase in SST. The increase of deep water species such as *G. truncatulinoides* and *G. inflata* suggests that deep convection was occurring during this time. Associated with the transition from the more humid to present arid conditions of the Mediterranean region (Jalut et al., 2009) this phase also identifies increased salinity levels in the Gulf of Lion from the mid to late Holocene (Melki et al., 2009). The final phase associated with the late Holocene presents an increasing SST associated with modern environmental conditions. Faunal abundances reflect the modern hydrographic conditions associated with the site of WMDW formation that is conducive to deep vertical mixing and temporal stratification as indicated by the presence of *G. truncatulinoides* and *N. pachyderma* (dextral).

Chapter 10: Conclusions and Further Work

10.1 Conclusions

The focus of this research was divided between biostratigraphy and palaeoclimatological reconstruction in the western Mediterranean Sea using planktonic foraminifera. Four cores were analysed in 3 distinct regions, the Tyrrhenian Sea, the Balearic basin and the Gulf of Lion. The research aims were; to assess the potential of coiling variation in *G. truncatulinoides* as a biostratigraphic marker and to examine the relationship with environmental parameters such as sea surface temperatures (SSTs), to establish a new ecozonation for the Gulf of Lion and Balearic Basin based on planktonic foraminiferal species abundance and to provide a palaeoenvironmental reconstruction for the climatically sensitive Gulf of Lion during the Holocene employing artificial neural network analysis of faunal assemblage data.

Chapter 7 addressed the potential of *G truncatulinoides* as a biostratigraphic marker, and attempted to establish a relationship between the coiling variation of the species and environmental parameters. The results indicated that *G. truncatulinoides* can be used as a biostratigraphic marker in the western Mediterranean Sea with all 4 cores identifying a mid Holocene dextral dominance at ~5.0 cal kyr BP. However, this must be applied using relative coiling abundance of *G. truncatulinoides* as a percentage of the total *G. truncatulinoides* population based on total sample counts of 50 specimens or more. This quantitative method provides a more accurate biostratigraphical signal. The associations of coiling ratios with reconstructed ANN SSTs indicate a poor correlation, in particular for the dextral variant, this corroborates the findings of Ujiié et al. (2010) that suggests SST does not determine coiling direction. Modern day studies indicate that water column stratification represents the most influential environmental factor for the species abundance and for individual coiling type distribution (Lohmann and Schweitzer, 1990, Ujiié et al., 2010).

Chapter 8 presented the first ecozonation for the Gulf of Lion and the Balearic Basin in the western Mediterranean Sea. Ecozonation was established based on the relative faunal abundance variation of planktonic foraminifera, with the subsequent establishment of 3 Ecozones extending from the early Holocene to the present. Each Ecozone (EZ) can be identified with independent climatological and environmental features. EZ3 (11.2-8.6 cal kyr BP) is associated with the transition from glacial to interglacial conditions, with SST

reconstructions demonstrating a significant summer SST increase of ~6-8°C. The presence of *G. truncatulinoides* indicates the occurrence of deep vertical mixing. EZ3 (8.6-5.1 cal kyr BP) is indicative of a period of enhanced stratification, likely associated with post glacial sea level rise and environmental conditions associated with the deposition of S1 in the eastern basin and the African humid period that extended up to ~5.5 cal kyr BP (deMenocal et al., 2000). EZ1 (5.1 cal kyr BP -Present) signifies the onset of deep vertical mixing associated with an increase in SST and the stabilisation of post glacial sea level rise to reflect the modern day hydrological conditions of the western basin.

The ecozonation established by this research indicates partial correlations between the relative faunal distribution patterns of both cores (M40/4 82-2SL and ODP 95B) however, an increase in core sampling would be needed to verify the proposed spatial extent of the biozonation. In the absence of a comparative biozonation with the previous biozonation studies in the western Mediterranean Sea, the findings substantiate the findings of Hayes et al. (2005) that planktonic foraminiferal biostratigraphy provides a useful palaeoenvironmental tool but on a local rather than regional scale.

The final aim of this research addressed a palaeoclimatological reconstruction of a high resolution core in the Gulf of Lion using planktonic foraminifera to reconstruct SST (Chapter 9). The findings identified four cooling events (CE) at 7.2, 5.2 2.4 and 1.2 cal kyr BP, also identified in North Atlantic and/or Mediterranean Sea proxies. Three phases of climatic variability were established in core M40/4 82-2 SL associated with specific environmental conditions. The early/mid-mid Holocene is represented by a reduction or possible termination of deep water ventilation associated with a decrease in SST with minimum SST occurring at ~ 5.0 kyr BP. Terrestrial and marine proxies (Bernasconi and Pika-Biolzi, 2000; Ali et al., 2008; Di Donato et al., 2008) indicate increased precipitation during the early to mid Holocene in addition to post glacial sea level rise resulting in reduced salinities and hydrological conditions conducive to reduced vertical mixing and enhanced water column stratification (Kallel et al., 2004). This is reflected by the absence of *G. truncatulinoides* in the faunal record during this time. The mid-late Holocene (coeval with Biozone 2) suggests a re-establishment of deep water convection in the Gulf of Lion and an increase in SST. This phase is associated with the transition from the more humid to present arid conditions associated with the Mediterranean region (Jalut et al., 2009). Increased salinity levels identified in the Gulf of Lion from the mid to late Holocene (Melki

et al., 2009) likely facilitated the preconditioning phase required for deep water mixing thereby allowing the growth of deep water species such as *G. truncatulinoides* and *G. inflata*. The final phase associated with the late Holocene (coeval with biozone 1) presents an increasing SST associated with modern environmental conditions. Faunal abundances reflect the modern hydrographic conditions associated with the site of WMDW formation that is conducive to deep vertical mixing and temporal stratification as indicated by the presence of *G. truncatulinoides* and *N. pachyderma* (dextral).

10.2 Limitations and Recommendations

Despite the advantages and usefulness of planktonic foraminifera for marine micropalaeoentological studies, limitations do exist. Such limitations include preservation of fossils and the effect of dissolution. However, many of the samples in this research contained pteropods that are more susceptible to dissolution than planktonic foraminifera and as such their presence reduces this concern. Recent discoveries of cryptic diversity in planktonic foraminifera (Kucera and Darling, 2002; Darling and Wade, 2008) have demonstrated the impact of different genetic variations when interpreting environmental calibrations. This relatively new development could help explain noise in palaeoclimatological reconstructions. To limit this, where possible, modern analogues used to infer palaeoenvironmental conditions were based on known cryptic species distribution. This approach was used throughout chapter 7 where only ecological preferences of *G. truncatulinoides* Type 2 were used for analysis, as this cryptic species represents that which is located in the Mediterranean Sea (de Vargas et al., 2001).

As the nature of this research depends on understanding the modern environmental parameters that control the numerous aspects of distribution, abundance and indeed coiling direction, further research on the present day ecological requirements and habitats of planktonic foraminifera would greatly facilitate our understanding of past environments. To further advance this research I would suggest extending the sampling resolution of core M40/4 82-2 SL to extend the full Holocene time frame as the time limits of this research did not allow for this. In addition, further cores would be required to determine the full spatial extent of the biostratigraphic potential of *G. truncatulinoides*.

References

Ali, A.A., Roiron, P., Chabal, L., Ambert, P., Gasco, J., Andre, J. and Terral, J. (2008) 'Holocene hydrological and vegetation changes in southern France inferred by the study of an alluvial travertine system (Saint-Guilhem-le-Desert, Herault)', Geoscience, 340, 356-366.

Alley, R.B. and Águstsdottír, A.M., (2005) 'The 8k event: cause and consequences of a major Holocene abrupt climate change' Quaternary Science Reviews, 24, 1123-1149.

Alley, R.B., Mayewski, P.A., Sowers, T., Stuiver, M., Taylo, K.C. and Clark, P.U. (1997) 'Holocene climatic instability: A prominent, widespread event 8200 yr ago', Geology, 25(6), 483-486.

Alpert, P., Baldi, M., Ilani, R., Krichak, S., Price, C., Rodó, X., Saaroni, H., Ziv, B., Kishcha, P., Barkan, J.,Mariotti, A., Xoplaki, E. (2006) 'Relations between Climate Variability in the Mediterranean Region and the Tropics: ENSO, South Asian and African Monsoons, Hurricanes and Saharan Dust' in P. Lionello, P. Malanotte-Rizzoli, and R. Boscolo (eds). Mediterranean Climate Variability. Oxford: Elsevier.

Armstrong, H.A. and Brasier, M.D. (2005) Microfossils, 1st ed., Blackwell Publishing.

Baldini, J.U.L., McDermott, F. and Fairchild, I.J. (2002) 'Structure of the 8200-Year Cold Event Revealed by a Speleothem Trace Element Record', Science, 296, 2203-2206.

Barale, V., Jaquet, J.M., and Ndiaye, M.(2008) 'Algal blooming patterns and anomalies in the Mediterranean Sea as derived from the SeaWiFS data set (1998–2003)', Remote Sens. Env., 112, 3300-3313

Barber, D.C., Dyke, A., Hillaire-Marcel, C., Jennings, A.E., Andrews, J.T., Kerwin, M.W., Bilodeau, G., McNeely, R., Southon, J., Moorhead, M.D. and Gagnon, J.M. (1999) 'Forcing of the cold event of 8,200 years ago by catastrophic drainage of Laurentide lakes', Nature, 400, 344-348.

Bé, A.W.H. and Hamlin, W.H. (1967) 'Ecology of Recent Planktonic Foraminifera: Part 3: Distribution in the North Atlantic during the Summer of 1962', Micropaleontology, 13(1), 87-106.

Bé, A.W.H., and Tolderlund, D.S., 1971. Distribution and ecology of living planktonic foraminifera in surface waters of the Atlantic and Indian Oceans. In Funnel, B.M., and Riedel, W.R. (Eds.), The Micropaleontology of Oceans: Cambridge (Cambridge Univ. Press), 105-149

Bé, A.W.H. (1959) 'Ecology of Recent planktonic foraminifera: Part 1- Areal distribution in the western North Atlantic', Micropaleontology, 5(1), 77-100.

Bé, A.W.H. (1960) 'Ecology of Recent Planktonic Foraminifera: Part 2: Bathymetric and Seasonal Distributions in the Sargasso Sea off Bermuda', Micropaleontology, 6(4), 373-392.

Bé, A.W.H. (1967) 'Foraminifera Families:Globigerinidae and Globorotaliidae' Conseil Permanent International pour L'exploration De La Mer, Lamont Geological Observatory of Columbia University, New York, No 982.

Bell, M., and M.J.C. Walker. 2005. Late Quaternary Environmental Change-Physical and human perspectives-Second Edition. Glasgow: Prentice Hall.

Bernasconi, S.M. and Pila-Biolzi, M. (2000) 'A stable isotope study of multiple species of planktonic foraminifera across sapropels of the Tytrrhenian Sea, ODP Site 974', Palaeogeography, Palaeoclimatology, Palaeoecology, 158, 281-292.

Bolli, H. M., (1950) 'The direction of coiling in the evolution of some Globorotaliidae' Contrib. Cushman foundation foramin. Res., 2, 82-89

Bolli, H. M., (1951) 'Notes on the direction of coiling of ratalid foraminifera' Contrib. Cushman foundation foramin. Res., 2, 139-143

Bond, G. C. and R. Lotti, 1995: Iceberg discharges into the North Atlantic on millenial time scales during the last glaciation. Science, 267, 1005-1010.

Bond, G., Showers, W., Cheseby, M., Lotti, R., Almasi, P., deMenocal, P., Priore, P., Cullen, H., Hajdas, I. and Bonani, G. (1997). 'A Pervasive Millennial-Scale Cycle in North Atlantic Holocene and Glacial Climates'. Science 278 (5341):

Bond, G., Kromer, B., Beer. J., Muscheler, R., Evans, M., Showers, W., Hoffman, S., Lotti-Bond, R., Hajdas, I. and Bonani, G. (2001). 'Persistent Solar Influence on North Atlantic Climate During the Holocene' Science 294 (5549), 2130–2136

Bout-Roumazeilles, V., Nebout, N.C., Peyron, O., Cortijo, E., Landais, A. and Masson-Delmotte, V. (2007) 'Connection between South Mediterranean climate and North African atmospheric circulation during the last 50,000 yr BP North Atlantic cold events', Quaternary Science Reviews, 26, 3197-3215.

Buccheri, G., Capretto, G., Di Donato, V., Esposito, P., Ferruzza, G., Pescatore, T., Ermolli, E.R., Senatore, M.R., Sprovieri, R., Bertoldo, M., Carella, D. and Madonia, M. (2002) 'A high resolution record of the last deglaciation in teh southern Tyrrhenian Sea: environmental and climatic evolution.', Marine Geology, 186, 447-470.

Budillon, F., Lirer, F., Iorio, M., Macrí, P.,Sagnotti, L., Vallefuoco, M., Ferraro, L., Garzigilia, S., Innangi, S., Sahabi, M., Tonielli, R. (2009) 'Intergrated stratigraphic reconstruction for the last 80 kyr in a deep sector of the Sardinia Chanel (Western MEditerranean)',Deep Sea Research, doi:10.1016/j.dsr2.2008.07.026

Cacho, I., Grimalt, J.O., Pelejero, C., Canals, M., Sierro, F.J., Flores, J.A. and Shackleton, N. (1999) 'Dansgaard-Oeschger and Heinrich event imprints in Alboran Sea paleotemperatures', Paleoceanography, 14(6), 698-703.

Cacho, I., Grimalt, J.O., Canals, M., Sbaffi, L., Shackleton, N., SchÖnfeld, J. and Zahn, R. (2001) 'Varaibility of teh western Mediterranean Sea surface temperature during

the last 25,000 years ans its connection with the Northern Hemishpere climatic changes', Paleoceanography, 16(1), 40-52.

Cacho, I., Grimalt, J.O. and Canals, M. (2002) 'Response of the western Mediterranean Sea to rapid climatic variability during the last 50,000 years: a molecular biomarker approach', Journal of Marine Systems, 33, 253-272.

Campins, J., Jansa, A , and Genoves, A., (2006) 'Three-dimensional structure of Western Mediterranean cyclones', Int. J. Climatol. 26(3), 323-343.

Capotondi, L., Borsetti, A.M. and Morigi, C. (1999) 'Foraminiferal ecozones, a high resolution proxy for the late Quaternary biochronology in the central Mediterranean Sea', Marine Geology, 153 253-274.

Casford, J.S.L., Abu-Zied, R., Rohling, E.J., Cooke, S., Boessenkool, K.P., Brinkhuts, H., De Vries, C., Wefer, G., Geraga, M., Papatheodorou, G., Croudace, I., Thomson, J. and Lykousis, V. (2001) 'Mediterranean climate variability during the Holocene', Mediterranean Marine Science, 2(1), 45-55.

Cifelli, R. (1974) 'Planktonic Foraminifera from the Mediterranean and Adjacent Atlantic Waters (Cruise 49 of the Atlantis II, 1969)', Journal of foraminiferal Research, 4(4), 171-183.

Cléroux, C., Lynch-Stieglitz, J., Schmidt, M., Cortijo, E., Duplessy, JC. (2009) 'Evidence for calcification depth change of *Globorotalia truncatulinides* between deglaciation and Holocene in the Western Atlantic Ocean' Marine Micropaleontology, 73, 57-61

CLIMAP. 1976. The Surface of the Ice-Age Earth. Science, Vol. 191, 1131-1137.

Coloma, C., Marchant, M., and Hebbeln, D. (2005) 'Planktonic Foraminifera during El Niño 1997-98 off Coquimbo (30°S; 73°W), Chile' Gayana 69(1) 48-77.

Comas, M.C., Zahn, R. and Klaus, A., et al. (1996) 'Site 975', Proceedings of the Ocean Drilling Program, Initial Reports, 161, 113-177.

Constantin, S., Bojar A-V., Lauritzen, S-E., Lundberg, Joyce., (2007) 'Holocene and Late Pleistocene climate in the sub-Mediterranean continental environment: A speleothem record from Poleva Cave(Southern Carpathians, Romania)' Palaeogeography, Palaeoclimatology, Palaeoecology 243, 322–338.

Dansgaard, W., S. J. Johnsen, H. B. Calusen, J.-D. Dahl, N. S. Gundestrup, C. U.Hammer, C. S. Hvidberg, J. P. Steffensen, A. E. Sveinbjornsdottir, J. Jouzel and G.Bond, 1993: Evidence for general instability of past climate from a 250-kyr ice-core record. Nature, 364, 218-20.

Davis, B.A.S., Brewer, S., Stevenson, A.C., Guiot, J. and Data Contributors (2003) 'The temperature of Europe during the Holocene reconstructed from pollen data', Quaternary Science Reviews, 22, 1701-1716.

Darling, K.F., and C. M. Wade. (2008). The gentic diversity of planktic foraminifera and the and the global distribution of ribosomal RNA genotypes. Marine Micropalaeontology, 67 (3) 216-238.

De Vargas, C., S. Renaud, H. Hilbrecht, and J. Pawlowski. 2001. Pleistocene adaptive radiation in Globorotalia truncatulinoides: genetic, morphologic, and environmental evidence. Paleobiology, Vol. 27: p. 104-125.

deMenocal, P., Ortiz, J., Guilderson, T., Adkins, J., Sarnthein, M., Baker, L., Yarusinsky, M. (2000) ' Abrupt onset and termination of the African Humid Period:rapid climate responses to gradual insolation forcing' Quaternary Science Reviews 19 347-361

Debret, M., Bout-Roumazeilles, V., Grousset, E., Desmet, M., McManus, J.F., Massei, N., Sebah, D., Petit, J.R., Copard, Y. and Trentesaux, A. (2007) 'The origin of the 1500-year climate cycles in Holocene North-Atlantic Records', Climate of the Past, 3 569-575.

Debret, M.,Sebag, D.,Crosta, X.,Massei, N., Tetit, J-R., Chapron, E., Bout-Roumazeilles, V. (2009) 'Evidence from wavelet analysis for a mis-Holocene transition in global climate forcing', Quaternary Science Reviews, doi:10.1016/j.quascirev.2009.06.005

Di Donato, V., Esposito, P., Russo-Ermolli, E., Scarano, A. and Cheddadi, R. (2008) 'Coupled atmospheric and marine palaeoclimatic reconstruction for the last 35ka in the Sele Plain-Gulf of Salerno area (southern Italy)', Quaternary International, 190 146-157.

Duplessy, J., Cortijo, E. and Kallel, N. (2005) 'Marine records of Holocene climatic variation', Geoscience, 337 87-95.

Emeis, K., Struck, U., Schulz, H., Rosenberg, R., Bernasconi, S., Erlenkeuser, H., Sakamoto, T. and Martinez-Ruiz, F. (2000) 'Temperature and Salinity variations of Mediterranean Sea surface waters over the last 16,000 years from records of planktonic stable oxygen isotopes and alkenone unsaturation ratios', Palaeogeography, Palaeoclimatology, Palaeoecology, 158 259-280.

Ericson, D.B., Wollin, G. and Wollin, J. (1954) 'Coiling diriction of *Globorotalia truncatulinoides* in deep-sea cores', Deep-Sea Research, 2 152-158.

Erricson, D.B., Ewing, M., Wollin, G. and Heezen, B.C. (1961) 'Atlantic Deep-Sea Sediment Cores', Geological Society of America Bulletin, 72 193-286.

Fischer, G.,and Wefer, G. (1999) 'Use of proxies in paleoceanography: examples from the South Atlantic' Fischer, G.,and Wefer, G. (Eds.) Springer-Verlag, New York

Fleitmann, D., M. Mudelsee, S.J. Burns, R.S. Bradley, J. Kramers, and A. Matter. 2008. Evidence for a widespread climatic anomaly at around 9.2ka before present. Paleoceanography, 23, doi: 10.1029/2007PA001519.

Fletcher, W.J., and M. F. Sánchez Goni. 2008. Orbital and sub-orbital-scale climate impacts on vegetation of the western Mediterranean basin over the last 48,000 yr. Quaternary Research, 70, 451-464.

Frigola, J., Moreno, A., Cacho, I., Canals, M., Sierro, F.J., Flores, A., Grimalt, J.O., Hodell, D.A. and Curtis, J.H. (2007) 'Holocene Climate variability in the western Mediterranean region from a deepwater sediment record', Paleoceanography, 22.

Frigola, J., A. Moreno, I. Cacho, M. Canals, F.J. Sierro, J. A. Flores, and J. O. Grimalt. 2008. Evidence of abrupt changes in Western Mediterranean Deep Water circulation during the last 50 kyr: A high-resolution marine record from the Balearic Sea. Quaternary International, 181, 88-104.

González-Donoso J.M., Serrano F., Linares D. (2000) Sea surface temperature during the Quaternary at ODP sites 976 and 975 (western Mediterranean). Palaeogeography, Palaeoclimatology, Palaeoecology, 162, 17–44.

Hayes, A., E.J. Rohling, S. De Rijk, D. Kroon, and W.J. Zachariasse. 1999. Mediterranean planktonic foraminiferal faunas during the last glacial cycle. Marine Geology, 153, 239-252.

Hayes, A., Kucera, M., Kallel, N., Sbaffi, L. and Rohling, E.J. (2005) 'Glacial Mediterranean sea surface temperatures based on planktonic foraminiferal assemblages', Quaternary Science Reviews, 24, 999-1016.

Hemleben, C., M. Spindler, and O.R. Anderson. 1989. Modern Planktonic Foraminifera. New York: Springer.

Herman, Y. (1972) *'Globorotalia truncatulinoides*: a Palaeo-oceanographic Indicator', Nature, 238, 394-395.

'DFG Senatskommission für Ozeanographie'. 2010. [Online]. Available: http://www.dfg-ozean.de/de/berichte/fs_meteor/m_40/ (Accessed 01.01.2010)

Hughen, K., Baillie, M., Bard E., Bayliss, A., Beck, J., Bertrand, C., Blackwell, P., Buck, C.,Burr, G., Butler, K., Damon, P., Edwards, R., Fairbanks, R., Friedrich, M., Guilderson, T., Kromer, B., McCormac, F., Manning, S., Bronk Ramsey,C., Reimer, P., Remmele, S., Southon, J., Stuiver, M., Talamo, S., Taylor, F., van der Plicht, J., Remmele,C., Southon, J., Stuiver, M., Talamo, S., Taylor, F., van der Plicht, J., and Weyhenmeyer., C. (2004). Radiocarbon, 46, 1059-1086. Marine04 Marine radiocarbon age calibration, 26-0ka BP.

Hurrell, J.W. (1995) 'Decadal Trends in the North Atlantic Oscillation: Regional Temperatures and Precipitation' ,Science, 269, 676-679

Imbrie, J., J.D. Hays, D.G. Martinson, A. McIntyre, A.C. Mix, J.J. Morley, N.J. Pisias, W.L. Prell, and N.J. Shackleton. 1984. The Orbital Theory of Pleistocene Climate: support form a revised chronology of the 18O record, in A. Berger, J. Imbrie, J. Hays, G. Kukla, and B. Saltzman (eds). Milankovitch and Climate. Dordrech: Reidel.

Jalut, G., Amat, A.E., Bonnet, L., Gauquelin, T. and Fontugne, M. (2000) 'Holocene climatic changes in the Western Mediterranean, from south-east France to south-east Spain', Palaeogeography, Palaeoclimatology, Palaeoecology, 160, 255-290.

Jian, Z., Li, B., Huang, B. and Wang, J. (2000) *'Globorotalia truncatulinoides* as indicator of upper-ocean thermal structure during the Quaternary: evidence from the South China Sea and Okinawa Trough', Palaeogeography, Palaeoclimatology, Palaeoecology, 162, 287-298.

Jimenez-Espejo, F.J., Martinez-Ruiz, F., Sakamota, T., Iijima, K., Gallego-Torres, D. and Harada, N. (2007) 'Paleoenvironmental changes in the western Mediterranean since the last glacial maximum: High resolution multiproxy record from the Algero-Balearic basin', Palaeogeography, Palaeoclimatology, Palaeoecology, 246(2), 292-306.

Jones, J.I. (1967) 'Significance of distribution of planktonic foraminifera in the Equatorial Atlantic Undercurrent', Micropaleontology, 13(4), 489-501.

Jorissen, F.J., Asioli, A., Borsetti, A.M., Capotondi, L., de Visser, J.P., Hilgen, F.J., Rohling, E.J., van der Borg, K., Vergnaud Grazzini, C. and Zachariasse, W.J. (1993) 'Late Quaternary central Mediterranean biochronology', Marine Micropaleontology, 21, 169-189.

Kallel, N., Duplessy, J.C., Labeyrie, L., Fontugne, M., Paterne, M., Montacer, M., (2000) 'Mediterranean pluvial periods and sapropel formation over the last 200000 years' , Palaeogeogr. Palaeoclimat. Palaeoecol. 157, 45–58.

Kallel, N., Paterne, M., Labeyrie, L., Duplessy, J. and Arnold, M. (1997) 'Temperature and Salinity records of the Tyrrhenian Sea during the last 18,000 years', Palaeogeography, Palaeoclimatology, Palaeoecology, 135, 97-108.

Kallel, N., Duplessy, J.-C., Labeyrie, L., Fontugne, M., Paterne, M., (2004). 'Mediterranean sea palaeohydrology and pluvial periods during the late Quaternary'. In: Batterbee, R.W., Gasse, F., Stickley, C.E. (Eds.), Past Climate Variability through Europe and Africa. Springer,Dordrecht, pp. 307–324.

Kerwin, M.W., Overpeck, J.T., Webb, R.S., DeVaernal, A., Rind, D.H., Healy, R.J. (1999) 'The Role of Oceanic Forcing in Mid-Holocene Northern Hemisphere climatic change', Paleoceanography, 14(2) 200-210.

Kucera, M.D. (2003) 'Numerical approach to microfossil proxy daya. Lecture notes for Summer school Paleoceanography: Theory and Field evidence.', IAMC Geomare, 66-90.

Kucera, M., A. Rosell-Melé, R. Schneider, C. Waelbroeck, and M. Weinelt. 2005. Multiproxy approach for the reconstruction of the glacial ocean surface (MARGO). Quaternary Science Reviews, 24, 813-819.

Kucera, M. (2007) 'PLanktonic Foraminifera as Tracers of Past Oceanic Environments', in Hillaire-Marcel, C. and de Vernal, A. (eds.) Proxies in Late Cenozoic Paleocenography, 1st ed., Amsterdam, The Netherlands: Elsevier.

Kuroyanagi, A. and Kawahata, H. (2004) 'Vertical distribution of living planktonic foraminifera in the seas around Japan', Marine Micropaleontology, 53, 173-196.

Kustanowich, S. (1963) 'Distribution of Planktonic Foraminifera in Surface Sediments of the South-West Pacific Ocean', New Zealand Journal of Geology and Geophysics, 6(4), 534-565.

LaGrande, A.N., Lynch-Stieglite, J. and Farmer, E.C. (2004) 'Oxygen Isotopic composition of *Globorotalia trucatulinoides* as a proxy for intermediate depth density' Paleocanography, 19 (PA4025): 10,1029/2004PA001045

La Voilette, P.E. (1994) 'Overview of the Major Forcings and Water Masses of the Western Mediterraenan Sea' In Costal and Estuarine Studies: Seasonal and Interannual Variability of the Western Mediterranean Sea. La Voilette, P.E. (Ed.) AGU, Washington, DC.

Lal, D., Jull, A.J.T., Pollard, D., Vacher, L., (2005) 'Evidence for large century time-scale changes in solar activity in the past 32 Kyr, based on un-situ cosmogenix 14C in ice at Summit, Greenland' , Earth and Planetary Science Letters, 234, 335-439

Leduc, G., Schneider, R., Kim, J.H., Lohmann, G., (2010) 'Holocene and Eemian sea Surface temperature trends as revealed by alkenone and Mg/Ca paleothermometry' Quaternary Science Reviews, 29, 989-1004

Lionello, P., P. Malanotte-Rizzoli, R. Boscolo, P. Alpert, V. Artale, L. Li, J. Luterbacher, W. May, R. Trigo, M. Tsimplis, U. Ulbrich, and E. Xoplaki. 2006. 'The Mediterranean climate: an overview of the main characteristics and issues', in P. Lionello, P. Malanotte-Rizzoli, and R. Boscolo (eds). Mediterranean Climate Variability. Oxford: Elsevier.

Lohmann, G.P. and Malmgrenm B.A. (1983) 'Equatorward migration of *Globorotalian truncatulinoides* ecophenotypes through the Late Pleistocene:Gradual evolution or ocean change?',Paleobiology, 414-421

Lohmann, G.P. and Schweitzer, P.N. (1990) *'Globorotalia truncatulinoides'* Growth and chemistry as probes of the past thermocline: 1. Shell size. Paleoceanography, 5(1), 55-75.

Magny M., V., B., Zanchetta, G., Fouache, E., Touchais, G., Petrika, L., Coussot, C., Walter-Simonnet, A. and Arnaud, F. (2009) 'Possible complexity of the climatic event around 4300-3800 cal. BP in the central and western Mediterranean', The Holocene, 19(6), 823-833.

Magny, M., Galop, D., Bellintani, P., Desmet, M., Didier, J., Haas, J.N., Martinelli, N., Pedrotti, A., Scandolari, R., Stock, A. and Vannière, B. (2009) 'Late-Holocene climatic variability south of the Alps as recorded by lake-level fluctuations at lake ledro, Trentino, Italy', The Holocene, 575(589),.

Magny, M., Vannière, B., Zanchetta, G., Fouache, E., Touchaise, G., Pertika, L., Coussot, C., Walter-Simonnet, A. and Arnaud, F. (2009) 'Possible complexity of the climatic event around 4300-3800 cal. BP in the central and western Mediterranean', The Holocene, 19(6), 823-833.

Melki, T., Kallel, N., Jorissen, F.J., Guichard, F., Dennielou, B., Berné, L., Labeyrie, L. and Fontugne, M. (2009) 'Abrupt climate change, sea surface salinity and paleoproductivity in the western Mediterranean Sea (Gulf of Lion) during teh last 28 kyr', Palaeogeography, Palaeoclimatology, Palaeoecology, 279, 96-113.

MFSTEP, (2005) Mediterranean Forcasting System toward Environmental Predictions, 17. Available at http://www.bo.ingv.it/mfstep

Myers, P.G. (2002) 'Flux-forced simulations of the paleocirculation of the Mediterranean', Paleoceanography, 17(1), 1009, doi:10.1029/2000PA000613

Orr, W.N. (1967) 'Secondary Calcification in the Foraminiferal Genus Globorotalia' Science New Series,157(3796) 1554-1555

O'Brien, S.R., Mayewski, P.A., Meeker, L.D., Messe, D.A., Twickler, M.S., Whitlow, S.I. (1995) 'Complexity of Holocene Climate as Reconstructed from a Greenland Ice Core' ,Science,270 (5244) 1962-1964.

Peel, M.C., Finlayson, B.L., and McMahon, T.A., (2007) 'Updated world map of the Köppen-Geiger climate classification' ,Hydrology and Earth Systems Sci.ence, 11, 1633-1644.

Pérez-Folgado, M., Sierro, F.J., Flores, J.A., Cacho, I., Grimalt, J.O., Zahn, R. and Shackleton, N. (2003) 'Western Mediterranean planktonic foraminifera events and millennial climatic variability during the last 70 kyr', Marine Micropaleontology, 48, 49-70.

Pilcher, J.R. 2005. 'Radiocarbon Dating and Environmental Radiocarbon Studies', in A. Mackay, R. Battarbee, J. Birks, and F. Oldfield (eds). Global Change in the Holocene. London: Hodder Arnold.

Pujol, C. and Vergnaud Grazzini, C. (1989) 'Palacoceanography of the last deglaciation in the Alboran Sea (western Mediterranean). Stable Isotopes and planktonic forminiferal records' Marine Micropaleontology. 15, 153-179.

Pujol, C. and Vergnaud Grazzini, C. (1995) 'Distribution patterns of live planktic foraminifers as related to regional hydrography and productive systems of the Mediterranean Sea', Marine Micropaleontology, 25, 187-217.

Rasmussen, S.O., Vinther, B.M., Clausen, H.B. and Andersen, K.K. (2007) 'Early Holocene climate oscillations recorded in three Greenland ice cores', Quaternary Science Reviews, 26, 1907-1914.

Reddy, M.P.M., (2001) 'Water Masses of the Oceans' In Descriptive Physical Oceanograpy, Reddy, M.P.M. (ed) Balkema, India.

Rixen, M., Beckers, J., Levitus, S., Antonov, L., Boyer, T., Maillard, C., Fichaut, M., Balopoulos, E., ,Iona, S., Dooley, H., Garcia,M -J., Manca, B., Giorgetti, A., Manzella, G., Mikhailov N., Pinardi, N., Zavatarelli, M., (2005) 'The Western Mediterranean Deep Water: A proxy for climate change' Geophysical Research Letters, 32.

Robinson, A.R., W.G. Leslie, A. Theocharis, and A. Lascaratos. 2001. Mediterranean Sea Circulation. Encyclopedia of Ocean Sciences, Academic Press, 44, 1689-1706.

Rohling, E.J. and De Rijk, S. (1999) 'Holocene Climate Optimum and Last Glacial Maximum in the Mediterranean: the marine oxygen isotope record', Marine Geology, 153, 57-75.

Rohling, E.J., and Gieskes. W.W.C. (1989). Late Quaternary changes in Mediterranean intermediate water density and formation rate. Paleoceanography, 4 (5), 531-545.

Rohling, E.J., and Palike. H. (2005). Centennial-scale climate cooling with a sudden cold event around 8,200 years ago. Nature, 434, 975-979.

Rohling, E.J., Hayes, A., Rijk, D., Kroon,D., Zachariasse, W.J. and Eisma, D. (1998) Abrupt cold spells in the northwest Mediterranean. Palaeoceanography, 13, 316-322.

Rohling, E. J., Abu-Zied, R.H., Casford, J.S.L., Hayes, A. and Hoogakker, B.A.A. (2009). 'The marine environment: present and past', in Woodward, J. C., (ed.). The Physical Geography of the Mediterranean. Oxford: Oxford University Press.

Rouis-Zargouni, I., Turon, J., Londeix, L., Essallami, L., Kallel, N. and Sicre, M. (2009) 'Environmental and climatic changes in the central Mediterranean Sea (Siculo-Tunisisn Strait) during the last 30 ka based on dinoflagellate cyst and planktonic foraminifera assemblages', Palaeogeography, Palaeoclimatology, Palaeoecology.

Sabatier, P., Dezileau, L., Barbier, M., Raynal, O., Lofi, J., Briqueu, L., Condomines, M., Bouchette, F., Certain, R., Van Grafenstein, U., Jorda, C. and Blanchemanche, P. (2010) 'Late-Holocene evolution of a costal lagoon in the Gulf of Lions (South of France)', Bulletin Société géologique France, 181(1), 27-36.

Sbaffi, L., Wezel, F.C., Kallel, N., Paterne, M., Cacho, L., Ziveri, P. and Shackleton, N. (2001) 'Response to the pelagic environment to palaeoclimatic changes in the central Mediterranean Sea during the Late Quaternary', Marine Geology, 178, 39-62.

Schiebel, R., and C. Hemleben. 2005. Modern planktic foraminifera. Paläontologische Zeitschrift, 79 (1) 135-148.

Schmuker, B. and Schiebel, R. (2002) 'Planktic forminifers and hydrography of the eastern and northern Caribbean Sea', Marine Micropaleontology, 46, 387-403.

Shaw, A.B. 1964. Time in Stratigraphy. New York: McGraw-Hill.

Siani, S., Paterne, M., Michel, E., Sulpizo, R.,Sbrana, A., Arnold, M., Haddad, G. (2001) 'Mediterraeann Sea Surface Radiocarbon Reservoir Age Changes since the Last Glacial Maximum' Science, 294, 1917-1920.

Smith, R.O., H.L. Bryden, and K. Stansfield. 2008. Observations of new western Mediterranean deep water formation using Argo floats 2004-2006. Ocean Science, 4, 133-149.

Spencer-Cervato, C., and Thierstein, H.R. (1996) 'First appearance of Globorotalia truncatulinoides: cladogenesis and Immigration' Marine Micropaleontology, 30, 267-291

Sprovieri, R., Di Stefano, E., Incarbona, A. and Gargano, M.E. (2003) 'A high-resolution record of the last deglaciation in the Sicily Channel based on foraminifera and calcareous nannofossil quantitative distribution', Palaeogeography, Palaeoclimatology, Palaeoecology, 202, 119-142.

Stuiver, M., Reimer, P.J., Bard, E., Warren-Beck, J., Burr, G.S., Hughen, K.A., Kromer, B., McCormac, G., Van Der Plicht, J. and Spurk, M. (1998). INTCAL98 Radiocarbon Age Calibration 24,000-0 cal. BP. Radiocarbon, 40(3) 1041-1083.

Thiede, J. (1971) 'Variations in Coiling Ratios of Holocene Planktonic Foramifera', Deep Sea Research and Oceanography, 18, 823-831.

Thunell, R.C. (1978) 'Distribution of Recent Planktonic Foraminifera in Surface Sediments of the Mediterranean Sea', Marine Micropaleontology, 3, 147-173.

Ujiié, Y., and J.H. Lipps. 2009. Cryptic diversity in planktic foraminifera in the northwest Pacific Ocean. Journal of Foraminiferal Research, 39(3) 145-154.

Ujiié, Y., Garidel-Thoron, T., Watanabe, S., Wiebe, P., de Vargas, C. (2010) 'Coiling dimorphism within a genetic type of the planktonic foraminifer *Globorotalia truncatulinoides*' Marine Micropaleontology 77, 145–153.

Veski, S., Seppa, H. and Ojola, A.E.K. (2004) 'Cold event at 8200 yr B.P. recorded in annually laminated lake sediments in eastern Europe', Geological Society of America, 32(8), 681-684.

Walker, M. 2005. Quaternary Dating Methods. London: John Wiley & Sons Ltd.

Wilke, I., Meggers, H. and Bickert, T. (2009) 'Depth habitats and seasonal distributions of recent planktic foraminifers in the Canary Islands region(29°N) based on oxygen isotopes', Deep-Sea Research, 1(56), 89-106.

Williams, M., Dunkerley, D., De Deckker, P., Kershaw, P. and Chappell, J. (1998) Quaternary Environments, 2nd ed., London: Arnold.

Wilson, R.C.L., S.A. Drury, and J.L. Chapman. 2005. The Great Ice Age-Climate Change and Life. Cornwall: Routledge.

Xoplaki, E., F. J. Gonzalez-Rouco, J. Luterbacher, and H. Wanner (2003) 'Mediterranean summer air temperature variability and its connection to the large-scale atmospheric circulation and SSTs', Clim. Dyn., 20, 723–739.

Websites:

- National bathymetric chart of the Mediterranean Sea: http://ngdc.noaa.gov/mgg/ibcm/seismicity/IBCM-S-5M-254m-Shaded.jpg; Accessed July 2011.

- CIBRA: The Mediterranean Sea, http://www..unipv.it/cibra/edu_Mediterraneo_uk.html. Last Updated August 2005, Accessed July 2011-09-07

Appendix A: Species Pictures

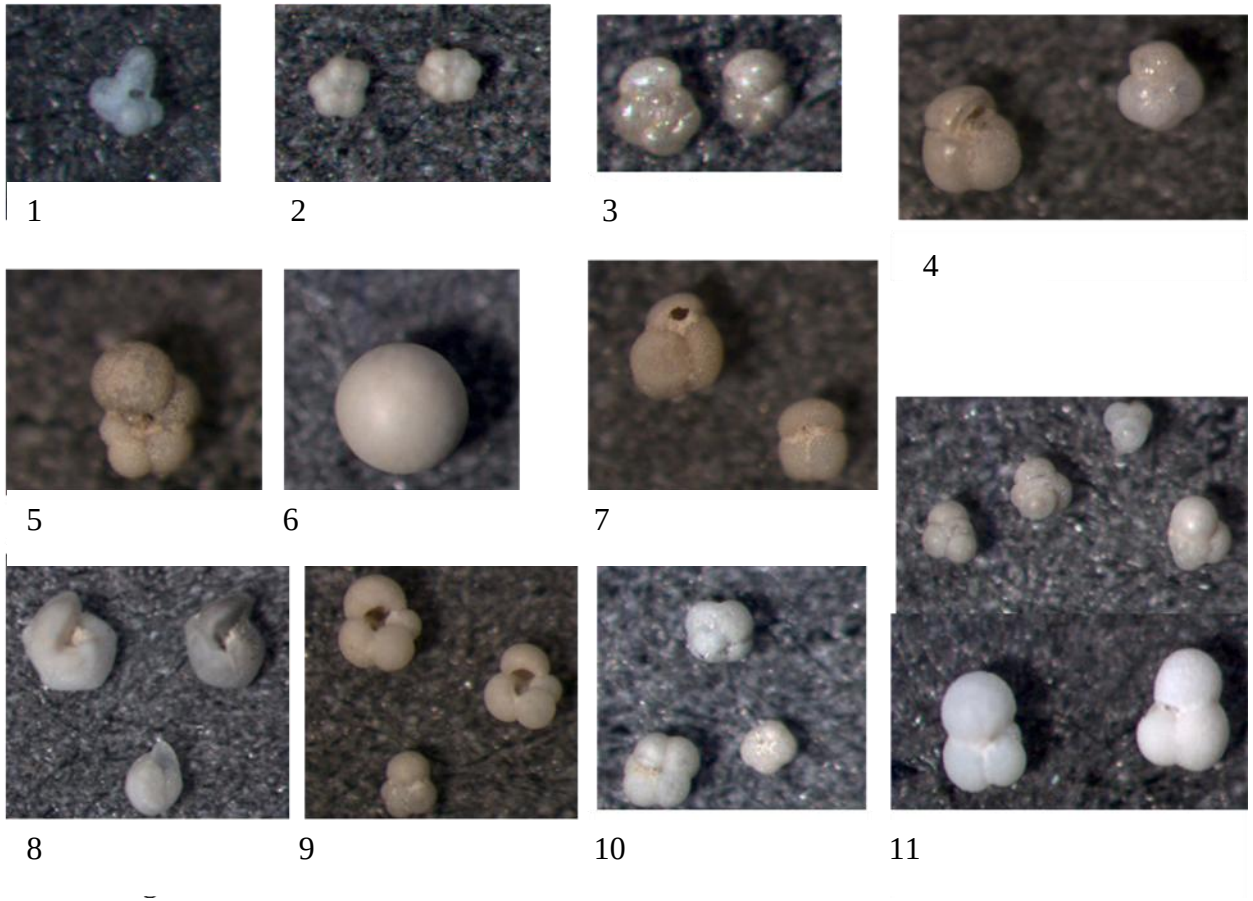

Plate 1. Digital images of planktonic foraminifera taken on stereo microscope (20 X objective lens) *1=B. digitata, 2=T. quinqueloba, 3=G. scitula, 4=G. inflata, 5=G. siophonifera, 6=O. universa, 7= G.ruber, 8=G. truncatulinoides (left coiling) 9=G. bulloides, 10=N.pachyderma, 11=G. glutinata (with and without bulla).*

Appendix B: Four Cores Raw Data